Small regulatory RNAs controlling complex phenotypes in *Vibrio cholerae*

Dissertation

Zur Erlangung des Doktorgrades

der Naturwissenschaften

(Dr. rer. nat.)

der Fakultät für Biologie

der Ludwig-Maximilians-Universität München

vorgelegt von

Roman Herzog

aus Augsburg

München, Juli 2020

Diese Dissertation wurde angefertigt

unter der Leitung von Prof. Dr. Kai Papenfort

im Bereich von Department Biologie I

an der Ludwig-Maximilians-Universität München

Gutachter:

1. Prof. Dr. Kai Papenfort
2. Prof. Dr. Heinrich Jung

Datum der Abgabe: 21.07.2020

Tag der mündlichen Prüfung: 15.12.2020

Eidesstattliche Erklärung

Ich versichere hiermit an Eides statt, dass die vorgelegte Dissertation von mir selbstständig und ohne unerlaubte Hilfe angefertigt wurde. Des Weiteren erkläre ich, dass ich nicht anderweitig ohne Erfolg versucht habe, eine Dissertation einzureichen oder mich der Doktorprüfung zu unterziehen. Die folgende Dissertation liegt weder ganz, noch in wesentlichen Teilen einer anderen Prüfungskommission vor.

Roman Herzog, München, den 20. Juli 2020

Statutory Declaration

I declare that I have authored this thesis independently, that I have not used other than the declared sources/resources. As well I declare, that I have not submitted a dissertation without success and not passed the oral exam. The present dissertation (neither the entire dissertation nor parts) has not been presented to another examination board.

Roman Herzog, Munich, 20 July 2020

Contents

Nomenclature

Base-pairing interactions of an sRNA with an mRNA are indicated in the format sRNA/*mRNA*, e.g., VqmR/*aphA*.

Numbers above sRNA sequences and promoter regions denote the distance relative to the transcriptional start site.

Numbers above mRNA sequences indicate the relative distance to the translational start site.

Gene deletions are indicated by the "Δ" symbol, e.g., Δ*vqmR*.

Genes or genomic fragments that follow a "p" are expressed from a plasmid, e.g., pVqmR.

"P" indicates a promoter, e.g., P*vqmR*.

Abbreviations

(v/v)	volume per volume
(w/v)	weight per volume
[^{32}P]	phosphorus-32
°C	degree Celsius
A	adenosine
a.k.a.	also known as
A.U.	arbitrary units
A-22	*S*-(3,4-dichlorobenzyl) isothiourea
AA	aminoacetone
AI	autoinducer
AI-2	autoinducer-2
AI-3	autoinducer-3
Ala-AA	*N*-alanyl-aminoacetone
Amp	ampicillin
AMP	antimicrobial peptide
ANOVA	analysis of variance
bp	base-pair
C	cytosine
CAI-1	cholera autoinducer-1
c-di-GMP	cyclic diguanylate monophosphate
cDNA	complementary DNA
CDS	coding sequence
Cef	cefalexin
CFU	colony forming units
Cm	chloramphenicol
Co-IP	co-immunoprecipication
conc.	concentration
CPM	counts per million
CT	cholera toxin
Da	Dalton
DNA	deoxyribonucleic acid

DNase	deoxyribonuclease
DPD	4,5-dihydroxy-2,3-pentanedionine
DPO	3,5-dimethylpyrazin-2-ol
dRNA-seq	differential RNA-sequencing
DTT	dithiothreitol
e.g.	*exempli gratia*
ECF	extracytoplasmic function σ factor
EDTA	ethylene diamine tetraacetic acid
ESR	envelope stress response
EtOH	ethanol
f.c.	final concentration
FDR	false discovery rate
fMet	N-formylmethionine
g	gravitational force equivalent
G	guanosine
GFP	green fluorescent protein
GO	gene ontology
h	hour
HCD	high cell density
IGR	intergenic region
Kan	kanamycin
kb	kilobase-pairs
LB	lysogeny broth
LCD	low cell density
LNA	locked nucleic acid
$\log_2$	binary logarithm
LPS	lipopolysaccharide
M	marker
M.U.	miller units
MGO	methylglyoxal
min	minute
mRNA	messenger RNA
n	number

N	any nucleotide
nt	nucleotide
n.a.	not available
OD_{600}	optical density at 600 nanometer
OMP	outer membrane (β-barrel) protein
ONPG	O-nitrophenyl-ß-D-galactopyranoside
PBP	penicillin binding protein
PBS	phosphate buffered saline
PCR	polymerase chain reaction
PenG	penicillin G
PG	peptidoglycan
qRT-PCR	quantitative real-time PCR
QS	quorum sensing
R	purine nucleotide
RBS	ribosome binding site
Rcs	regulator of capsule synthesis
RIP-seq	RNA immunoprecipitation followed by high-throughput sequencing
RNA	ribonucleic acid
RNAP	RNA polymerase
RNAPα	alpha subunit of RNA polymerase
RNase	ribonuclease
rpm	revolutions per minute
rRNA	ribosomal RNA
SAM	(S)-adenosylmethionine
SD	standard deviation or Shine-Dalgarno
SDS-PAGE	sodium dodecyl sulfate polyacrylamide gel electrophoresis
SE	standard error
s(ec)	second
sfGFP	superfolder GFP
sRNA	small regulatory RNA
T	tyrosine
TCP	toxin-co-regulated pilus
TCS	two-component system

TIR	translation initiation region
Tris-HCl	tris(hydroxymethyl)aminomethane-hydrochloride
tRNA	transfer RNA
TSS	transcriptional start site
U	uridine, unit
UTR	untranslated region
VPS	*Vibrio* polysaccharide
W	watt
WT	wild-type
X-gal	5-bromo-4-chloro-3-indolyl-β-D-galactopyranoside

List of Publications

Included in this thesis:

Chapter 2:

Herzog R, Peschek N, Fröhlich KS, Schumacher K, Papenfort K. Three autoinducer molecules act in concert to control virulence gene expression in *Vibrio cholerae*. **Nucleic Acids Res.** 2019;47(6):3171-3183. doi:10.1093/nar/gky1320

Chapter 3:

Herzog R*, Peschek N*, Singh PK, Fröhlich KS, Schröger L, Meyer F, Bramkamp M, Drescher K, Papenfort K. RNA-mediated control of cell shape modulates antibiotic resistance in *Vibrio cholerae*. **Manuscript**

*these authors contributed equally to the work

Chapter 4:

Peschek N, Hoyos M, Herzog R, Förstner KU, Papenfort K. A conserved RNA seed-pairing domain directs small RNA-mediated stress resistance in enterobacteria. **EMBO J.** 2019;38(16). doi:10.15252/embj.2019101650

Not included in this thesis:

Herzog R, Papenfort K. Transcriptomic Approaches for Studying Quorum Sensing in *Vibrio cholerae*. **Methods Enzymol.** 2018;612:303-342. doi:10.1016/bs.mie.2018.09.008

Declaration of contributions

Chapter 2:

RH and KP initiated and designed the study. RH generated the majority of strains and plasmids. MD generated most of the transcriptional reporter plasmids used in Fig. 4C. RH performed all experiments except the ribosome-profiling analyses of Fig. S3, which were conducted by KFS. KS assisted RH with experiments and strain construction. NP initially identified *aphA* as a target of VqmR, and RH and NP analyzed the RNA-sequencing data (Table 1, Fig. 6, Table S1, Fig. S7). RH constructed the figures, and RH and KP wrote the manuscript.

_____   _____

Roman Herzog   Prof. Dr. Kai Papenfort

Chapter 3:

NP and KP initiated and NP, RH, and KP conceptualized the study. RH performed all phase-contrast microscopy experiments (Fig. 1A, Fig 4B, C, Fig. S4). RH generated the alignment of the *vadR* gene among *Vibrios* in Fig. 1B. NP characterized the gene expression of *vadR* on Northern blots (Fig. 1C). KSF performed structure probing experiments (Figs. S1A; B), and RH tested the half-life of VadR in the presence or absence of *hfq* (Fig. S1C). NP performed the genetic screen to identify the transcription factor driving *vadR* expression (Fig. S1E), and RH and NP performed validation experiments (Fig. 1D, Figs. S1D, F). RH reanalyzed publicly available ChIP-seq dataset for HIS-tagged VxrB (Fig. S1G), and RH and LS characterized putative transcription factor binding sites in the *vadR* promoter region (Fig. S1H). NP identified VadR targets using RNA-seq (Figs. 2A-C, Table S1), validated the results using qRT-PCRs (Fig. S2A), and NP and LS validated base-pairing of VadR and targets using a GFP-based reporter system (Fig. 3, Fig. S3A). LS and NP validated the expression of VadR mutants using Northern blot analyses (Fig. S3B). RH performed Western blot analyses of the biofilm-related protein RbmA (Fig. S2B). RH and NP analyzed CrvA protein levels using Western blots (Fig. 4A). RH investigated the effect of penicillin G on *vadR* expression (Figs. 5A, B), and NP tested the effect of A-22 on the promoter activity of *vadR* (Fig. S5A). NP performed experiments to test the effects of penicillin G treatment in *vadR* and *crvA* mutants on cell survival (Fig. 5C, Fig. S5D). RH tested *crvA* mRNA levels in *vadR* and *crvA* mutants (Fig. S5C), and the effect of *crvA* overexpression on cell survival after PenG treatment (Fig. S5B). PKS designed and performed experiments to characterize the effects of VadR on biofilm formation (Figs. 2D-I, Figs. 6A-C). FM set up the microscopy analysis pipeline to test for cell curvature and other cell shape parameters. NP and RH performed statistical analyses and created the figures. KP wrote the manuscript with the help of all authors. NP was assisted by the research students: Elena Evertz and Alexandra Eklund.

We hereby confirm the above statements:

_____   _____

Roman Herzog   Nikolai Peschek

_____

Prof. Dr. Kai Papenfort

Chapter 4:

NP and KP initiated and conceptualized the study. KUF contributed by analyzing the transcriptional start sites identified in [1] for sigma factor binding motifs. NP constructed the majority of plasmids and strains and performed the majority of experiments and data analyses (Figs. 1- 3, Figs. 4A; B; D, Fig 5A, Fig. 6D, Fig. 7, Figs. EV1A-C; E, Fig. EV2, Fig. EV4D, Appendix Fig. S1B; C, Appendix Fig. S2, Appendix Fig. S3). RH measured the *micV* promoter activities in *E. coli* and monitored the composition of OMPs in *V. cholerae* and *E. coli* cells carrying sRNA overexpression plasmids (Fig. 4C, Fig. EV1F, Fig. Appendix Fig. S1A). MH constructed and validated the synthetic sRNA library, MH and NP performed the selection experiments and analyzed the resulting sequencing data (MH: Figs. 5B; C, Figs. EV4A; B; C; Figs. EV5A; B, MH and NP: Fig. EV3, Figs. EV5A; B). NP and MH identified and validated OmpA as the key target for ethanol resistance (NP: Fig. 6D, Figs. EV5C; D; E, MD: Fig. 6C, Fig. EV4A, NP and MH: Figs. 6A; B). NP constructed the figures, KP, NP, MH, and RH wrote the manuscript. NP was assisted by the research students: RH and Raphaela Götz.

_____   _____

Roman Herzog   Prof. Dr. Kai Papenfort

Summary

Small RNAs (sRNAs) are central regulators of post-transcriptional gene expression in bacteria. In the major human pathogen *Vibrio cholerae*, > 100 sRNA candidates have recently been identified. However, little is known about their biological functions. In this work, the mRNA target spectra of four sRNAs of *V. cholerae*, namely VqmR, VadR, MicV, and VrrA were defined and validated using a combination of RNA-sequencing and biochemical methods. Moreover, transcriptional activators of *vadR* and *micV* were identified, and the role of all three sRNAs was investigated in the context of diverse phenotypes.

Virulence factor production and biofilm formation are two key processes for the pathogenicity of *V. cholerae*. Both are controlled by bacterial communication systems referred to as quorum sensing (QS), which is based on small signaling molecules called autoinducers (AI). DPO is the latest discovered AI in *V. cholerae* and an activating ligand of the transcription factor VqmA. In a bound state, VqmA drives the expression of the VqmR sRNA, which was previously described as a repressor of biofilm formation. The present work revealed that VqmR also controls the production of virulence factors in *V. cholerae* by inhibiting the synthesis of the QS master regulator AphA. Specifically, VqmR uses a third base-pairing site located in the single-stranded region of its Rho-independent terminator loop to block the ribosome binding site of *aphA*. The two other known AIs of *V. cholerae*, CAI-1 and AI-2, also regulate *aphA* expression by a shared signal transduction pathway. Global transcriptome analyses were performed to study the effect of each of the AIs, i.e., CAI-1, AI-2, or DPO, as well as all possible AI combinations on the production of virulence factors and other important QS-controlled phenotypes.

A characteristic phenotype of many *Vibrios* is their curved rod morphology. Recently, the periplasmic polymer CrvA was identified as the first structural determinant of cell curvature in *V. cholerae*. However, the regulation of *crvA* remained poorly understood. In this work, the VadR sRNA was shown to be a direct regulator of *crvA*, and thus, cell curvature. In a genetic screen, the response regulator of the VxrAB two-component system (TCS) was identified as the transcriptional regulator of *vadR*. VxrAB is activated under cell wall damaging conditions and promotes the synthesis of new peptidoglycan to restore cell envelope homeostasis. The data presented here demonstrate that VadR also plays a central role in the cell envelope stress response by regulating *crvA* mRNA levels. Further, the majority of the mRNA targets of VadR are biofilm-related, and VadR overexpression strongly inhibited the process of biofilm formation in *V. cholerae*.

Another crucial component of the cell envelope stress response in *V. cholerae* is the alternative sigma factor σ^E, which is encoded on the *rpoE* gene and activated in the presence of misfolded outer membrane β-barrel proteins (OMPs) in the periplasm. The sigma factor σ^E associates with RNA polymerase and functions by default as a strict activator of gene expression. In *V. cholerae*, the σ^E response includes the induction of the VrrA sRNA to downregulate detrimental transcripts during cell envelope stress conditions. This work identified MicV as a second σ^E-dependent sRNA. MicV and VrrA both repress a shared and a specific set of mRNA targets, thereby forming the repressive arm of the σ^E response. Shared targets, e.g., *ompA* and *ompT*, are regulated by an almost identical seed sequence present in both sRNAs. A highly similar sequence also exists in the seed region of the σ^E-dependent RybB sRNA from *E. coli* providing evidence for a conserved base-pairing domain. Overexpression of MicV, VrrA, or RybB, in either *V. cholerae* or *E. coli*, resulted in reduced OMP levels. Further, the overexpression of either of these three sRNAs in a *V. cholerae rpoE* deletion mutant strongly suppressed its sensitivity towards ethanol. In a laboratory selection experiment, using a randomized sRNA library and ethanol to induce the σ^E response, the sequence matching the putative base-pairing domain of MicV, VrrA, and RybB, was strongly enriched. The most abundant sRNA variants obtained from the selection experiment all repressed the synthesis of OmpA, which was further characterized as the key factor for ethanol resistance in *V. cholerae*.

Zusammenfassung

Kleine RNAs (sRNAs) sind zentrale Regulatoren der post-transkriptionellen Genexpression in Bakterien. In dem bedeutenden humanpathogenen Bakterium *Vibrio cholerae* wurden vor Kurzem > 100 sRNA-Kandidaten identifiziert. Allerdings ist nur wenig über ihre biologische Funktion bekannt. In dieser Arbeit wurden die mRNA-Zielspektren von vier sRNAs von *V. cholerae*, nämlich VqmR, VadR, MicV und VrrA unter Verwendung einer Kombination aus RNA-Sequenzierung und biochemischen Methoden definiert und validiert. Darüber hinaus wurden die Transkriptionsaktivatoren von *vadR* und *micV* identifiziert und die Rolle aller drei sRNAs im Kontext verschiedener Phänotypen untersucht.

Die Produktion von Virulenzfaktoren und die Bildung von Biofilmen sind zwei Schlüsselprozesse für die Pathogenität von *V. cholerae*. Beide werden von einem bakteriellen Kommunikationssystem gesteuert, das als Quorum Sensing (QS) bezeichnet wird und auf kleinen Signalmolekülen basiert, die als Autoinduktoren (AI) bezeichnet werden. DPO ist der zuletzt entdeckte AI in *V. cholerae* und ein aktivierender Ligand des Transkriptionsfaktors VqmA. Mit gebundenem DPO-Liganden steuert VqmA die Expression der VqmR sRNA, die zuvor als Repressor der Biofilmbildung beschrieben wurde. Die vorliegende Arbeit zeigt, dass VqmR auch die Produktion von Virulenzfaktoren in *V. cholerae* steuert, indem es die Synthese des QS-Hauptregulators AphA hemmt. Dazu verwendet VqmR eine dritte Basenpaarungsstelle, die sich in der einzelsträngigen Region des Rho-unabhängigen Terminators befindet, um die Ribosomenbindungsstelle von *aphA* zu blockieren. Die beiden anderen bekannten AI von *V. cholerae*, CAI-1 und AI-2, regulieren ebenfalls die Expression von *aphA* über einen gemeinsamen Signaltransduktionsweg. Globale Transkriptomanalysen wurden durchgeführt, um die Wirkung jedes AI, also von CAI-1, AI-2 oder DPO, sowie aller möglichen Kombinationen von AI auf die Produktion von Virulenzfaktoren und anderen wichtigen QS-kontrollierten Phänotypen zu untersuchen.

Ein charakteristischer Phänotyp vieler Vibrionen ist ihre gekrümmte, stäbchenförmige Morphologie. Kürzlich wurde das periplasmatische Polymer CrvA als erste strukturelle Determinante der Zellkrümmung von *V. cholerae* identifiziert. Es blieb jedoch ungeklärt, wie *crvA* reguliert wird. In dieser Arbeit wurde gezeigt, dass die VadR sRNA ein direkter Regulator von *crvA* ist und damit auch einen indirekten Effekt auf die Zellkrümmung hat. In einem genetischen Screen wurde der Antwortregulator des VxrAB-Zweikomponentensystems (TCS) als Transkriptionsregulator von *vadR* identifiziert. VxrAB wird unter zellwandschädigenden

Bedingungen aktiviert und fördert die Synthese von neuem Peptidoglycan, um die Homöostase der Zellhülle wiederherzustellen. Die hier präsentierten Daten zeigen, dass VadR auch eine zentrale Rolle bei der Zellhüllen-Stressreaktion spielt, indem es die *crvA* mRNA reguliert. Des Weiteren ist die Mehrheit der Ziel-mRNAs von VadR biofilmbezogen, und die Überexpression von VadR inhibierte den Prozess der Biofilmbildung in *V. cholerae* deutlich.

Eine weitere entscheidende Komponente der Zellhüllen-Stressreaktion von *V. cholerae* ist der alternative Sigma-Faktor σ^E, der vom *rpoE*-Gen codiert und in Gegenwart von fehlgefalteten β-Fass-Proteinen der äußeren Membran (OMPs) im Periplasma aktiviert wird. Der Sigma-Faktor σ^E bindet die RNA-Polymerase und fungiert unausweichlich als strikter Aktivator der Genexpression. Die σ^E-Antwort von *V. cholerae* umfasst die Induktion der VrrA sRNA, um die Anzahl an schädlichen Transkripten während Zellhüllstresses zu reduzieren. Diese Arbeit identifizierte MicV als eine zweite σ^E-abhängige sRNA. MicV und VrrA unterdrücken beide einen gemeinsamen und einen spezifischen Satz von Ziel-mRNAs und bilden so den repressiven Arm der σ^E-Antwort. Gemeinsame Zieltranskripte, wie z. B. *ompA* und *ompT*, werden durch eine nahezu identische „Seed"-Sequenz reguliert, die in beiden sRNAs vorhanden ist. Eine sehr ähnliche Sequenz existiert auch in der „Seed"-Region der σ^E-abhängigen RybB sRNA in *E. coli*, was auf eine konservierte Basenpaarungsdomäne hindeutet. Die Überexpression von MicV, VrrA oder RybB in *V. cholerae* oder *E. coli* führte zur verringerten Anzahl an OMP Proteinen. Außerdem verringerte die Überexpression jeder der drei sRNAs die Empfindlichkeit einer *V. cholerae rpoE*-Deletionsmutante gegenüber Ethanol deutlich. In einem Labor-Selektionsexperiment war, unter Einsatz einer randomisierten sRNA-Bibliothek sowie von Ethanol zur Induktion der σ^E-Antwort, die Sequenz, die mit der mutmaßlichen Basenpaarungsdomäne von MicV, VrrA und RybB übereinstimmt, stark angereichert. Die am häufigsten vorkommenden sRNA-Varianten, die sich aus dem Selektionsexperiment ergaben, unterdrückten alle die Synthese von OmpA, das im weiteren Verlauf der Studie als Schlüsselfaktor für die Ethanolresistenz von *V. cholerae* charakterisiert wurde.

1 Introduction

1.1 Post-transcriptional gene regulation in γ-proteobacteria

Bacteria occupy the most diverse ecological niches and their overall global abundance is estimated to be in the range of 10^{29} to 10^{31} cells [2]. A key feature of their evolutionary success is their ability to adapt to ever-changing environmental conditions, which requires gene regulatory mechanisms.

For decades these regulatory functions were assumed to be almost exclusively executed by transcription factors at the DNA level. Following the "Central Dogma of Molecular Biology" (Figure 1, green box), transcription factors recruit RNA polymerase to specific promoter regions on the chromosome to initiate transcription of a subset of genes. Ribosomes translate the resulting messenger RNAs (mRNA) into proteins, which then fulfill designated enzymatic, regulatory, or structural functions. Interestingly, mRNAs constitute only ≈ 4-5 % of the total bacterial RNA pool, consisting predominantly of untranslated, a.k.a. non-coding, RNA [3]. Ribosomal RNA (rRNA) and transfer RNAs (tRNA) are the most abundant RNA species in bacteria (≈ 80 % and ≈ 15 % of total RNA, respectively), and they are essential to translate genetic information from mRNAs into proteins (Figure 1).
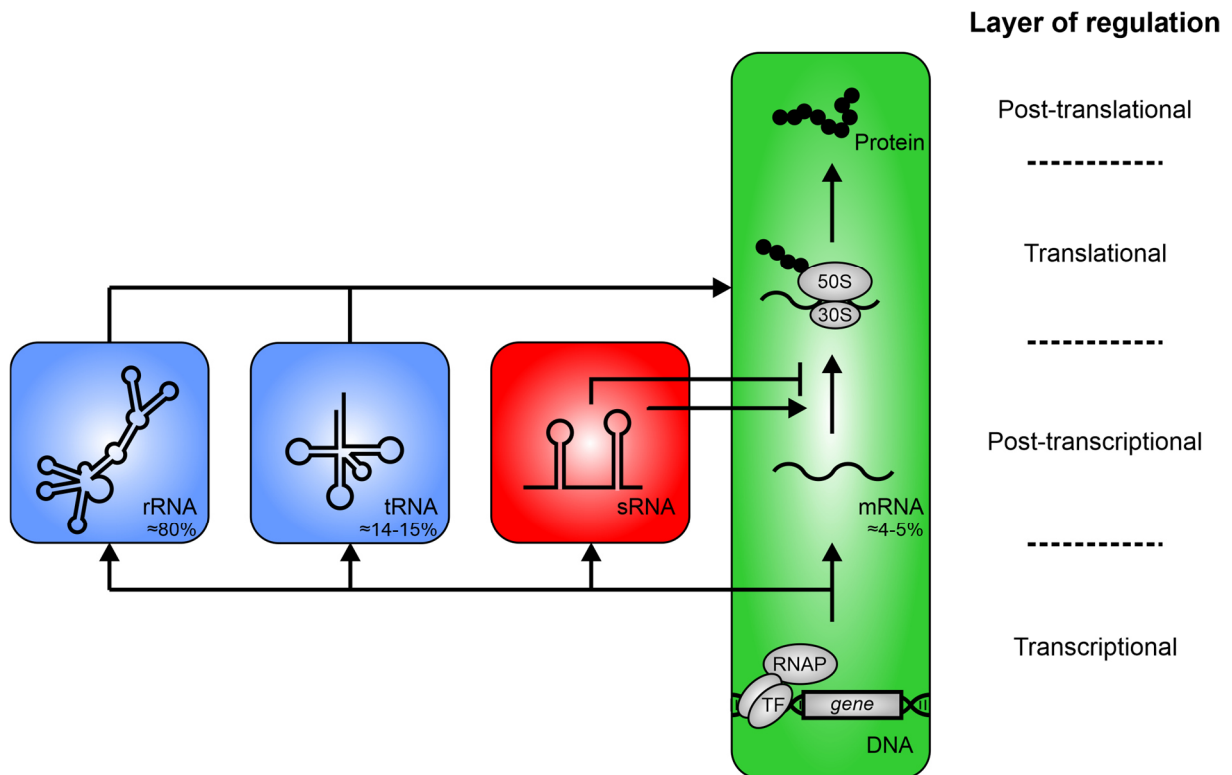

Figure 1 Four major RNA classes are involved in bacterial protein biosynthesis. TF: transcription factor; RNAP: RNA polymerase. Percentages indicate the abundance of a specific RNA species relative to the total bacterial RNA pool according to [3].

Besides executing housekeeping and protein-coding functions, RNA molecules can also act as post-transcriptional regulators of gene expression. In some cases, the mRNA itself contains a regulatory element that controls its translation. These *cis*-acting regulatory elements are primarily located in the 5' untranslated region (UTR) of an mRNA, where they form stable secondary structures to govern ribosome accessibility or transcript stability. They fold or unfold in response to temperature changes or the presence of ligands and are called RNA thermometers and riboswitches, respectively [4], [5]. However, most post-transcriptionally controlled mRNAs are targeted by base-pairing RNAs, which are referred to as small regulatory RNAs (sRNAs). sRNAs can be categorized based on the chromosomal origin of the sRNA and its target. *Cis*-sRNAs are transcribed in the antisense direction of their targets and thus, by default, show perfect sequence complementary to them. In contrast, *trans*-acting sRNAs and their targets are encoded at different loci on the chromosome.

Trans-encoded sRNAs dominate post-transcriptional gene regulation in bacteria. They typically control large sets of mRNAs by imperfect complementary base-pairing [6] and can even compete with transcription factors in terms of numbers and regulatory scope [7]. A prototypic *trans*-encoded sRNA, i) is expressed from a free-standing gene, ii) varies between 50-400 nts in length, iii) harbors a Rho-independent terminator, and iv) requires chaperone activity to base-pair with its targets [8], [9]. Indeed, all sRNAs investigated in this work match these "classic" criteria. However, recent results from global transcriptomic analyses challenge the universal validity of these prototypic features. For instance, 3' UTRs contain an unexpected plethora of sRNAs, which are either transcribed from internal promoters or generated by endonucleolytic cleavage of a primary RNA [1], [10], [11]. Further, the extent and necessity of RNA chaperone activities seem to differ drastically between various bacteria [12]. One prime example is the RNA chaperone Hfq, which is indispensable for most *trans*-encoded sRNA functions in *E. coli*, *Salmonella*, and *Vibrio*, and disruption of *hfq* causes pleiotropic phenotypes [13]–[15]. In contrast, many sRNAs of Gram-positive bacteria, such as *Staphylococcus aureus* or *Bacillus subtilis*, do not require Hfq to efficiently regulate their targets [16], [17].

1.1.1 The RNA chaperone Hfq

Hfq belongs to the Sm/LSm protein family and was discovered as "Host factor for bacteriophage Qβ" in *E. coli* [18]. However, it is now primarily recognized as a global sRNA-mRNA matchmaker protein. Hfq is a ring-shaped homohexamer [19], [20] that contains at least three distinct RNA contact surfaces: the proximal face, the distal face, and the lateral rim [21]. In γ-proteobacteria,

the proximal face displays a strong affinity towards single-stranded U-rich regions in the Rho-independent terminator of sRNAs [19], [22]–[24]. The distal face recognizes (AAN) triplets (N = any nucleotide), which are often located 5' to the sRNA binding-site on an mRNA [20], [25] or in distinct sRNAs [21]. The outer rim of Hfq presents clusters of arginine and lysine residues, which are crucial for Hfq's chaperone activity since they stabilize the RNA substrates [26]–[28]. Additionally, the proximal side of the rim binds single-stranded A/U-rich motifs [22], [29]. The N-terminus of Hfq is exposed on the proximal face of the protein and highly conserved [19]. In contrast, the C-terminal domain (CTD) varies drastically in sequence and length and often carries an acidic tip [30]–[32].

As a matchmaker chaperone, Hfq catalyzes the formation of RNA-RNA duplexes [33]. Many sRNAs utilize a conserved sequence, a.k.a. the "seed"-sequence, to efficiently recognize their antisense mRNA target sites [34], [35]. Hfq alters the secondary structure of bound RNAs to promote base-pairing between the "seed"-sequence and its mRNA target in proximity to the arginine/lysine patches of the lateral rim [36], [37]. The stabilization of this RNA-RNA helix initiation complex by Hfq is key for the subsequent annealing elongation ("zipping") of the two RNAs [38]. Finally, the sRNA-mRNA duplex is released from the chaperone.

How RNA-RNA duplexes are liberated from Hfq is not fully understood. Although *in vivo* experiments highlighted the rapid turnover of target mRNAs by Hfq-binding sRNAs within minutes, Hfq-RNA complexes are extremely stable *in vitro* with half-lives in the range of hours [39], [40]. Given this kinetic discrepancy and the fact that the intracellular number of Hfq-binding RNAs exceeds the approximately 400 – 10,000 copies of hexameric Hfq per cell, two assumptions can be made [41]–[44]. First, RNA continuously occupies every Hfq molecule in the cell, and second, an active mechanism to liberate Hfq from RNA and RNA-RNA complexes is required.

One proposed mechanism involves the CTD of Hfq. According to this model, the acidic tip of the CTD competes with RNAs for binding to the basic residues of the outer rim, thus continually "sweeping" weak Hfq binders and RNA-RNA duplexes [45], [46]. Indeed, a recently resolved X-ray crystal structure of *Caulobacter crescentus* Hfq confirmed the interaction between the CTD and the basic patches of the lateral rim [32]. However, this model can not explain how Hfq homologs that lack a CTD release RNA or RNA-RNA duplexes [30], [31]. Additionally, earlier studies demonstrated that C-terminally truncated *E. coli* Hfq proteins were still able to fulfill their riboregulatory functions, indicating that the CTD is not solely responsible for RNA release from Hfq [31], [47].

A second model suggests that sRNAs "actively cycle" on Hfq [33]. More precisely, several sRNAs interact with the proximal face of Hfq simultaneously, and thereby, reciprocally affect their dissociation rates. Thus, increasing concentrations of an sRNA drastically accelerate its chance to outcompete other RNA species at the proximal face of Hfq and to regulate its target mRNAs. Indeed, *in vitro* and *in vivo* RNA-competition experiments for Hfq-binding support this model [40], [48].

Besides its role as an sRNA-mRNA matchmaker protein, Hfq executes versatile post-transcriptional functions. For instance, it protects bound sRNAs against nucleolytic decay through Ribonucleases II and III (RNase II/III), or the RNA degradosome, a multiprotein complex consisting of Ribonuclease E (RNase E), Polynucleotide Phosphorylase (PNPase), RNA helicase B (RhlB), and enolase [49], [50]. On the other hand, Hfq was repeatedly co-purified with PNPase and RNase E [51], [52]. Indeed, the regulatory functions of many sRNAs require Hfq-mediated recruitment of the degradosome, causing mRNA or coupled sRNA/mRNA decay [9], [51].

1.1.2   Gene-regulatory mechanisms of *trans*-encoded base-pairing sRNAs

sRNAs activate or inhibit the translation of a target mRNA by altering its accessibility towards ribosomes, its stability, or, as in most cases, both. In this respect, sRNAs can act either directly through base-pairing with the target sequence or indirectly through sequestration or modification of another regulator. All sRNAs investigated in this work function as direct, *trans*-encoded, and base-pairing regulators in *V. cholerae.* However, mechanistic studies of sRNAs were predominantly conducted in *E. coli* or *Salmonella*. Consequently, this section focuses on gene-regulatory mechanisms that were reported for direct, *trans*-encoded, and base-pairing sRNAs in *E. coli*, *Salmonella*, or *Vibrio* species.

The majority of studied sRNAs are negative regulators that bind within the translation initiation region (TIR) of their target mRNAs, most often covering the Shine-Dalgarno (SD) or start-codon sequence [9]. MicF, the first described *trans*-acting sRNA, is one of many examples that employ this mechanism to regulate their targets. More precisely, MicF sequesters the RBS and the start-codon sequence of *ompF* in *E. coli*. As a consequence, this mRNA becomes inaccessible for the ribosomal 30S subunit, and thus, translation is prevented [53] (Figure 2A).

Translation can be inhibited even when the sRNA base-pairing site does not overlap with the TIR. For instance, the GcvB sRNA in *Salmonella* represses *gltI* mRNA expression by annealing to a translational enhancer element upstream of its RBS (Figure 2B) [54], [55]. Likewise, the SgrS sRNA

sequesters a translational enhancer element in the *manY* 5' UTR in *E. coli* and *Salmonella*. This interaction renders the enhancer element inaccessible for binding of the small ribosomal subunit protein S1 and thus prevents translation initiation [56]. The *E. coli* sRNAs IstR, RyhB, and Spot42 also base-pair upstream of the RBS of their target genes to inhibit translation. IstR occupies a ribosome standby site in the *tisAB* messenger. Without 30S binding to this site, the highly structured mRNA remains untranslated [57]. The RyhB sRNA inhibits *fur* synthesis by repressing the synthesis of a translationally coupled leader peptide upstream of the *fur* TIR [58]. Spot42 binds a sequence upstream of the TIR of its target mRNA, *sdhCDAB*, and still prevents ribosome binding. Here, the sRNA functions as a guide RNA to recruit the Hfq chaperone towards the RBS, where it acts as a steric repressor of 30S attachment (Figure 2C) [59].

Translation inhibition of a target mRNA is most often associated with mRNA destabilization. In the absence of bound ribosomes, the transcript remains unprotected against exo- or endonucleolytic decay. Hfq-binding sRNAs can further accelerate the degradation of unprotected mRNAs since Hfq can recruit the major endoribonuclease RNase E (chapter 1.1.1). Thus, the majority of sRNAs that block translation of an mRNA additionally alter its stability as a secondary effect. The question of whether translation inhibition or the subsequent target degradation leads to a more significant impact on gene silencing was investigated for the SgrS/*ptsG* and RyhB/*sodB* interactions in *E. coli*. Both sRNAs eliminate the synthesis of their target mRNAs in two ways. First, they block the respective TIR through base-pairing, and second, they recruit RNase E, causing translation inhibition and sRNA-mRNA duplex degradation, respectively (Figure 2D) [60]. Interestingly, the use of a temperature-sensitive RNase E mutant demonstrated that RNase E does not contribute to either IICB^{Glc} (encoded by *ptsG*) or SodB reduction. However, RNase E is required for the irreversible degradation of the target mRNA and its sRNA regulator [61].

Some sRNAs do not prevent ribosome binding at all, neither directly nor indirectly, but still repress protein synthesis. The underlying mechanism was first characterized for the MicC sRNA in *Salmonella* and its regulated target, *ompD*. Structure probing revealed that MicC anneals to the *ompD* mRNA deep inside the coding sequence (CDS) (Figure 2E). Instead of blocking translation initiation, this interaction recruits RNase E, which rapidly degrades the transcript [62]. This "target degradation" mode of action is particularly surprising since the CDS is thought to be continuously protected by ribosomes. One explanation could be that weaker SD sequences lead to low ribosome assembly rates or that secondary structures block ribosome binding. As a consequence, parts of the mRNA remain "naked" and accessible for sRNA annealing [63].
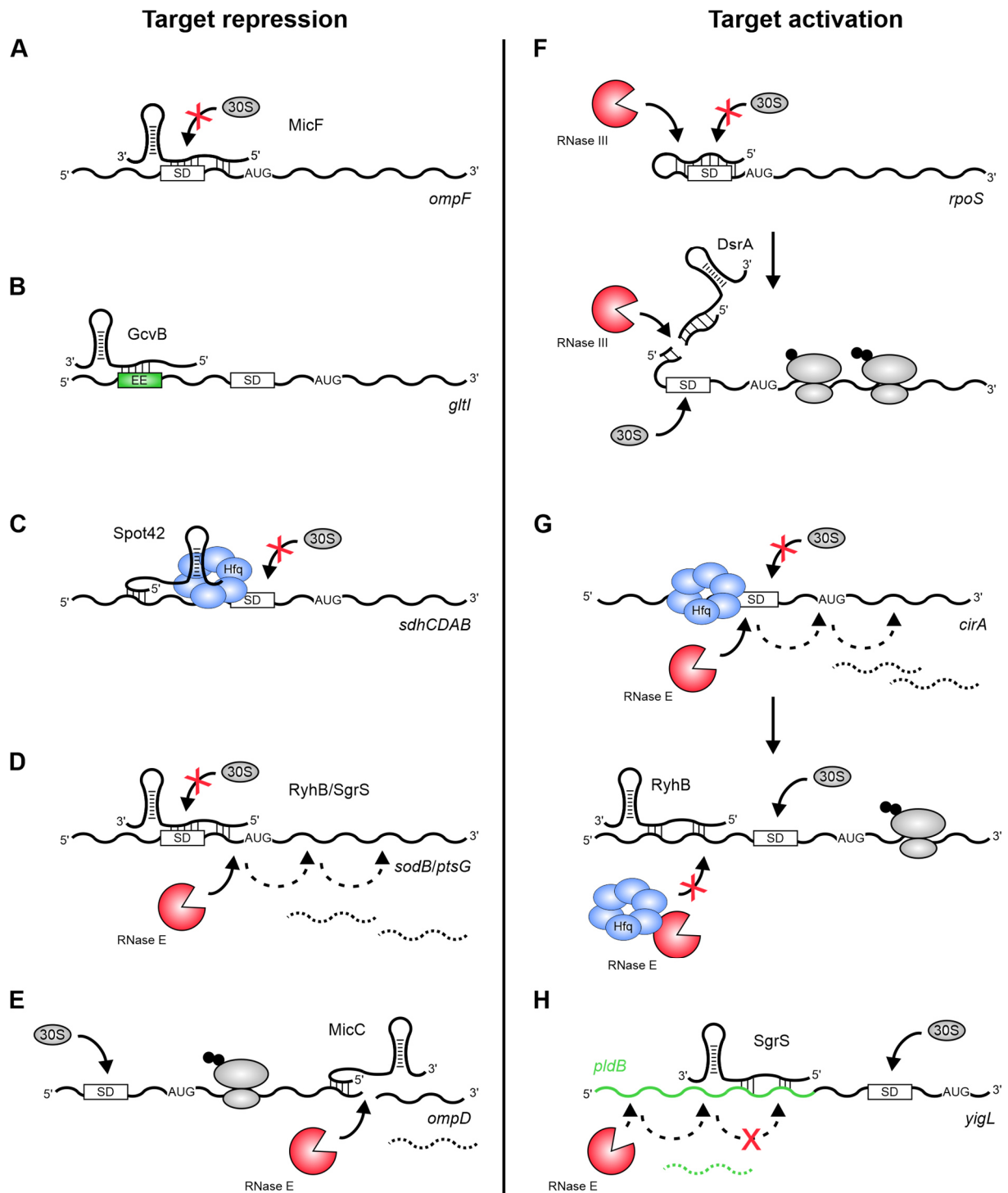
Figure 2 Regulatory mechanisms of base-pairing sRNAs that act in *trans*. A) – H) Detailed description of each mechanism in the main text. sRNAs and elements within the mRNA are not drawn to scale. SD: Shine-Dalgarno sequence; AUG: start codon; EE: enhancer element.

Albeit less frequently than negative regulation, sRNAs can promote target expression most commonly by a mechanism referred to as "anti-antisense" [64], [65]. A requirement for this mechanism is a secondary hairpin-structure in the 5' UTR of a target mRNA that prevents ribosome

binding and thus, translation initiation. Upon sRNA base-pairing with the 5' UTR, the hairpin unfolds, and the RBS becomes accessible for the 30S ribosomal subunit. This mode of action was initially discovered in *Staphylococcus aureus* for the RNAIII/*hla* interaction [66], however, multiple sRNAs in γ-proteobacteria regulate their targets in the same way. The most extensively studied example of a post-transcriptionally activated mRNA in *E. coli* is *rpoS*. Three independent sRNAs, DsrA, ArcZ, and RprA, activate *rpoS* translation under specific environmental conditions by an anti-antisense mechanism [67]. Interestingly, DsrA-mediated unfolding of the *rpoS* 5' UTR not only prevents an RNase III cleavage event that reduces translation initiation, but it also creates a new RNase III cleavage site within the DsrA/*rpoS* duplex, which stabilizes the *rpoS* transcript (Figure 2F)[68].

Contrary to the described negative regulation of *sdhCDAB* by Spot42 and Hfq (Figure 2C), sRNA base-pairing can also prevent Hfq-mediated target repression. For example, Hfq negatively regulates the translation and stability of the *cirA* mRNA in *E. coli*. RyhB base-pairs with the 5' UTR of *cirA*, upstream of the TIR. The RNA-duplex leads to a conformational change in the 5' UTR, which occludes Hfq binding sites and prevents RNase E-recruitment (Figure 2G). Thus, RyhB reduces translational inhibition and transcript destabilization [69].

sRNAs can also activate target mRNAs in a translation-independent manner. In *Salmonella*, the Hfq-binding SgrS sRNA positively regulates *yigL* expression, the second gene of the bicistronic *pldB-yigL* messenger. SgrS binds within the *pldB* sequence ≈ 200 nts upstream of the *yigL* start codon and does not affect *yigL* translation. However, this duplex masks an RNase E cleavage site, which prevents sustained 5' to 3' directional processing by RNase E (Figure 2H). Consequently, the stabilized '*pldB-yigL* fragment accumulates and YigL is expressed, while PldB is not [70], [71].

To summarize, sRNAs employ a variety of mechanisms to orchestrate global gene expression at the post-transcriptional level. Their ability to rapidly silence or activate target transcripts is crucial for bacterial fitness in fast-changing environments, and it is therefore not surprising that the majority of characterized sRNAs act as key players in various stress response systems [72]. The environment also contains valuable information about intra- and interspecies population densities. Bacteria perceive this information in the form of chemical signaling molecules and adapt their lifestyles accordingly. In *Vibrios*, this process of adaptation is orchestrated by multiple sRNAs that act in concert, which allows an optimal response to complex mixtures of environmental signals [73], [74].

1.2 The life-cycle of *Vibrio cholerae*

V. cholerae spends most of its life-cycle in an aquatic environment, where it attaches to diverse biotic and abiotic surfaces. Here, *V. cholerae* is frequently involved in microbial communities, called biofilms (chapter 1.4). The dense extracellular matrix of biofilms protects *V. cholerae* from protozoan grazing and attacks by bacteriophages [75], [76]. Further, biofilms enhance the infectivity upon oral ingestion by the human host compared to planktonic cells in two ways. First, they offer protection from the acidic environment of the stomach and thus, promote the successful transmission of *V. cholerae* into the small intestine [77]. Second, *V. cholerae* cells derived from biofilms express high levels of virulence factors, and this hyperinfective phenotype increases *V. cholerae*'s potential to colonize the small intestine [78], [79]. The pathogenicity of *V. cholerae* relies on two major virulence factors: the toxin co-regulated pilus (TCP), which facilitates the attachment to the intestinal epithelial cells, and the cholera toxin (CT) (chapter 1.3.3) [80]. The latter causes the uncontrolled efflux of ions and water from the epithelial cells into the gut lumen, which ultimately leads to the massive watery diarrhea known as cholera disease [81], [82]. During late stages of infection, *V. cholerae* detaches from the epithelial surface and is excreted via the stool, from where it eventually finds its way back into the aquatic environment [83].

1.3 Quorum sensing in *V. cholerae*

In its complex biphasic life-cycle, inside and outside the human host, *V. cholerae* critically depends on group behaviors like the formation of biofilms and the production of virulence factors. In order to act as a group, the individual cells have to communicate and synchronize gene expression, a process, which is commonly referred to as "quorum sensing" (QS). QS relies on the synthesis of small signaling molecules, a.k.a. autoinducers (AI), which are secreted into the environment and subsequently recognized by their cognate receptors [84]. AI concentrations in the environment correlate with bacterial cell densities. Consequently, AI recognition at low cell density (LCD) is a rare event, whereas, at high cell density (HCD), AIs are frequently bound to their receptors. Both receptor states lead to different global gene expression profiles, ultimately resulting in distinct group phenotypes [85].

1.3.1 Autoinducer molecules

V. cholerae uses at least three AI molecules to track intra- and interspecies population densities. One AI is (S)-3-hydroxytridecan-4-one, a.k.a. cholera autoinducer-1 (CAI-1) (Figure 3) [86]. CAI-1 is

synthesized by the enzyme CqsA, which combines the substrates (S)-adenosylmethionine (SAM) and decanoyl-coenzyme A [87], [88]. CqsA and thus, CAI-1, are produced under carbon source limited conditions, which primarily occur at high population densities [89], [90]. Of note, homologs of CqsA exist in many *Vibrio* species but only a few other genera, indicating that CAI-1 is utilized to track intragenus populations [91], [92].

In contrast, the autoinducer-2 (AI-2) serves as an interspecies communication signal since it is estimated to be produced and recognized by over 500 bacterial species [93]. Its synthase, LuxS, transforms the SAM cycle intermediate S-ribosylhomocysteine into 4,5-dihydroxy-2,3-pentanedionine (DPD) and homocysteine. DPD converts spontaneously into a thermodynamically favored ring-structure, which induces QS activity in *Salmonella* but not in *Vibrios* [94], [95]. In *Vibrios*, the additional incorporation of a boric atom is required to yield the functional AI-2 molecule (Figure 3) [96]–[98].
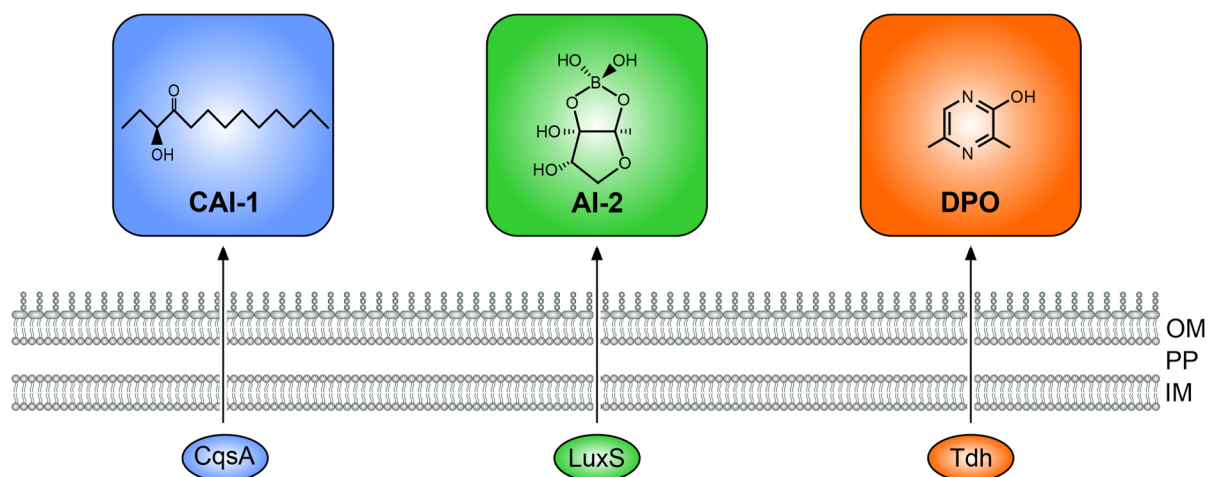

Figure 3 Identified AI molecules of *V. cholerae*. The enzymes CqsA, LuxS, and Tdh lead to the production of the three AI molecules CAI-1, AI-2, and DPO, respectively. The molecules are transported across the cell envelope either passively via diffusion or actively via unknown export mechanisms. OM: outer membrane; PP: periplasm; IM: inner membrane.

Recently, the molecule 3,5-dimethylpyrazin-2-ol (DPO) was identified as the third autoinducer in *V. cholerae* (Figure 3) [74]. DPO derives from the catalytic degradation of L-threonine through the enzyme threonine-dehydrogenase (Tdh). Tdh catalyzes the oxidation of L-threonine to 2-amino-3-ketobutyric acid (AKB), which decarboxylates to aminoacetone. Aminoacetone reacts with an activated form of L-alanine to the linear intermediate *N*-alanyl-aminoacetone. Upon intramolecular condensation, oxidation, and tautomerization of this intermediate, DPO is formed

[74]. The biological significance of DPO-signaling is not yet fully understood. On the one hand, the Tdh enzyme is ubiquitous and found in all domains of life, indicating that the use of DPO as a communication signal is widespread. Indeed, DPO accumulated in spent media of *E. coli* cultures [74]. On the other hand, homologs of the DPO receptor protein, VqmA, are only present among *Vibrios*, suggesting a role for DPO as an intragenus QS signal. Intriguingly, one DPO-binding VqmA homolog was discovered in the vibriophage VP882. Using its VqmA homolog, this phage eavesdrops on the DPO-mediated communication of *V. cholerae* and makes its lysis-lysogeny decision dependent on the surrounding concentration of DPO [99]. However, since this phage lacks *tdh* and thus, own DPO production, this interaction can be seen as one-sided exploitation of information rather than interspecies communication.

1.3.2 Recognition and integration of quorum sensing signals

The AIs CAI-1, AI-2, and DPO are recognized by their cognate receptors CqsS, LuxPQ, and VqmA, respectively (Figure 4) [74], [91], [100]–[103]. LuxP is a periplasmic binding protein that senses AI-2 and tightly associates with LuxQ [96], [101]. CqsS and LuxQ are integral inner membrane-bound signal transduction proteins with cytoplasmic histidine kinase domains [104]. Although both receptors, CqsS and LuxPQ, detect different ligands, they share the same signaling pathway [100].

In an unbound state at LCD, when AI concentrations are low, the histidine kinases of CqsS and LuxPQ are autophosphorylated. The phosphates are channeled to the shared phosphotransfer protein LuxU, which in turn activates the response regulator LuxO (Figure 4, left) [105]–[107]. LuxO-P recruits the alternative sigma factor σ^{54} (RpoN) to induce the transcription of the four homologous sRNAs Qrr1-4 [73], [108]. The Hfq-binding Qrrs reciprocally control the fate of the transcripts of the two QS master regulators, AphA and HapR. Specifically, they efficiently destabilize the *hapR* mRNA, and Qrr2-4 post-transcriptionally activate *aphA* translation [73], [109], [110]. Further, the Qrr-mediated down-regulation of *hapR* indirectly activates *aphA* on the transcriptional level since HapR represses *aphA* transcription. Thus, at LCD AphA is made, while HapR is not. The LCD master regulator AphA initiates pathogenic group behaviors since it acts on top of the virulence cascade (chapter 1.3.3) and promotes biofilm formation (chapter 1.4) by activating the transcription factor VpsT [111]–[113].

AI-binding converts the enzymatic activity of CqsS and LuxPQ from kinases to phosphatases [104], [114], [115]. As a consequence, the LuxU/O pathway remains inactive, and the Qrrs are no longer transcribed (Figure 4, right). Now, the master regulator at HCD, HapR, is made. HapR inhibits *aphA*

transcription and thus virulence factor production [116]. Further, HapR represses biofilm formation by blocking the expression of multiple biofilm components and regulators, including *vpsT*, and instead, induces motility [117]–[119].
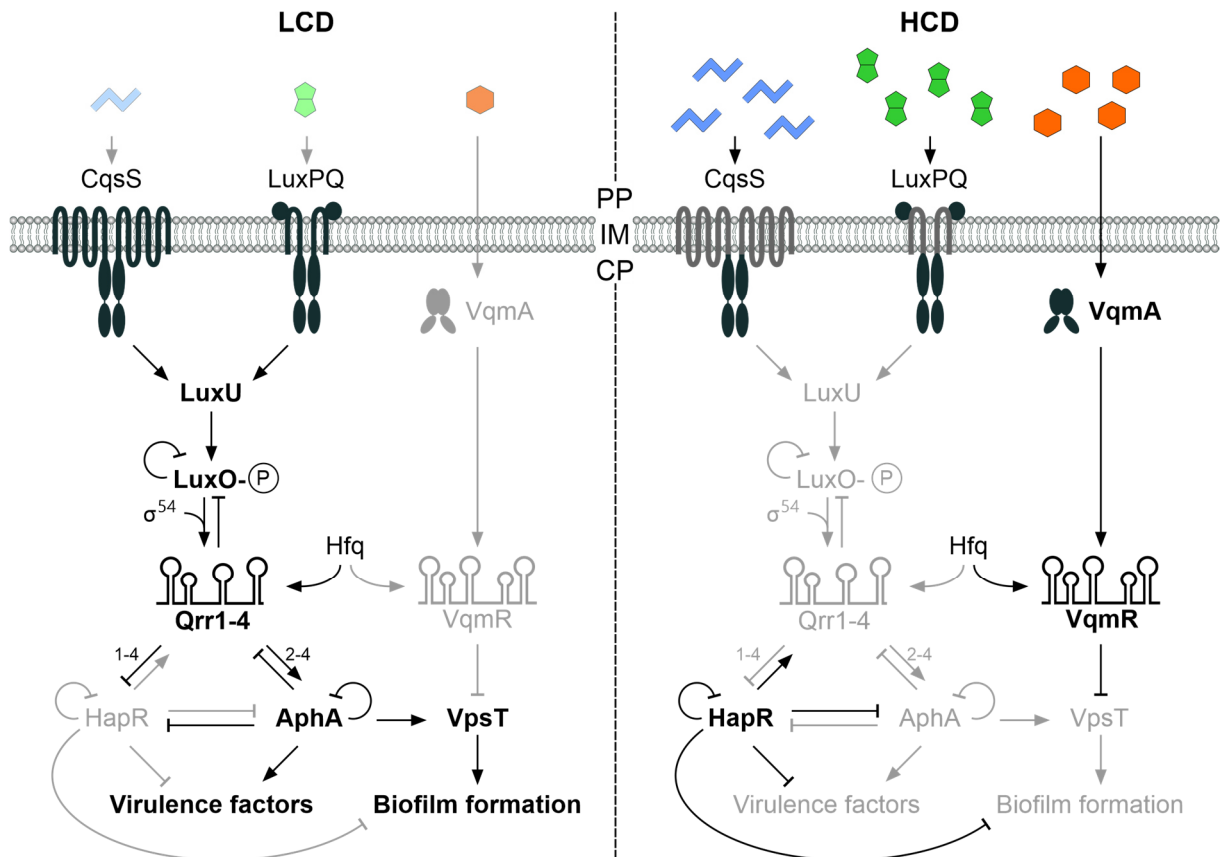

Figure 4 Overview of AI signaling in *V. cholerae*. Left: At low AI concentrations, the CqsS and LuxPQ receptors function as kinases and phosphorylate LuxU. LuxU transfers the phosphate group (P) to the regulator LuxO. In concert with σ54, LuxO drives the expression of the Qrr sRNAs. The Hfq-binding Qrrs destabilize the *hapR* mRNA and induce AphA synthesis. AphA promotes the production of virulence factors as well as biofilm formation by activating *vpsT* expression. Right: AIs accumulate at HCD. Upon AI-binding, the CAI-1 and AI-2 receptors function as phosphatases and thereby silence the pathway. HapR is produced and represses virulence factor production and biofilm formation by repressing *aphA*. DPO binds and activates its cytoplasmic receptor protein VqmA. The active complex induces VqmR expression. VqmR requires Hfq to repress *vpsT* translation and thus biofilm formation. AI molecules are depicted in the same color as in Figure 3. Feedback loops are explained in the main text. PP: periplasm; IM: inner membrane; CP: cytoplasm.

The CAI-1/AI-2 signal transduction pathway contains a multitude of additional feedback loops. For instance, each of the key regulators LuxO, AphA, and HapR negatively autoregulates its expression (Figure 4) [120]–[122]. These regulatory circuits stabilize the system as they minimize fluctuations within the pathway, and further, they prevent unhindered QS outputs [123]. The Qrr sRNAs are involved in two feedback loops that guarantee their fine-tuned expression. First, the Qrrs negatively regulate their expression by sequestering the mRNA of their activator, LuxO, causing a

"buffered" equilibrium of Qrr and *luxO* levels [120], [124]. Second, the Qrrs are indirectly upregulated by HapR, their primary target at LCD, which allows a rapid transition from HCD to LCD QS mode [125], [126]. Additionally, AphA and HapR function as reciprocal inhibitors and thus prevent HapR expression at LCD and AphA production at HCD, respectively (Figure 4) [109], [122].

DPO signal transduction is independent of LuxU/O and the Qrrs. In contrast to CqsS and LuxPQ, the DPO receptor protein, VqmA, is i) found in the cytoplasm and ii) a DNA-binding transcriptional regulator [1]. Extracellular DPO accumulates with increasing cell numbers in L-threonine-rich environments. Thus, DPO primarily binds and activates VqmA at HCD (Figure 4, right). The active DPO-VqmA complex induces the expression of the VqmR sRNA, which belongs to the large group of Hfq-binding sRNAs [1], [74], [102]. VqmR is a direct regulator of at least eight mRNAs, including *vpsT* [1]. Intriguingly, DPO-mediated activation of VqmR sufficiently represses *vpsT* and thus inhibits biofilm formation independent of the CAI-1/AI-2 signaling pathway [74].

1.3.3 AphA and the virulence cascade

The LCD master regulator AphA is key for virulence factor production in *V. cholerae,* and cells lacking *aphA* fail to colonize the small intestine in the infant mouse infection model [127]. AphA requires another transcriptional regulator, AphB, to activate the expression of the *tcpPH* operon (Figure 5) [112], [113], [127]. The TcpP protein integrates into the inner membrane and depends on the interaction with TcpH in the periplasm to escape proteolytic decay [128], [129]. To drive the expression of the next element in the virulence cascade, TcpPH associates with a second membrane protein complex, namely ToxRS [130], [131]. TcpP and ToxR recognize distinct binding sites in the promoter region of *toxT* and thereby activate gene expression [132]. ToxT is the direct activator of the two main virulence factors, the toxin co-regulated pilus (TCP) and the cholera toxin (CT), which are encoded on the *tcpA-F* and the *ctxAB* operons, respectively (Figure 5) [80], [133]. Of note, *ctxAB* is part of the genome of a chromosomally integrated filamentous phage called CTXɸ, which is present in all toxigenic *Vibrio* strains [81], [134]. The CT, consisting of one CtxA and five CtxB subunits (Figure 5), attaches to the GM_1 receptor on the surface of intestinal epithelial cells and is internalized via endocytosis [135], [136]. Inside the cell, CtxA is proteolytically cleaved and thereby activated. Next, it ADP-ribosylates the GTP-binding component of the adenylate cyclase, causing an increased cAMP production inside the host cell and, as a consequence, the massive secretion of ions and water into the intestinal lumen [136], [137]. If untreated, about 50 % of infected individuals die because of severe dehydration [138].
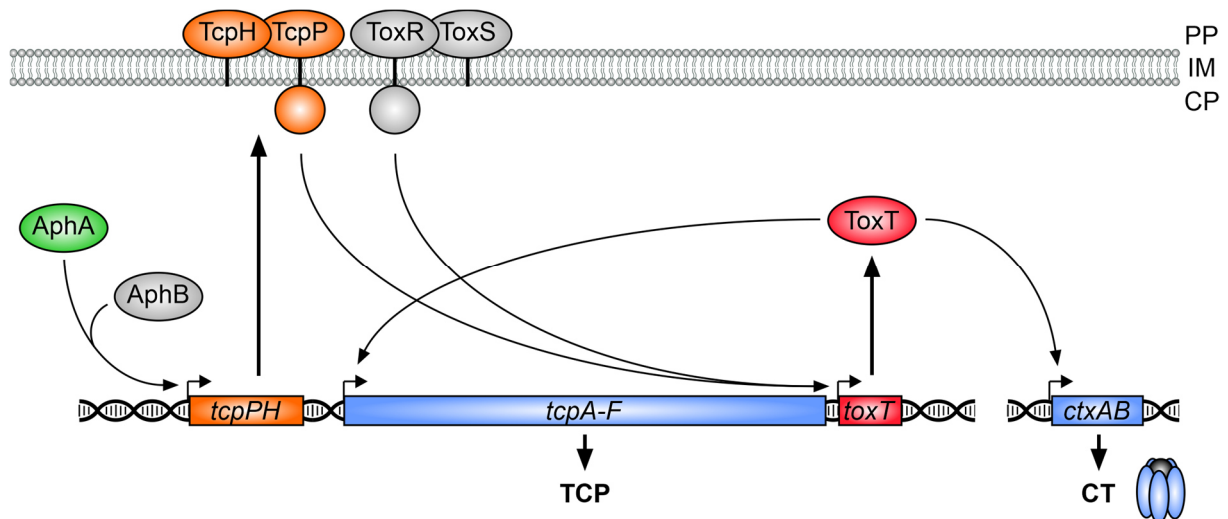
Figure 5 The virulence cascade of *V. cholerae*. AphA, in concert with AphB, activates the *tcpPH* operon. The encoded proteins assemble at the inner membrane to associate with the ToxRS complex. Together, TcpPH and ToxRS activate the *toxT* promoter. ToxT activates the two operons encoding the main virulence factors TCP and CT. CT consists of five CtxB subunits and one CtxA subunit, depicted in blue and grey, respectively.

1.4 Biofilm formation

At low AI levels, multiple factors induce the formation of biofilms in *V. cholerae*. Here, the AphA-mediated activation of VpsT plays a pivotal role. VpsT depends on its ligand, the second messenger molecule cyclic di-guanosine monophosphate (c-di-GMP), to become a functional regulator [139]. VpsT activates the master regulator of biofilm formation, VpsR, which in turn induces VpsT and AphA production [140], [141]. The regulons of VpsR and VpsT largely overlap and include the genes encoding the key components for biofilm formation: *Vibrio* polysaccharide (VPS) and the secreted biofilm matrix proteins RbmA, RbmC, and Bap1 [142].

The development of biofilms in *V. cholerae* is a multistep process. Initially, one *V. cholerae* cell uses its flagellum to swim and simultaneously specific type IV pili to attach to a surface [143], [144]. Once attached, the cell continuously secretes VPS, expressed from two VpsR/VpsT-controlled gene clusters [145]. Next, RbmA accumulates on the cell surface and facilitates cell-cell adhesion between the parental cell and its daughter cell after cell division [146]. At the interface of the two cells and the surrounding surface, the second matrix protein, Bap1, is secreted, enhancing cell-cell and cell-surface attachment [146]. The third major matrix protein, RbmC, is then secreted at distinct sites of the cells' surfaces. In growing biofilms, RbmC and Bap1 interact with the VPS to form a flexible and protective envelope [142], [146]. Besides polysaccharides and proteins, the biofilm matrix contains significant amounts of extracellular DNA (eDNA).

Interestingly, *V. cholerae* cells lacking the two secreted nucleases Dns and Xds produce thicker and less organized biofilms, supporting the substantial role of eDNA in the biofilm matrix and of nucleases in the formation of a characteristic biofilm architecture [147].

Flagella, pili, and matrix components are not the only factors that determine the success of biofilm formation. Recent studies suggest that the overall cell shape of a bacterium contributes to its ability to colonize surfaces and to the spatial architecture of a biofilm [148]–[150]. For example, a filamenting *V. cholerae* strain was shown to have a significant advantage in the early colonization of the natural substrate chitin when compared to non-filamentous *V. cholerae* cells [148]. Another study demonstrated that the curved vibrioid cell shape of *C. crescentus* is beneficial for biofilm formation since *C. crescentus* wild-type cells outcompeted straight mutant cells under constant flow. This observation was explained with the fact that under the tested conditions, curved cells experienced a decreased distance towards the surface when compared to straight cells, which accelerated initial attachments [150]. Intriguingly, different cell morphologies were also reported in single-species *V. cholerae* biofilms, which predominantly consisted of relatively straight cells [151]. So far, it is not clear whether this atypical straight cell phenotype derives solely from the physical forces inside a biofilm or whether *V. cholerae* actively modulates its cell shape during biofilm formation.

1.5 Cell shape

The cell shape of almost any given bacterium is defined by its cell wall structure, with *V. cholerae* being no exception [152], [153]. In Gram-negative bacteria like *V. cholerae*, the cell wall, a.k.a. the sacculus, forms a stable mesh in the periplasm, sandwiched between the inner and the outer membrane. It consists of peptidoglycan (PG), which is composed of glycan strands cross-linked by short peptide sidechains. The process of PG synthesis can be divided into three steps. First, a disaccharide-pentapeptide precursor molecule is synthesized in the cytoplasm and coordinated to the inner membrane. Next, the precursor is "flipped" across the inner membrane into the periplasm. In the last step, so-called Penicillin Binding Proteins (PBP), a group of proteins targeted by β-lactam antibiotics such as penicillin, insert the translocated monomer into the polymeric sacculus [154]. To achieve a specific shape, a bacterial cell has to coordinate cell wall synthesis and degradation [152], [155].

V. cholerae has a curved rod morphology. The rod shape is caused by the interplay of a multiprotein complex, referred to as the elongasome and the actin homolog MreB [156]–[159]. The elongasome moves circumferentially around the cell in a perpendicular orientation to its long axis. It comprises PBPs, which consistently drive peptidoglycan polymerization, causing elongated rod-like cell shapes [156], [157]. The elongasome requires guidance by a cytoplasmic and inner membrane-associated MreB polymer [160], [161]. In *V. cholerae*, depletion of MreB, or disruption of its polymerization by the MreB-targeting drug A-22, results in spherical cells [158].

The first structural determinant of *V. cholerae*'s comma shape was recently identified as the CrvA protein, which forms a cell-spanning polymer in the periplasm at the inner face of the cell (Figure 6) [153]. Deletion of *crvA* results in a straight rod phenotype. The CrvA polymer does not alter the chemical composition of PG, instead, it causes the asymmetric insertion of new PG components. Specifically, the amount of newly inserted PG is higher along the outer face when compared to the inner face [153]. This biased PG expansion causes the cell to bend towards the inner face. *V. cholerae* cell curvature increases with cell density, indicating a QS-mediated control of *crvA* and curvature (Figure 6). Indeed, *hapR* mutant cells displayed decreased curvature compared to wild-type, whereas AI supplementation with AI-2 and CAI-1 increased cell bending. However, the cell curvature of *luxS*/*cqsA* double-mutant cells did not differ from wild-type cells [153]. Thus, the regulatory control of *crvA* and curvature remains somewhat unclear and requires a more detailed investigation.

Interestingly, the curved morphology of *V. cholerae* was demonstrated to be beneficial for the penetration of high-density agar surfaces, which to some extent, mimic the dense mucoid matrices encountered in the human small intestine. Indeed, straight *crvA* mutant cells were less successful in colonizing animal hosts, which could be explained with their reduced ability to penetrate mucoid matrices [153], [162].
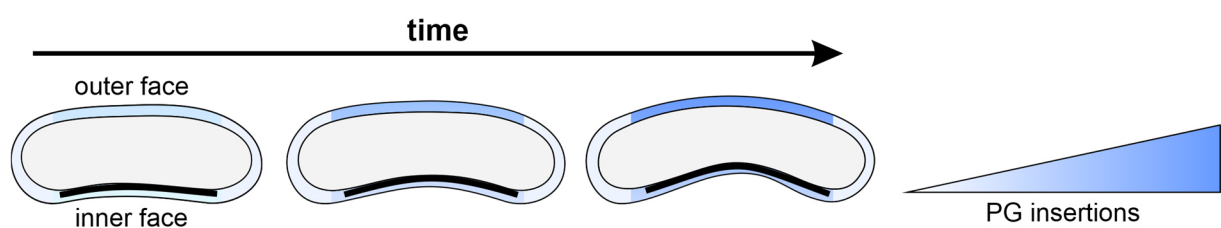

Figure 6 The periplasmic CrvA polymer curves *V. cholerae* cells. CrvA (black curve) causes the asymmetric insertion of new PG, which leads to increased cell bending over time.

1.6 Cell envelope stress responses

The outer membrane, the periplasm, the peptidoglycan layer, and the inner membrane form the cell envelope of Gram-negative bacteria. It protects from harmful substances, enables a spatial organization, shapes the cell, and allows the controlled import or export of ions and molecules. Therefore, cell envelope homeostasis is essential for bacterial survival. However, in its biphasic life-cycle, *V. cholerae* faces multiple factors that cause cell envelope damage [163]. These include changes in temperatures, osmolarity, and pH, as well as antimicrobial peptides or antibiotics. Given the importance of an intact cell envelope, it is not surprising that several stress response systems exist in *V. cholerae* to sense and counteract cell envelope stresses by altering the processes of envelope biogenesis. Well-known systems are the alternative sigma factor σ^E and the Cpx response, which are mainly activated under outer membrane- and inner membrane-damaging conditions, respectively [164]–[166]. Additionally, the phage shock protein (PSP) response supports the Cpx system in cases of severe inner membrane damage [167]. Interestingly, *V. cholerae* lacks the Rcs and Bae response systems, which exist in many Gram-negative bacteria and respond, among other triggers, to cell wall damages [168], [169]. Recent studies indicate that the VxrAB (a.k.a. WigKR) two-component system (TCS) of *V. cholerae* could fill this role and mediate cell wall homeostasis during cell wall stress [170]–[172].

Most relevant for this work are the σ^E and VxrAB (WigKR) response systems, which are discussed in more detail below.

1.6.1 σ^E response

Alternative sigma factors are valuable tools to deal with specific environmental stresses. They bind to and redirect RNA polymerase to a specific subset of promoters to mediate situation-dependent gene expression on a global scale. The accumulation of misfolded outer membrane β-barrel proteins (OMPs) in the periplasm is the activating signal for the σ^E response, which is best studied in *E. coli* [164]. However, the core components of the system are also present in *V. cholerae*, indicating a conserved signal transduction cascade.

In the absence of inducing triggers, σ^E is tethered to the inner membrane by its anti-sigma factor RseA, which is protected from proteolysis by the RseB protein (Figure 7A, left) [173], [174]. Under membrane-damaging conditions, OMPs misfold and remain in the periplasm. Although the exact mechanism remains unknown, previous results indicated that misfolded OMPs and off-pathway lipopolysaccharides (LPP) release RseB-mediated protection of RseA [174], [175]. The accessible

C-termini of misfolded OMPs are recognized by the inner membrane protease DegS, which subsequently cleaves the periplasmic domain of RseA [176]. A second protease, RseP, cleaves RseA and releases σ^E into the cytoplasm, where it associates with RNAP to activate its regulon (Figure 7A, right) [177]. In *E. coli*, the σ^E response induces the expression of ≈ 100 genes to restore membrane homeostasis [178].

By default, σ^E is a strict positive regulator of gene expression. However, perturbations of the outer membrane force the bacterial cell to immediately stop *de novo* synthesis of OMPs and other unfavored proteins. To this end, bacteria employ σ^E-dependent sRNAs, which act as the repressive arm of the σ^E response [39], [179]. In *E. coli*, three Hfq-dependent sRNAs, namely MicA, RybB, and MicL, are highly activated upon σ^E induction [180], [181]. MicA and RybB control large sets of shared and specific targets, including several mRNAs encoding OMPs or lipoproteins associated with the cell envelope [179]. In contrast to the larger regulons of MicA and RybB, the *lpp* transcript is the only validated target of MicL [181]. Notably, the outer membrane lipoprotein Lpp is the most abundant protein in the cell and its post-transcriptional repression by MicL alleviates membrane damage repair [181].
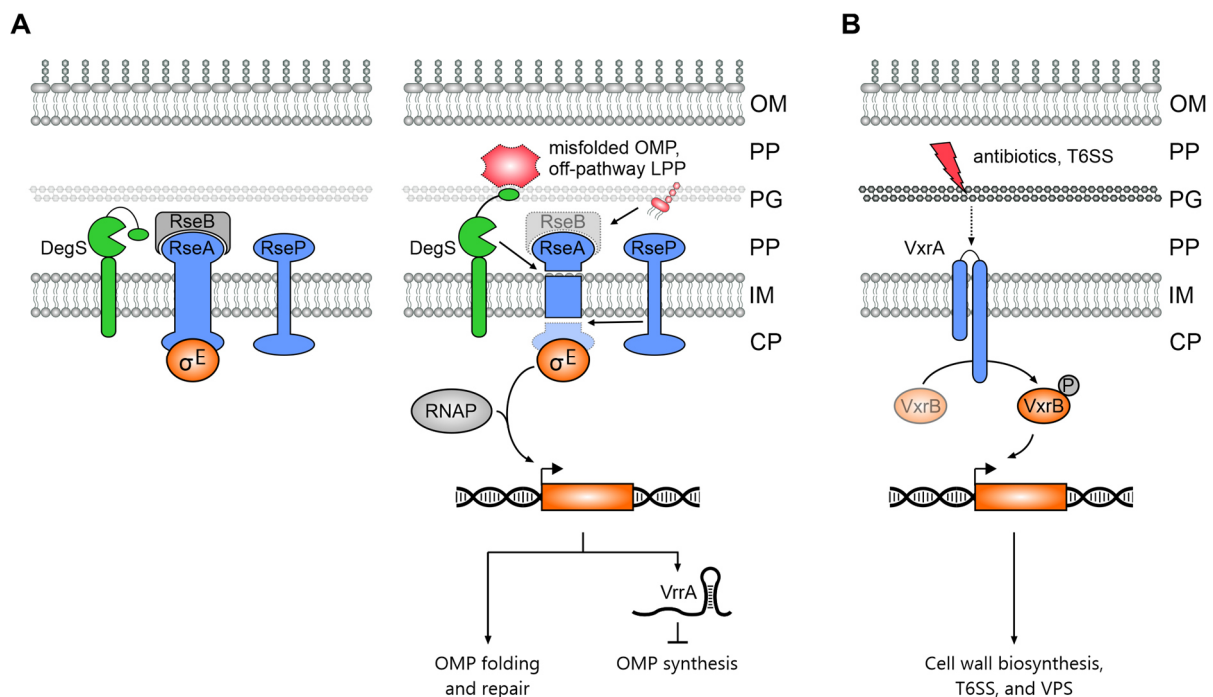
Figure 7 The σ^E and VxrAB response systems of *V. cholerae*. A) Left: The alternative σ^E is sequestered at the inner membrane by its anti-sigma factor RseA. Proteolytic cleavage of RseA by DegS and RseP is prevented. Right: Accumulating OMPs in the periplasm activate the proteolytic function of DegS and off-pathway LPPs release protection of RseA through RseB. DegS cleaves RseA and thus allows RseP to access RseA. σ^E is released into the cytoplasm. In association with RNAP, it activates a large regulon. VrrA acts as the repressive arm of the system. B) Cell wall damage activates the VxrAB TCS via an unknown signal. P: phosphate group; OM: outer membrane; PP: periplasm; PG: peptidoglycan; IM: inner membrane; CP: cytoplasm.

In *V. cholerae*, VrrA is the only described σ^E-dependent sRNA (Figure 7A, right)[182]. VrrA is a direct repressor of the two major OMPs OmpA and OmpT, the biofilm matrix protein RbmC (chapter 1.4), and the ribosome hibernation protein Vrp [182]–[185]. Given that *E. coli* employs three sRNAs in its σ^E response system, which together govern > 30 mRNA targets, it seems likely that VrrA regulates yet unidentified targets, or, that *V. cholerae* expresses additional σ^E-dependent sRNAs to restore cell envelope integrity.

1.6.2 Vxr response

The VxrAB TCS was recently identified as a potent cell wall damage response system in *V. cholerae* [170]. It is encoded by the first and second gene of the *vxrABCDE* operon, with VxrA being the histidine kinase and VxrB functioning as the cognate response regulator [186]. The roles of VxrC, VxrD, and VxrE during the cell envelope stress response are currently unknown.

Multiple stimuli that disrupt the cell wall integrity activate the VxrAB system in *V. cholerae*. These include antibiotics like penicillin, fosfomycin, and D-cycloserine, as well as effector proteins delivered by type VI secretion systems (T6SS) during bacterial attacks (Figure 7B) [170], [172]. Of note, the VxrA homolog in *V. parahaemolyticus*, VbrK, functions as a receptor of the β-lactam antibiotic penicillin [171]. However, given that VxrAB responds to structurally highly diverse agents and T6SS effector proteins in *V. cholerae* [170], [172], it seems more likely that VxrA in *V. cholerae* senses a cell wall degradation product rather than one specific antibiotic.

The VxrB regulon comprises all genes required for cell wall biosynthesis and its activation was shown to be critical to restore cell wall homeostasis [170]. Indeed, exposure of a *V. cholerae vxrAB* deletion mutant to β-lactam antibiotics decreased its fitness ≈100-fold in a laboratory setting and even >10,000-fold in an infant mouse model [170]. Additionally, VxrB promotes biofilm formation and virulence factor production by activating VPS production and the T6SS, respectively [186], [187]. Intriguingly, these two phenotypes indirectly contribute to cell envelope integrity. For example, members of a biofilm show increased tolerance and persistence towards (cell wall-targeting) antibiotics, and a dense VPS matrix mitigates T6SS attacks [172], [188]. Counterattacking via an own T6SS is another evident strategy to prevent cell envelope perturbation caused by T6SS-mediated attacks [172], [186].

Importantly, the VxrAB system also plays a role during normal growth conditions, in the absence of cell wall-damaging stimuli. Under standard laboratory growth conditions, cells that lack *vxrAB* experience minor growth defects in the early stationary phase, but strikingly, they show a

significant increase in cell diameter and cell volume [170]. These observations indicate that the VxrAB system is not only involved in the cell envelope stress response, but also fulfills critical house-keeping functions to maintain the global peptidoglycan architecture, and thus, the characteristic cell shape of *V. cholerae*.

1.7 Aim of this work

Small regulatory RNAs have been extensively studied in *E. coli* and *Salmonella*. In both model organisms, sRNAs play vital roles in physiology, metabolism, virulence, and stress response systems [6]. However, only a few sRNAs have been identified and functionally characterized in the human pathogen *V. cholerae*. A differential RNA-sequencing (dRNA-seq) approach in *V. cholerae* set the starting point to determine the scope of sRNA abundance in this organism systematically. In total, 107 new sRNA candidates were revealed, and at the beginning of this work, only one of them, Vcr107, was further investigated and renamed VqmR [1].

VqmR, which is controlled by the VqmA transcription factor, is a direct regulator of 16 mRNAs, including *vpsT*, and VqmR-mediated repression of *vpsT* inhibits biofilm formation in *V. cholerae*. Recently, DPO was discovered as the third AI molecule in *V. cholerae* and as the activating signal of VqmA [74]. The aim of chapter 2 of this work was to further explore the target regulon of VqmR using RNA-sequencing (RNA-seq) and lower cell densities compared to the previously tested condition [1]. This approach yielded the *aphA* transcript as a new repressed target of VqmR. AphA is the QS master regulator at LCD, and down-regulation of AphA by VqmR reduced virulence factor production. AphA is also controlled by the shared QS pathway of CAI-1 and AI-2. Global transcriptome analyses of *V. cholerae* cells treated with single AIs or AI combinations revealed that not only *aphA*, but hundreds of genes were co-regulated by CAI-1, AI-2, and DPO. This comprehensive dataset deepens our understanding of QS functions in this human pathogen and can be considered of major importance for future QS-related studies.

QS was recently proposed to mediate cell curvature in *V. cholerae* [153]. The authors of this study also demonstrated that the curved-rod morphology of *V. cholerae* increases its ability to colonize animal infection models [153]. However, no direct regulator of cell curvature in *V. cholerae* has been identified. The aim of chapter 3 was to investigate whether one or more of the previously identified sRNA candidates [1] affects cell curvature in *V. cholerae*. Indeed, the Vcr090 sRNA, which was renamed VadR, was identified as a negative regulator of cell curvature and as a direct

repressor of the structural protein CrvA. The *vadR* gene was shown to be transcriptionally controlled by the VxrAB TCS, which plays a crucial role in cell wall homeostasis. Likewise, VadR was demonstrated to contribute to *V. cholerae* survival after treatment with cell wall-damaging agents through the regulation of *crvA*.

Cell envelope-damaging conditions induce several stress response systems in bacteria, which frequently involve sRNAs [72]. For example, the σ^E response in *E. coli* activates three sRNAs that fulfill designated functions to relieve outer membrane stress [180], [181]. However, VrrA is the only known σ^E-dependent sRNA in *V. cholerae* [182]. Thus, the main objective in chapter 4 was to identify and functionally characterize additional σ^E-dependent sRNAs in *V. cholerae*. The promoter region of the *vcr089* sRNA gene matched the σ^E binding motif, and σ^E-dependent expression of the sRNA was validated experimentally. Vcr089 was renamed MicV and demonstrated to act partially redundant with VrrA due to highly similar seed sequences in both sRNAs. Laboratory selection experiments provided evidence that sRNAs could be functionally annotated based on their base-pairing sequences.

2 Three autoinducer molecules act in concert to control virulence gene expression in *Vibrio cholerae*

Herzog R, Peschek N, Fröhlich KS, Schumacher K, Papenfort K. Three autoinducer molecules act in concert to control virulence gene expression in Vibrio cholerae. ***Nucleic Acids Res.*** 2019;47(6):3171-3183. doi:10.1093/nar/gky1320

The full-text article is available online at:

https://academic.oup.com/nar/article/47/6/3171/5289484

The supplementary data is available online at:

https://academic.oup.com/nar/article/47/6/3171/5289484#supplementary-data

3 RNA-mediated control of cell shape modulates antibiotic resistance in *Vibrio cholerae*

Manuscript

Roman Herzog[1,2*], Nikolai Peschek[1,2*], Praveen K. Singh[3], Kathrin S. Fröhlich[1,2], Luise Schröger[1,2], Fabian Meyer[1,4], Marc Bramkamp[1,4], Knut Drescher[3,5], and Kai Papenfort[1,2,6#]

[1] Friedrich Schiller University, Institute of Microbiology, 07745 Jena, Germany

[2] Faculty of Biology I, Ludwig-Maximilians-University of Munich, 82152 Martinsried, Germany

[3] Max Planck Institute for Terrestrial Microbiology, 35043 Marburg, Germany

[4] Institute for General Microbiology, Christian-Albrechts-University, Kiel, Germany,

[5] Department of Physics, Philipps-Universität Marburg, 35032 Marburg, Germany

[6] Microverse Cluster, Friedrich Schiller University Jena, 07743 Jena, Germany.

* These authors contributed equally

Corresponding author

RNA-mediated control of cell shape modulates

antibiotic resistance in *Vibrio cholerae*

Roman Herzog[1,2*], Nikolai Peschek[1,2*], Praveen K. Singh[3], Kathrin S. Fröhlich[1,2], Luise Schröger[1,2], Fabian Meyer[1,4], Marc Bramkamp[1,4], Knut Drescher[3,5], and Kai Papenfort[1,2,6#]

[1] Friedrich Schiller University, Institute of Microbiology, 07745 Jena, Germany

[2] Faculty of Biology I, Ludwig-Maximilians-University of Munich, 82152 Martinsried, Germany

[3] Max Planck Institute for Terrestrial Microbiology, 35043 Marburg, Germany

[4] Institute for General Microbiology, Christian-Albrechts-University, Kiel, Germany,

[5] Department of Physics, Philipps-Universität Marburg, 35032 Marburg, Germany

[6] Microverse Cluster, Friedrich Schiller University Jena, 07743 Jena, Germany.

* These authors contributed equally

Corresponding author:

Kai Papenfort

E-mail: kai.papenfort@uni-jena.de

Phone: +49-3641-939-5753

Friedrich Schiller University of Jena

Institute of Microbiology

General Microbiology

Winzerlaer Straße 2

07745 Jena, Germany

Key words: *Vibrio cholerae*, small RNA, cell shape, biofilm formation, CrvAB

Abstract

Vibrio cholerae, the cause of cholera disease, exhibits a characteristic curved rod morphology, which promotes infectivity and motility in dense hydrogels. Periplasmic protein CrvA determines cell curvature in *V. cholerae*, yet the regulatory factors controlling CrvA are unknown. Here, we discovered the VadR small RNA (sRNA) as a post-transcriptional inhibitor of the *crvA* mRNA. Mutation of *vadR* increases cell curvature, whereas over-expression has the inverse effect. We show that *vadR* transcription is activated by the VxrAB two-component system and triggered by cell-wall-targeting antibiotics. *V. cholerae* cells failing to repress *crvA* by VadR display decreased survival upon challenge with penicillin G indicating that cell shape maintenance by the sRNA is critical for antibiotic resistance. VadR also blocks the expression of various key biofilm genes and thereby inhibits biofilm formation in *V. cholerae*. Thus, VadR is an important new regulator for synchronizing peptidoglycan integrity, cell shape, and biofilm formation in *V. cholerae*.

Main text

Bacterial cell shape is highly diverse and tightly conserved at the species level. Certain cell morphologies have been associated with distinct physiological functions such as optimized nutrient uptake, efficient surface adherence, and increased evasion from protist grazing[1]. Cell shape is determined by the geometry of the cell-wall, which can be affected by filamentous protein factors that change or interfere with peptidoglycan insertion[2-4]. For example, the cytoskeleton-like filament, crescentin (CreS), controls cell curvature in the model bacterium *Caulobacter crescentus*[5]. In *Vibrio cholerae*, CrvA protein polymerizes in the periplasmic space to promote cell bending[6,7]. *V. cholerae* cells lacking the *crvA* gene display attenuated colonization in animal infection models and it has been reported that cell curvature of *V. cholerae* increases in a cell-density dependent manner[6]. These findings indicate that CrvA levels are continuously adjusted during growth, however, the necessary regulatory factors are currently unknown.

Recently, post-transcriptional control by small regulatory RNAs (sRNAs) in *V. cholerae* was shown to be key for modulating spatiotemporal processes such as virulence, biofilm formation, secondary messenger production, and stress resistance[8-11]. The largest class of sRNAs associates with the RNA chaperone Hfq and typically regulates the expression of target mRNAs by base-pairing *via* short stretches of imperfect complementarity[12,13]. The network regulated by a single sRNA frequently involves dozens of targets and therefore sRNAs can rival transcription factors with respect to their regulatory scope and biological importance[14]. For example sRNAs are crucial for iron, membrane, and sugar homeostasis, as well as motility, biofilm formation, and virulence[15,16], however, no sRNA has been yet reported to control cell shape.

Here, we employed the curved rod-shaped bacterium *V. cholerae* as a model system to study the impact of sRNAs on cell curvature. To this end, we used a forward genetic screen and quantified the effect of 21 previously uncharacterized Hfq-dependent sRNAs on cell shape in *V. cholerae*. We discovered that production of the VadR (<u>V</u>xrB <u>a</u>ctivate<u>d</u> small <u>R</u>NA, see below) sRNA efficiently reduced cell curvature in *V. cholerae* by inhibiting the expression of the *crvAB* mRNA at the post-transcriptional level. VadR also controls several main genes required for biofilm assembly, including *rbmA*[17]. Consequently, we show that VadR also inhibits biofilm formation in *V. cholerae*. We further show that transcription of VadR is controlled by the VxrAB two-component system (a.k.a. WigKR[18,19]) and is activated by ß-lactam antibiotics. *V. cholerae* mutants deleted for *vadR* display increased sensitivity towards penicillin and we pinpoint this phenotype to VadR-mediated repression of *crvAB*. Our results reveal how a non-coding RNA involved regulates a cytoskeleton-like filament in bacteria and establishes a link between cell shape, biofilm formation, and antibiotic resistance in *V. cholerae*.

RESULTS

To identify sRNAs regulating cell curvature in *V. cholerae*, we performed a microscopy-based forward genetic screen. We selected 21 uncharacterized sRNAs candidates from a pool of recently identified Hfq-dependent sRNAs[20] and cloned their respective genes onto multi-copy plasmids. We transferred these plasmids into *V. cholerae* and assayed the resulting strains for centerline curvature using phase contrast microscopy. In line with a previous report[6], we found that curvature decreased ~3-fold in *crvA* deficient cells, when compared to wild-type *V. cholerae* (Fig. 1a). Over-expression of 20 sRNAs did not render curvature significantly, however, cells overexpressing one sRNA, which we term VadR (a.k.a. Vcr090[20], see below), displayed ~2-fold reduced curvature (Fig. 1a).

The *vadR* gene is located on the plus strand of the smaller *V. cholerae* chromosome between the *vca0002* and *vca0003* genes[20]. The sRNA is present in numerous other *Vibrios* and carries a highly conserved 5' end (Fig. 1b) frequently involved in RNA duplex formation with *trans*-encoded target mRNAs[8,21]. Structure probing experiments confirmed that this region is unstructured and therefore available for base-pairing with other transcripts (Figs. S1a-b). Northern blot analysis revealed that VadR accumulates as a ~85 nt transcript and is most highly expressed at low cell densities (Fig. 1c). Stability of VadR was ~3 min in *V. cholerae* wild-type cells and ~4-fold reduced in cells lacking the *hfq* gene (Fig. S1c). Together, we conclude that VadR is a Hfq-dependent sRNA that is likely to act by base-pairing other transcripts.

Alignment of *vadR* promoter sequences revealed three conserved elements upstream the -10 box (Fig. 1b). While we were unable to directly assign a transcriptional regulator to these elements, we discovered that a *vadR* transcriptional reporter was ~150-fold more active in *V. cholerae* when compared to *Escherichia coli* (Fig. S1d). These results suggested that *vadR* expression depended on a *V. cholerae*-specific factor, which allowed us to perform another genetic screen. Here, we employed a plasmid library expressing ~2.5 kb *V. cholerae* genomic fragments, which we co-transformed with a P*vadR*::*lacZ* transcriptional reporter into *E. coli*. We assayed ~23,000 colonies for ß-galactosidase activity on plates containing X-gal and isolated seven blue colonies. Sequence analysis of the respective plasmids revealed that all mapped to the *vxrABCDE* (*vca0565-0569*) locus; five plasmids contained sequences of *vxrAB* and two plasmids contained sequences of *vxrABCDE* (Fig. S1e). To corroborate these results, we monitored *vadR* production in wild-type and Δ*vxrABCDE V. cholerae* by means of (i) promoter activity measurements and (ii) Northern blot analysis. Indeed, promoter activity was ~50-fold reduced in the *vxrABCDE* mutant (Fig. S1f) and VadR was no longer detectable on Northern blots (Fig. 1d). Successive complementation of the *vxrABCDE* genes from a plasmid revealed that *vxrAB* (constituting the histidine kinase and response regulator of the two component system, respectively) restored VadR expression, while *vxrCDE* were

dispensable for regulation (Fig. 1d). Finally, to pinpoint direct regulation of *vadR* by VxrB, we reanalyzed previously reported ChIP-Seq data[22] for binding of VxrB at the *vadR* promoter. Indeed, we discovered a pronounced, VxrB-specific peak upstream of the *vadR* gene (Fig. S1g). These analyses also revealed a putative VxrB binding motif (TTGACAAAA-N2-TTGAC), which matched the three conserved sequence elements in the *vadR* promoter (Fig. 1b). Deletion of each of these sites efficiently reduced *vadR* promoter activity with sites 2 and 3 being most critical for transcription activation (Fig. S1h). Together, we conclude that VadR is a VxrAB-activated sRNA that modulates cell shape in *V. cholerae*.

To explore the molecular mechanism of VadR-mediated inhibition of cell bending, we next aimed to identify base-pairing partners of VadR *in vivo*. We used RNA-seq analyses to assess changes in global transcriptome levels following transient (15 min) overexpression of *vadR* in a Δ*vadR V. cholerae* strain. In total, 28 mRNAs, including *crvA*, displayed significant changes following VadR expression (Fig. 2a and Table S1). We validated regulation of all targets, except *ibpA*, using quantitative real-time PCR (by testing all monocistronic genes and the first gene of all regulated operons; Fig. S2a). The majority of repressed targets (15) corresponded to a single biofilm gene cluster (*vc0916-vc0939*) required for the production of the VPS biofilm exopolysaccharide, as well as genes producing the auxiliary biofilm components, RbmA-F[23] (Fig. 2b). Gene ontology (GO) analyses revealed a significant overrepresentation of GO terms associated with polysaccharide synthesis in the downregulated targets (Fig. 2c). Indeed, using the wrinkly colony morphology phenotype of *V. cholerae* Δ*hapR* cells as a read-out for biofilm formation[20], we discovered that VadR over-expression resulted in strongly decreased biofilm formation (Fig. 2d). This phenotype was further corroborated by quantitative measurements of biofilm formation in microfluidic flow chambers, analyzed by confocal microscopy (Figs. 2e-h). Detailed analysis of the respective microscopic images revealed that VadR expression resulted in a phenotype mimicking *V. cholerae* cells lacking the *rbmA* gene (Figs. 2e-i). RbmA is required to form higher order structures in *V. cholerae* biofilms and depletion of the protein from the biofilm results in decreased biofilm density[17,24,25]. Indeed, we observed a significant reduction in local biofilm density in cells over-expressing VadR (Figs. 2f, i), which is consistent with reduced RbmA levels determined by quantitative Western blots (Fig. S2b). These results show that in addition to controlling cell shape, VadR also regulates biofilm formation in *V. cholerae*.

To investigate the molecular underpinnings of VadR-mediated gene control in *V. cholerae*, we cloned the 5' UTR (untranslated region) and the TIR (translation initiation region) of the 14 potential VadR targets into a GFP-based reporter plasmid designed to score post-transcriptional control[26]. Co-transformation of these plasmids with a VadR over-expression vector or a control plasmid in *E. coli* confirmed post-transcriptional repression of nine targets (*crvA*, *irpA*, *rbmA*, *rbmD*, *vpsL*, *vpsU*, *vc2352*, *vca0075*, and *vca0864*), while we were unable

to validate direct regulation of *bapI*, *rbmC*, *rbmF*, *rbsD*, and *vca0043* (Figs. 3a and S3a). Using the RNA hybrid algorithm[27], we predicted RNA duplex formations of VadR with *crvA*, *rbmA*, *vpsU*, and *vpsL* (Figs. 3b-e). In all four cases, pairing involved the target's TIR and sequence elements located in the first 30 nucleotides of VadR. Using compensatory base-pair exchange experiments (creating mutants M1, M2, and M3 in *vadR*, see Figs. S1a and S3), we validated binding at the predicted positions (Figs. 3f-i). To bolster these results at the phenotypic level, we tested biofilm formation of ∆*vadR* cells expressing a mutated VadR variant (VadR∆R1, see Figs. S1a and S3b) unable to repress three of the four target genes. In contrast to wild-type VadR (Figs. 2d, f), VadR∆R1 did not affect biofilm formation and architecture in *V. cholerae* (Fig. 2d, g, i).

Given that we confirmed VadR as a direct repressor of *crvA* (Figs. 3b, f), we next aimed to study the role of VadR in cell curvature in *V. cholerae*. Western blot analysis showed CrvA levels were ~1.5-fold elevated in ∆*vadR* cells, whereas VadR over-expression led to a ~2-fold reduction in CrvA production (Fig. 4a). We correlated these results with microscopic curvature analyses of single cells and discovered that *vadR*-deficient mutants displayed increased curvature, whereas plasmid-borne VadR production had the reverse effect (Figs. 4b top and 4c). This effect was further amplified when cells were treated with sub-inhibitory concentrations of cefalexin forcing filamentation in *V. cholerae* (Fig. 4b, bottom). Importantly, neither *vadR* deletion, nor its over-expression affected cell length or volume of *V. cholerae* (Figs. S4a-b), indicating that VadR specifically modulates cell curvature by inhibiting *crvA* expression.

CrvA regulates cell curvature by spatially modulating peptidoglycan insertion in *V. cholerae*[6] and the VxrAB regulon is induced by peptidoglycan-targeting antibiotics such as penicillin G[19]. Consequently, we tested the effect of penicillin G on VadR expression. Indeed, Northern blot analysis showed ~7-fold increased VadR levels in *V. cholerae* wild-type cells following treatment with penicillin G (Fig. 5a) and we observed ~25-fold induction when we tested *vadR* promoter activity using a transcriptional reporter (Fig. 5b). In both cases, penicillin G-dependent activation of *vadR* was abrogated in the ∆*vxrABCDE* strain (Figs. 5a-b). Expression of *vadR* was also activated by the MreB-targeting antibiotic A22[28], albeit to a lower extent when compared to penicillin G (Fig. S5a).

Based on these results, we speculated that resistance towards cell-wall damaging antibiotics requires the remodeling of cell shape-determining components by VxrAB and VadR. Following this hypothesis, we first determined the relationship between CrvA production and penicillin G resistance. To this end, we cloned the inducible P_{BAD} promoter upstream of the chromosomal *crvAB* gene in *V. cholerae* and activated expression for 1.5h using various concentrations of L-arabinose. Next, we added penicillin G and continued incubation for additional 3 h when we determined survival by counting colony-forming units on agar plates. Indeed, we obtained ~2-fold fewer colony counts at low L-arabinose concentrations (0.0125%

final conc.) and up to ~3.5-fold reduced colonies when the promoter was strongly induced (0.05% final conc.) (Fig. S5b). These data indicated that elevated CrvA levels impair penicillin G resistance in *V. cholerae*. In accordance with this observation, we also discovered reduced penicillin G survival rates for *vadR*-deficient *V. cholerae* cells and we were able to complement this phenotype using plasmid-borne VadR production (Fig. 5c). To pinpoint this effect to VadR-mediated repression of *crvA* in the presence of penicillin G, we introduced mutation M1* (Fig. 3b) at the chromosomal *crvA* locus. This mutation keeps *crvA* production intact (Fig. S5c), but renders the transcript immune towards post-transcriptional repression by VadR. This strain phenocopied the effect of a *vadR* mutant. We obtained almost identical results when we introduced the corresponding mutation (M1, Figs. 3b and S1a) at the chromosomal *vadR* gene (Fig. 5c). Combination of the two mutant alleles resulted in a partial restoration of penicillin G resistance (Fig. 5c), supporting our initial hypothesis that VadR is required to mitigate the detrimental effect of CrvA under antibiotic pressure. Notably, neither mutation nor over-expression of *vadR* affected survival of *V. cholerae* under standard growth conditions (Fig. S5d).

To connect the roles of VadR in cell curvature regulation and biofilm formation in *V. cholerae*, we monitored VadR expression (using a P*vadR*::mRuby2 transcriptional reporter) in growing biofilms employing single-cell confocal microscopy analysis[29]. When normalized for sfGFP production driven from the constitutive P$_{tac}$ promoter, we discovered that the *vadR* promoter is most active during the initial phases of biofilm formation, while expression is switched off in mature biofilms (Fig. 6a). In parallel, we also determined cell curvature of individual cells during biofilm development (Fig. 6b). Comparison of the two datasets showed that VadR expression and cell curvature are negatively correlated (Fig. 6c), suggesting that VadR expression results in straighter cells during early phases of biofilm development, whereas mature biofilms are more likely to contain a higher proportion of curved cells.

Given that VadR also controls the production of several mRNAs encoding important biofilm factors such as VPS, RbmA, RbmC and Bap1 (Fig. S2a), it seems possible that VadR also limits the expression of these components in early biofilms (Fig. 6d). Transcription of *vadR* is controlled by the VxrAB system (Fig. 1d), which has been reported to control cell-wall synthesis and repair, biofilm formation, type 6 secretion, and iron homeostasis in *V. cholerae*[18,19,22,30]. In closely related *Vibrio parahaemolyticus*, the VxrAB system (here called VbrKR) has been reported to respond to ß-lactam antibiotics *via* direct interaction with the histidine kinase, VbrK[31]. Our results support activation of the system by ß-lactam antibiotics, *i.e.* penicillin G (Figs. 5a-b), however, since we also discovered *vadR* activation in the presence of A22 (Fig. S5a) it is likely that additional cues also trigger the system.

Indeed, VadR is readily detectable under standard growth conditions (Fig. 1c) suggesting a regulatory role for the system under non-stress conditions. Here, VadR might

take the role of adjusting cell growth with the production of CrvA and biofilm-forming factors (Fig. 6d). CrvA is an abundant periplasmic protein[6] and biofilm components require transport across two membranes to reach their final destination[23]. Uncoordinated export of proteins and polysaccharides can clog the cellular transport machineries and compromise the permeability barrier or structural integrity of the cell[32,33]. It is therefore vital for the cell to synchronize these functions with cell growth and sRNAs have previously been implicated in this process[34]. For example, sRNAs activated by the alternative sigma-factor E promote envelope homeostasis by tuning the levels of newly synthesis outer membrane proteins in response to misfolded proteins in the periplasm[8,21,35,36]. VadR could take an analogous position in the VxrAB stress response system and given the relatively short half-life of VadR (~3min, Fig. S1c), sRNA-based regulation might provide regulatory dynamics that are superior over canonical protein-based regulation[14]. This hypothesis is supported by our finding that VadR directly base-pairs with the mRNAs of the multiple biofilm components (Fig. 3a), rather than acting through a higher-level transcriptional regulator such as VpsT. VpsT activates the transcription of the genes encoding biofilm components in *V. cholerae*[37] and is repressed by the VqmR sRNA, which blocks biofilm formation[20,38]. Therefore, over-expression of VadR or VqmR has similar consequences for biofilm formation in *V. cholerae*, however, the underlying molecular mechanisms differ. Deciphering these differences will allow important conclusions about the biological roles of these sRNAs and their associated pathway, but could also provide a deeper understanding of how sRNAs evolve and select their targets[39].

Our data further showed that besides repressing biofilm formation and cell curvature, VadR also inhibits the expression of *vc2352* (encoding a NupC-type nucleoside transporter[40]), *irpA* (encoding an iron-regulated membrane protein carrying a peptidase domain[41]), *vca0864* (encoding a methyl-accepting chemotaxis protein[42]), and *vca0075*, which has unknown functions[43] (Figs. 3a and 6d). We do not yet understand how these genes fit into the VadR regulon, however, *vca0075* is co-repressed with *cdgA*[20], a diguanylate cyclase gene with documented functions in biofilm formation[44]. In addition, Vca0864 has been reported to inhibit chemotaxis towards N-acetylglucosamine, which is a key component of peptidoglycan[45]. Simultaneous repression of biofilm formation and Vca0864 by VadR could promote cell motility towards N-acetylglucosamine and thereby replenish the necessary building blocks for peptidoglycan remodeling under conditions of cell-wall stress.

How CrvA affects peptidoglycan remodeling in *V. cholerae* is currently not fully understood. Previous reports revealed that filament-like proteins such as CrvA and CreS render the activity of enzymes involved in cell-wall synthesis and thereby reduce the rate of peptidoglycan insertion at one site of the cell[6,46]. This process results in asymmetric growth and cell curvature, but might also create an "Achilles heel" in the presence of ß-lactam

antibiotics or other cell-wall damaging agents. VadR-mediated repression of *crvA* mRNA could help to mitigate this effect by reducing the de-novo production of CrvA protein.

METHODS

Bacterial strains and growth conditions

Bacterial strains used in this study are listed in Supplementary Table S2. Details for strain construction are provided in the Supplementary Material and Methods section. *V. cholerae* and *E. coli* cells were grown under aerobic conditions (200rpm, 37°C) in LB (Lenox). Where appropriate, media were supplemented with antibiotics at the following concentrations: 100 µg/ml ampicillin; 20 µg/ml chloramphenicol; 50 µg/ml kanamycin; 50 U / ml polymyxin B; 5 mg/ml streptomycin, 5 µg/ml cefalexin, 50 µg/ml penicillin G.

Plasmids and DNA oligonucleotides

All plasmids and DNA oligonucleotides used in this study are listed in Supplementary Tables S3 and S4, respectively. Cloning details are provided in the Supplementary Material and Methods section.

RNA isolation and Northern blot analysis

Total RNA was prepared and blotted as described previously[47]. Membranes (GE Healthcare Amersham) were hybridized with [^{32}P] labelled DNA oligonucleotides at 42°C. Signals were visualized using a Typhoon phosphorimager (GE Healthcare) and quantified using Gelquant software (biochemlabsolutions).

Microscopy analysis

Samples for microscopy analyses were prepared by growing the respective *V. cholerae* strains in LB to OD_{600} of 0.4. Cells were pelleted, washed in 1xPBS, and finally resuspended in 2.5% paraformaldehyde in 1xPBS. Phase contrast imaging was performed on a Zeiss Axio Imager M1 microscope equipped with EC Plan Neofluar 100x/ 1.3 Oil Ph3 objective (Zeiss). For additional magnification a 2.5 x optovar was used. Image acquisition was conducted with the AxioVision software-package (Zeiss). For further analysis, e.g. measurements of cell center line curvature, cell length and cell area, the FIJI-plugin MicrobeJ was used[48,49].

Flow chamber biofilms and confocal imaging

The strains were grown in LB medium supplemented with 50 µg/mL kanamycin, to mid-exponential growth phase, before introducing into microfluidic flow chambers. Flow chambers were constructed from poly(dimethylsiloxane) bonded to glass coverslips using an oxygen plasma. The microfluidic channels measured 500 µm in width, 100 µm in height and 7 mm in

length. After the cultures were introduced into the channels, the channels were incubated at 24°C for 1 h without any flow, to allow cells to attach to the bottom glass surface of the channels. The flow was then set to 0.3 µl/min for approximately 18 h before images were acquired. Cells were stained with green fluorescent nucleic acid stain dye, SYTO 9 (Thermo Fisher Scientific), by exchanging the syringes containing LB with SYTO 9 for 30 min. Flow rates were controlled using a high-precision syringe pump (Pico Plus, Harvard Apparatus). To acquire the spatiotemporal information of individual cells in a growing biofilm, time lapse confocal microscopy was performed as described previously[50]. To reduce photobleaching and phototoxicity during time-lapse imaging, a live feedback between image acquisition, image analysis and microscope control was used to automatically detect the biofilm height to avoid imaging of empty space on top of the biofilms. Images were acquired with an Olympus 100x objective with numerical aperture of 1.35, using a Yokogawa spinning disk confocal scanner and laser excitation at 488 nm. Images were acquired at spatial resolution of 63 nm in the xy plane and 400 nm along the z direction. To detect all single cells, measure cell curvature of each cell, and quantify the relative *vadR* promoter-reporter strength from biofilm grown in flow chambers, biofilm images were analysed with the BiofilmQ software available from the Drescher Lab[51]. Kymograph heatmaps showing the strength of *vadR* promoter and cell curvature during biofilm growth were generated with BiofilmQ. 3-D cell rendering was done using BiofilmQ-analysed biofilm data using the ParaView software[52]. Biofilm images were prepared with the NIS-Elements AR Analysis software (Nikon) by cropping a fixed z-plane with xy and yz projections.

RNA-seq analysis

Biological triplicates of *V. cholerae* Δ*vadR* strains harboring pBAD-Ctr or pBAD-*vadR* plasmids were grown to exponential phase (OD_{600} of 0.2) in LB media. sRNA expression was induced by addition of L-arabinose (0.2% final conc.). After 10 min of induction, cells were harvested by addition of 0.2 volumes of stop mix (95% ethanol, 5% (v/v) phenol) and snap-frozen in liquid nitrogen. Total RNA was isolated and digested with Turbo DNase (Thermo Fischer Scientific). Ribosomal RNA was depleted using Ribo-Zero kits (Epicentre) for Gram-negative bacteria, and RNA integrity was confirmed using a Bioanalyzer (Agilent). Directional cDNA libraries were prepared using the NEBNext Ultra II Directional RNA Library Prep Kit for Illumina (NEB, #E7760). The libraries were sequenced using a HiSeq 1500 system in single-read mode for 100 cycles. The read files in FASTQ format were imported into CLC Genomics Workbench v11 (Qiagen) and trimmed for quality and 3' adaptors. Reads were mapped to the *V. cholerae* reference genome (NCBI accession numbers: NC_002505.1 and NC_002506.1) using the "RNA-Seq Analysis" tool with default parameters. Reads mapping to annotated coding sequences were counted, normalized (CPM) and transformed (log_2). Differential expression

between the conditions was tested using the "Empirical Analysis of DGE" command. Genes with a fold change ≥ 1.75 and an FDR adjusted p-value ≤ 1E-3 were defined as differentially expressed.

Fluorescence measurements

Fluorescence assays to measure GFP expression were performed as described previously[26]. *E. coli* strains expressing translational GFP-based reporter fusions were grown for 16h in LB medium and resuspended in 1xPBS. Fluorescence intensity was quantified using a Spark 10M plate reader (Tecan). *V. cholerae* and *E. coli* strains carrying mKate2 transcriptional reporters were grown in LB medium, resuspended in 1xPBS, samples were collected at the indicated time points and mKate2 fluorescence was measured using a Spark 10M plate reader (Tecan). Control samples not expressing fluorescent proteins were used to subtract background fluorescence.

Western blot analysis

Experiments were performed as previously described[47]. If not stated otherwise, 0.075 OD / lane were separated using SDS-PAGE and transferred to PVDF membranes for Western blot analysis. 3xFLAG-tagged fusions were detected using anti-FLAG antibody (Sigma, #F1804). RnaPα served as a loading control and was detected using anti-RnaPα antibody (BioLegend, #WP003). Signals were visualized using a Fusion FX EDGE imager (Vilber) and band intensities were quantified using BIO-1D software tools (Vilber).

ß-galactosidase reporter assays

A plasmid library, expressing *V. cholerae* genomic fragments[53], was screened for activation of *vadR* promotor (P*vadR*) activity. To this end, *lacZ*-deficient *E. coli* BW25113 strains, harboring pNP-122, were transformed with pZach library plasmids. Transformants were selected on LB plates, containing the respective antibiotics and 20 µg / ml 5-Brom-4-chlor-3-indoxyl-β-D-galactopyranosid (X-gal). 23,000 colonies (representing ~11-fold coverage) were monitored for ß-galactosidase activity.

Sequence alignment

VadR and its promoter sequences among various *Vibrio* species were aligned using the MultAlin webtool[55]. Vch: *Vibrio cholerae* (NCBI:txid243277), Vmi: *Vibrio mimicus* (NCBI:txid1267896), Van: *Vibrio anguillarum* (NCBI:txid55601), Vqi: *Vibrio qinghaiensis* (NCBI:txid2025808), Vfu: *Vibrio furnissii* (NCBI:txid29494), Vfl: *Vibrio fluvialis* (NCBI:txid676), Vme: *Vibrio mediterranei* (NCBI:txid689), Vvu: *Vibrio vulnificus* (NCBI:txid672), Val: *Vibrio alginolyticus* (NCBI:txid663), Vpa: *Vibrio parahaemolyticus* (NCBI:txid670).

Statistical analyses

Statistical parameters for the respective experiment are indicated in the corresponding figure legends. *n* represents the number of biological replicates. Details for the performed statistical tests are provided in the supporting information. Statistical analyses of CFUs were performed as follows: The data were log10-transformed and tested for normality and equal variance using Kolmogorov–Smirnov and Brown–Forsythe tests, respectively. The data were tested for significant differences using one-way ANOVA and post hoc Holm-Sidak tests. Significance levels are reported in the in the supporting information. Statistical analysis was performed using SigmaPlot v14 (Systat). No blinding or randomization was used in the experiments. No estimation of statistical power was used before performing the experiments, and no data were excluded from analysis.

DATA AVAILABILITY

The raw data of the transcriptome analyses are available at the National Center for Biotechnology Information Gene Expression Omnibus (GEO) under the accession number GSE145764. Additional raw and analyzed data that support the findings of this study are available from the corresponding author upon request.

CODE AVAILABILITY

The biofilm image analysis software tool BiofilmQ[51] is available online (https://drescherlab.org/data/biofilmQ/).

AUTHOR CONTRIBUTIONS

RH, NP, KSF, PKS, MB, KD, and KP designed the experiments; RH, NP, PKS, LS, and KSF performed the experiments; RH, NP, PKS, KSF, FM, KD and K.P. analyzed data; and KP wrote the manuscript with the help of all authors.

COMPETING INTERESTS

The authors declare no competing financial interests.

REFERENCES

1. Taylor, J.A., Sichel, S.R. & Salama, N.R. Bent Bacteria: A Comparison of Cell Shape Mechanisms in Proteobacteria. *Annu Rev Microbiol* **73**, 457-480 (2019).
2. Cabeen, M.T. & Jacobs-Wagner, C. The bacterial cytoskeleton. *Annu Rev Genet* **44**, 365-92 (2010).
3. Wagstaff, J. & Lowe, J. Prokaryotic cytoskeletons: protein filaments organizing small cells. *Nat Rev Microbiol* **16**, 187-201 (2018).
4. Govindarajan, S. & Amster-Choder, O. Where are things inside a bacterial cell? *Curr Opin Microbiol* **33**, 83-90 (2016).
5. Ausmees, N., Kuhn, J.R. & Jacobs-Wagner, C. The Bacterial Cytoskeleton: An Intermediate Filament-Like Function in Cell Shape. *Cell* **115**, 705-713 (2003).
6. Bartlett, T.M. et al. A Periplasmic Polymer Curves Vibrio cholerae and Promotes Pathogenesis. *Cell* **168**, 172-185.e15 (2017).
7. Altinoglu, I., Merrifield, C.J. & Yamaichi, Y. Single molecule super-resolution imaging of bacterial cell pole proteins with high-throughput quantitative analysis pipeline. *Sci Rep* **9**, 6680 (2019).
8. Peschek, N., Hoyos, M., Herzog, R., Forstner, K.U. & Papenfort, K. A conserved RNA seed-pairing domain directs small RNA-mediated stress resistance in enterobacteria. *EMBO J* **38**, e101650 (2019).
9. Herzog, R., Peschek, N., Frohlich, K.S., Schumacher, K. & Papenfort, K. Three autoinducer molecules act in concert to control virulence gene expression in Vibrio cholerae. *Nucleic Acids Res* **47**, 3171-3183 (2019).
10. Davies, B.W., Bogard, R.W., Young, T.S. & Mekalanos, J.J. Coordinated regulation of accessory genetic elements produces cyclic di-nucleotides for V. cholerae virulence. *Cell* **149**, 358-70 (2012).
11. Bradley, E.S., Bodi, K., Ismail, A.M. & Camilli, A. A genome-wide approach to discovery of small RNAs involved in regulation of virulence in Vibrio cholerae. *PLoS Pathog* **7**, e1002126 (2011).
12. Kavita, K., de Mets, F. & Gottesman, S. New aspects of RNA-based regulation by Hfq and its partner sRNAs. *Curr Opin Microbiol* **42**, 53-61 (2018).
13. Gorski, S.A., Vogel, J. & Doudna, J.A. RNA-based recognition and targeting: sowing the seeds of specificity. *Nat Rev Mol Cell Biol* **18**, 215-228 (2017).
14. Hor, J., Gorski, S.A. & Vogel, J. Bacterial RNA Biology on a Genome Scale. *Mol Cell* **70**, 785-799 (2018).
15. Waters, L.S. & Storz, G. Regulatory RNAs in bacteria. *Cell* **136**, 615-28 (2009).
16. Wagner, E.G.H. & Romby, P. Small RNAs in bacteria and archaea: who they are, what they do, and how they do it. *Adv Genet* **90**, 133-208 (2015).
17. Fong, J.C. et al. Structural dynamics of RbmA governs plasticity of Vibrio cholerae biofilms. *Elife* **6**(2017).
18. Cheng, A.T., Ottemann, K.M. & Yildiz, F.H. Vibrio cholerae Response Regulator VxrB Controls Colonization and Regulates the Type VI Secretion System. *PLoS Pathog* **11**, e1004933 (2015).
19. Dörr, T. et al. A cell wall damage response mediated by a sensor kinase/response regulator pair enables beta-lactam tolerance. *Proceedings of the National Academy of Sciences of the United States of America* **113**, 404-409 (2016).
20. Papenfort, K., Forstner, K.U., Cong, J.P., Sharma, C.M. & Bassler, B.L. Differential RNA-seq of Vibrio cholerae identifies the VqmR small RNA as a regulator of biofilm formation. *Proc Natl Acad Sci U S A* **112**, E766-75 (2015).

21. Papenfort, K., Bouvier, M., Mika, F., Sharma, C.M. & Vogel, J. Evidence for an autonomous 5' target recognition domain in an Hfq-associated small RNA. *Proc Natl Acad Sci U S A* **107**, 20435-40 (2010).

22. Shin, J.-H. et al. A multifaceted cellular damage repair and prevention pathway promotes high level tolerance to β-lactam antibiotics. *bioRxiv*, 777375 (2019).

23. Teschler, J.K. et al. Living in the matrix: assembly and control of Vibrio cholerae biofilms. *Nat Rev Microbiol* **13**, 255-68 (2015).

24. Drescher, K. et al. Architectural transitions in Vibrio cholerae biofilms at single-cell resolution. *Proceedings of the National Academy of Sciences of the United States of America* **113**, E2066-E2072 (2016).

25. Yan, J., Sharo, A.G., Stone, H.A., Wingreen, N.S. & Bassler, B.L. Vibrio cholerae biofilm growth program and architecture revealed by single-cell live imaging. *Proc Natl Acad Sci U S A* **113**, E5337-43 (2016).

26. Corcoran, C.P. et al. Superfolder GFP reporters validate diverse new mRNA targets of the classic porin regulator, MicF RNA. *Mol Microbiol* **84**, 428-45 (2012).

27. Rehmsmeier, M., Steffen, P., Hochsmann, M. & Giegerich, R. Fast and effective prediction of microRNA/target duplexes. *RNA* **10**, 1507-17 (2004).

28. Gitai, Z., Dye, N.A., Reisenauer, A., Wachi, M. & Shapiro, L. MreB actin-mediated segregation of a specific region of a bacterial chromosome. *Cell* **120**, 329-41 (2005).

29. Hartmann, R. et al. Emergence of three-dimensional order and structure in growing biofilms. *Nat Phys* **15**, 251-256 (2019).

30. Teschler, J.K., Cheng, A.T. & Yildiz, F.H. The Two-Component Signal Transduction System VxrAB Positively Regulates Vibrio cholerae Biofilm Formation. *Journal of Bacteriology* **199**, 1-16 (2017).

31. Li, L. et al. Sensor histidine kinase is a beta-lactam receptor and induces resistance to beta-lactam antibiotics. *Proc Natl Acad Sci U S A* **113**, 1648-53 (2016).

32. Typas, A., Banzhaf, M., Gross, C.A. & Vollmer, W. From the regulation of peptidoglycan synthesis to bacterial growth and morphology. *Nat Rev Microbiol* **10**, 123-36 (2011).

33. Mitchell, A.M. & Silhavy, T.J. Envelope stress responses: balancing damage repair and toxicity. *Nat Rev Microbiol* **17**, 417-428 (2019).

34. Papenfort, K., Espinosa, E., Casadesus, J. & Vogel, J. Small RNA-based feedforward loop with AND-gate logic regulates extrachromosomal DNA transfer in Salmonella. *Proc Natl Acad Sci U S A* **112**, E4772-81 (2015).

35. Gogol, E.B., Rhodius, V.A., Papenfort, K., Vogel, J. & Gross, C.A. Small RNAs endow a transcriptional activator with essential repressor functions for single-tier control of a global stress regulon. *Proc Natl Acad Sci U S A* **108**, 12875-80 (2011).

36. Thompson, K.M., Rhodius, V.A. & Gottesman, S. SigmaE regulates and is regulated by a small RNA in Escherichia coli. *J Bacteriol* **189**, 4243-56 (2007).

37. Casper-Lindley, C. & Yildiz, F.H. VpsT is a transcriptional regulator required for expression of vps biosynthesis genes and the development of rugose colonial morphology in Vibrio cholerae O1 El Tor. *J Bacteriol* **186**, 1574-8 (2004).

38. Papenfort, K. et al. A Vibrio cholerae autoinducer-receptor pair that controls biofilm formation. *Nat Chem Biol* **13**, 551-557 (2017).

39. Updegrove, T.B., Shabalina, S.A. & Storz, G. How do base-pairing small RNAs evolve? *FEMS Microbiol Rev* **39**, 379-91 (2015).

40. Gumpenberger, T. et al. Nucleoside uptake in Vibrio cholerae and its role in the transition fitness from host to environment. *Mol Microbiol* **99**, 470-83 (2016).

41. Davies, B.W., Bogard, R.W. & Mekalanos, J.J. Mapping the regulon of Vibrio cholerae ferric uptake regulator expands its known network of gene regulation. *Proc Natl Acad Sci U S A* **108**, 12467-72 (2011).

42. Boin, M.A., Austin, M.J. & Häse, C.C. Chemotaxis in Vibrio cholerae. *FEMS Microbiology Letters* **239**, 1-8 (2004).

43. Heidelberg, J.F. et al. DNA sequence of both chromosomes of the cholera pathogen Vibrio cholerae. *Nature* **406**, 477-83 (2000).

44. Lim, B., Beyhan, S., Meir, J. & Yildiz, F.H. Cyclic-diGMP signal transduction systems in Vibrio cholerae: modulation of rugosity and biofilm formation. *Mol Microbiol* **60**, 331-48 (2006).

45. Minato, Y. et al. Roles of the sodium-translocating NADH:quinone oxidoreductase (Na+-NQR) on vibrio cholerae metabolism, motility and osmotic stress resistance. *PLoS One* **9**, e97083 (2014).

46. Cabeen, M.T. et al. Bacterial cell curvature through mechanical control of cell growth. *EMBO J* **28**, 1208-19 (2009).

47. Frohlich, K.S., Haneke, K., Papenfort, K. & Vogel, J. The target spectrum of SdsR small RNA in Salmonella. *Nucleic Acids Res* **44**, 10406-10422 (2016).

48. Schindelin, J. et al. Fiji: an open-source platform for biological-image analysis. *Nat Methods* **9**, 676-82 (2012).

49. Ducret, A., Quardokus, E.M. & Brun, Y.V. MicrobeJ, a tool for high throughput bacterial cell detection and quantitative analysis. *Nat Microbiol* **1**, 16077 (2016).

50. Singh, P.K. et al. Vibrio cholerae Combines Individual and Collective Sensing to Trigger Biofilm Dispersal. *Curr Biol* **27**, 3359-3366 e7 (2017).

51. Hartmann, R. et al. BiofilmQ, a software tool for quantitative image analysis of microbial biofilm communities. 735423 (2019).

52. Ayachit, U. *The ParaView Guide: A Parallel Visualization Application*, (Kitware, Inc., 2015).

53. Donnell, Z. Regulation of cqsA and cqsS in Vibrio cholerae. (Princeton, NJ : Princeton University, 2015).

54. Frohlich, K.S., Papenfort, K., Berger, A.A. & Vogel, J. A conserved RpoS-dependent small RNA controls the synthesis of major porin OmpD. *Nucleic Acids Res* **40**, 3623-40 (2012).

55. Corpet, F. Multiple sequence alignment with hierarchical clustering. *Nucleic Acids Res* **16**, 10881-90 (1988).

56. Ashburner, M. et al. Gene ontology: tool for the unification of biology. The Gene Ontology Consortium. *Nat Genet* **25**, 25-9 (2000).
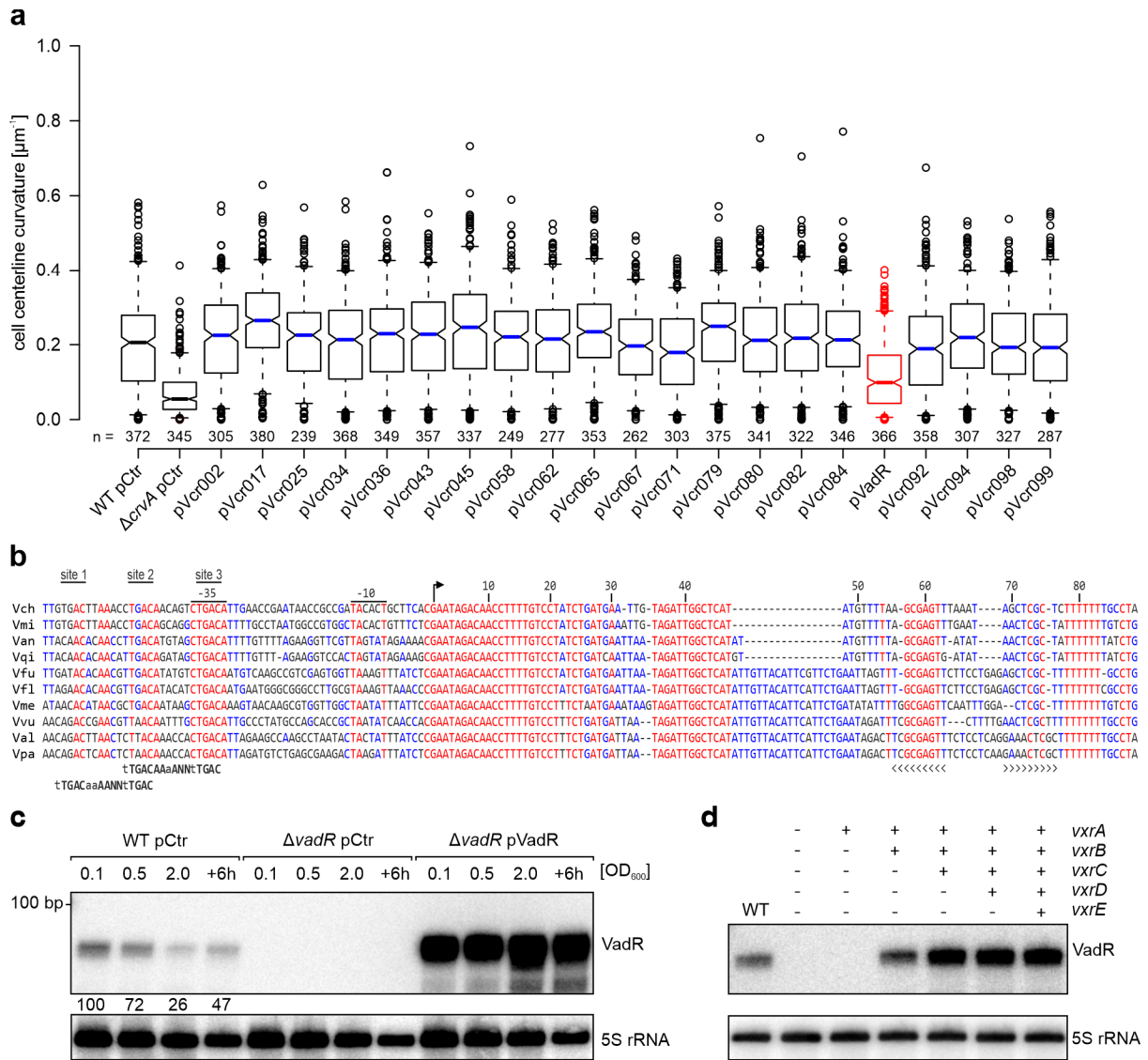
Figure 1

Figure 1: The VadR sRNA alters *V. cholerae* cell shape and is transcribed by VxrB
(a) Centerline curvature of *V. cholerae* cells expressing the indicated sRNAs (x-axis). The blue line indicates the median, boxes represent 25th and 75th percentiles, whiskers represent 5th and 95th percentiles and notches indicate 95% confidence intervals for each median. *n* of each set is listed above the x-axis. **(b)** Alignment of *vadR* and its promoter sequence from various *Vibrio* species. The -35 box, -10 box, TSS (arrow) and the Rho-independent terminator (brackets) are indicated. Putative VxrB binding sites and binding motifs (bold) are illustrated. **(c)** VadR expression throughout bacterial growth was tracked on Northern blots. *V. cholerae* wild-type or *vadR* mutant cells carrying either a control plasmid (pCtr) or a constitutive *vadR* overexpression plasmid (pVadR) were tested. **(d)** *V. cholerae* ΔvxrABCDE cells were complemented with various cistrons of the *vxrABCDE* operon and tested for VadR expression on Northern blots. Expression of the *vxrABCDE* fragments was driven by the inducible pBAD promoter (0.02 % L-arabinose final conc.) and exponentially growing cells were harvested (OD$_{600}$ of 0.2). A *V. cholerae* wild-type strain harboring an empty vector served as control. The experiment was performed with three independent biological replicates (*n* = 3).

Figure 2
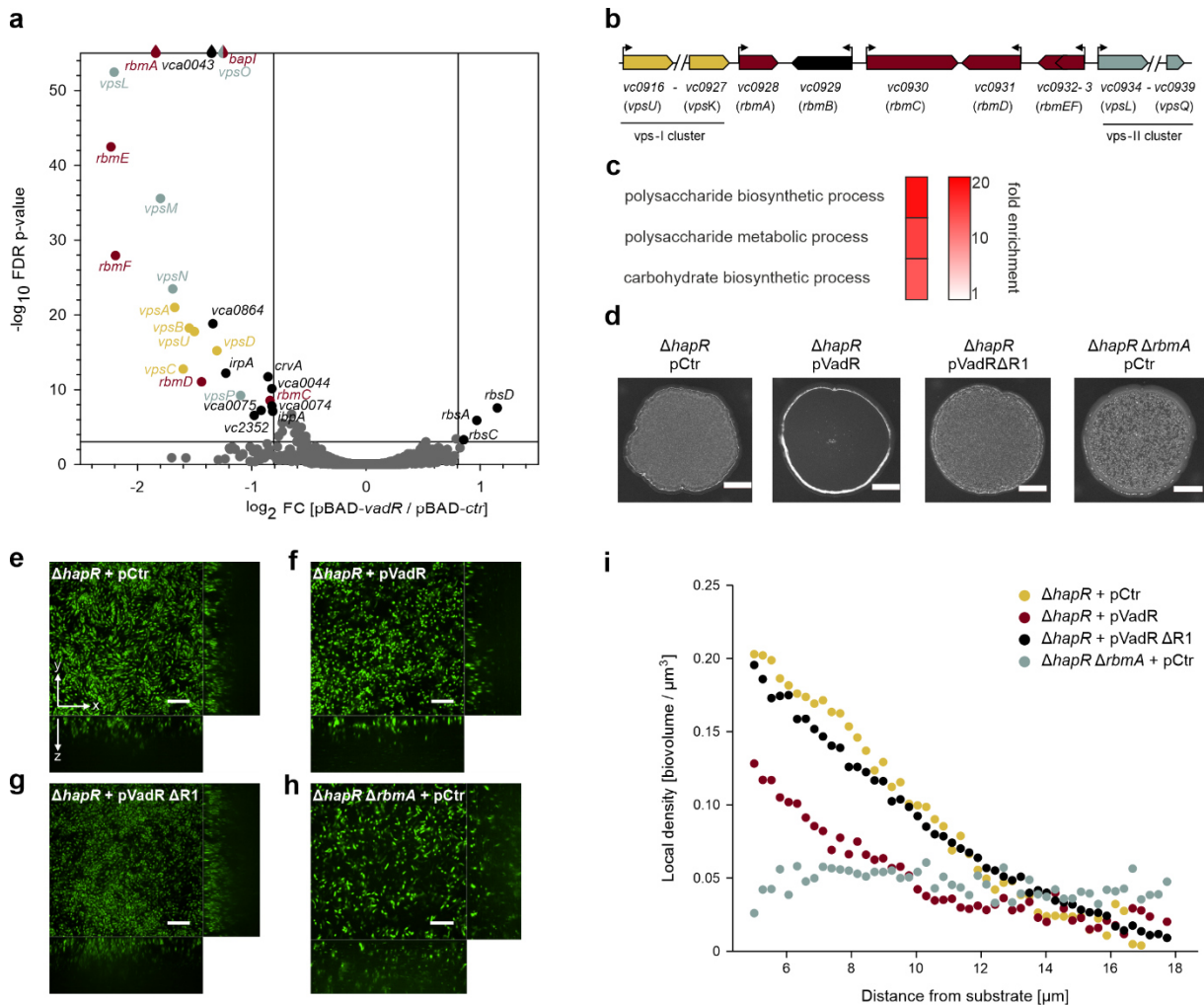
Figure 2: Target spectrum of VadR and its role in biofilm formation

(a) Volcano plot analysis showing differentially regulated genes after pulse induction of VadR. Genes with absolute fold changes ≥ 1.75 and an FDR corrected p-value of ≤ 0.001 were considered significantly expressed and are indicated. **(b)** Genomic context of the major biofilm cluster in *V. cholerae*. **(c)** Gene enrichment analysis of the differentially expressed genes shown in (a) using gene ontology analysis[56]. **(d)** Colony biofilm images of *V. cholerae* Δ*hapR* cells carrying the indicated plasmids. 5 μl of each strain were spotted on LB agar plates and incubated for 24h at room temperature before imaging. Scale bars = 2 mm. **(e-h)** Confocal Spin Disk Microscope images of biofilms (grown for 18 h) formed by *V. cholerae* Δ*hapR* cells carrying the following plasmids: (e) control plasmid, (f) *vadR* overexpression, (g) *vadR* ΔR1 overexpression. (h) A Δ*hapR*/Δ*rbmA* mutant harboring a control plasmid was used for comparison. The central images show bottom-up views, and the flanking images show vertical optical sections. Scale bars = 10 μm. **(i)** Local cell density as a function of distance from the substratum was plotted for each of the indicated strains using the BiofilmQ software[51].

Figure 3

Figure 3: VadR is a direct inhibitor of *crvA* and key biofilm transcripts
(a) Genes post-transcriptionally regulated by VadR. Fluorescence intensities of *E. coli* strains carrying the gene-specific reporters and the control plasmid (pCtr) were set to 1. Bars show mean of biological replicates ± SD, *n* = 4. **(b-e)** Prediction of RNA duplex formation between selected mRNAs and VadR. Numbers indicate the distances from the TSS for VadR and the start codons of the target mRNA sequences, respectively. Arrows indicate the mutations tested in (f-i). **(f-i)** Validation of the predicted mRNA-sRNA duplexes shown in (b-e) using compensatory base-pair mutations. Fluorescence levels of *E. coli* strains harboring an empty vector control (pCtr) were set to 1. Bars show mean of biological replicates ± SD, *n* = 6.
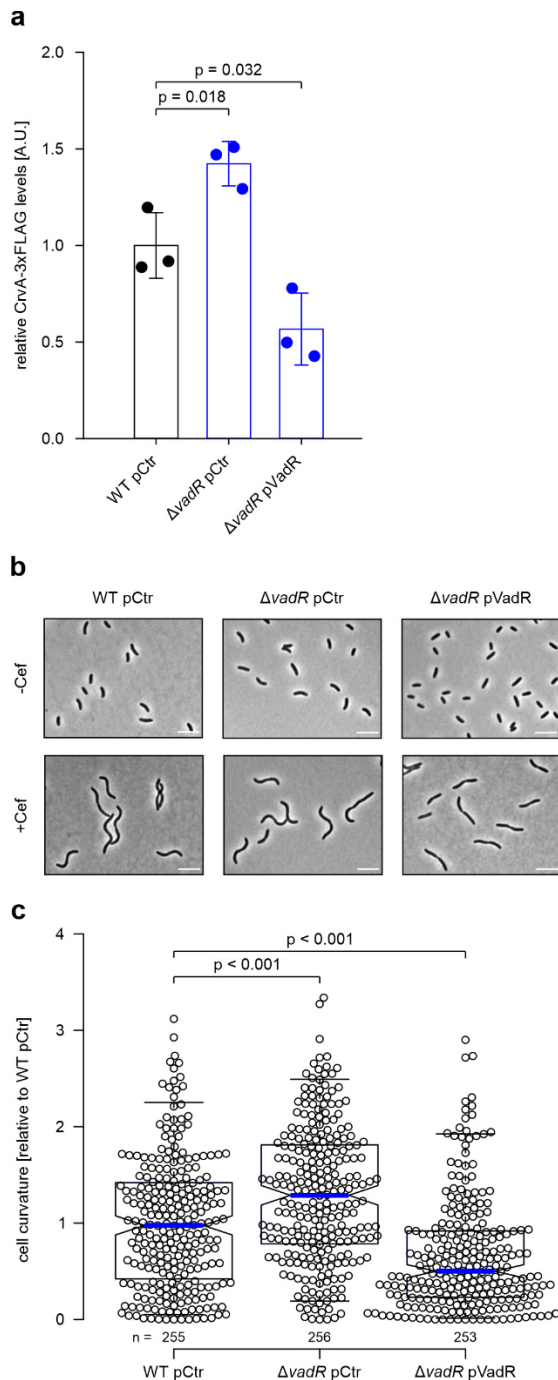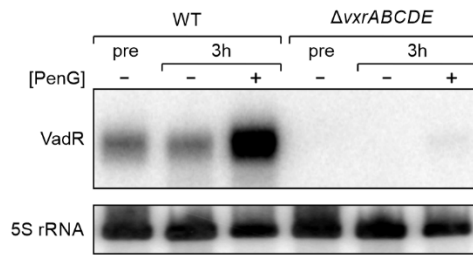
Figure 4

a

b

c

Figure 4: VadR modulates *V. cholerae* curvature by repressing CrvA

(a) Quantification of CrvA-3xFLAG protein levels in *V. cholerae* wild-type and *vadR*-deficient cells. Total protein samples of the indicated strains were harvested (OD_{600} of 0.5) and tested by Western blot analysis. CrvA-3xFLAG protein levels detected in the wild-type cells were set to 1. Bars show mean of biological replicates ± SD, *n* = 3. Statistical significance was determined using one-way ANOVA and post-hoc Holm-Sidak test. **(b)** Microscopy of cells used in (a; –Cef). A second set of cells was treated with cefalexin for 1h (+Cef) after reaching an OD_{600} of 0.5. Shown are representative fields of vision. Scale bars = 5 μm. **(c)** Analysis of cell centerline curvature in –Cef samples of (b). The curvature mean of wild-type cells was set to 1. A blue line indicates the median, boxes represent 25th and 75th percentiles, whiskers represent 5th and 95th percentiles and notches indicate 95% confidence intervals for each median. *n* of each set is listed above the x-axis. Statistical significance was determined using Kruskal-Wallis test and post-hoc Dunn's test.

Figure 5

a

b
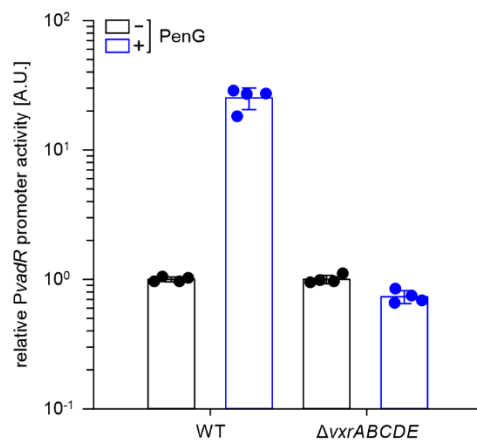
c
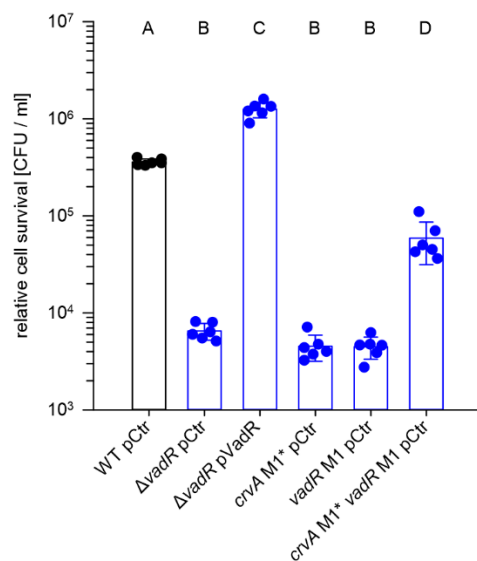
Figure 5: VadR mediates ß-lactam resistance through repression of CrvA

(a) *V. cholerae* wild-type and *vxrABCDE* mutant strains were grown to OD = 0.2 (pre) and split into two sets. One set was treated with penicillin G, while the other set received a mock treatment. After 3h, RNA was isolated and VadR expression was monitored by Northern analysis. **(b)** VadR promoter activity was tested under the same conditions as in (a) using a fluorescent transcriptional reporter. Promoter activities of mock-treated strains were set to 1. Bars represent mean of biological replicates ± SD, n = 4. **(c)** The indicated *V. cholerae* strains (x-axis) were grown to OD_{600} = 0.4 and treated with penicillin G for 3h. Survival after treatment was determined by counting colony forming units (CFUs). Bars represent mean of biological replicates ± SD, n = 6. Statistical significance was determined using one-way ANOVA and post-hoc Holm-Sidak test. Significantly different groups ($p < 0.01$) are labelled with corresponding letters.
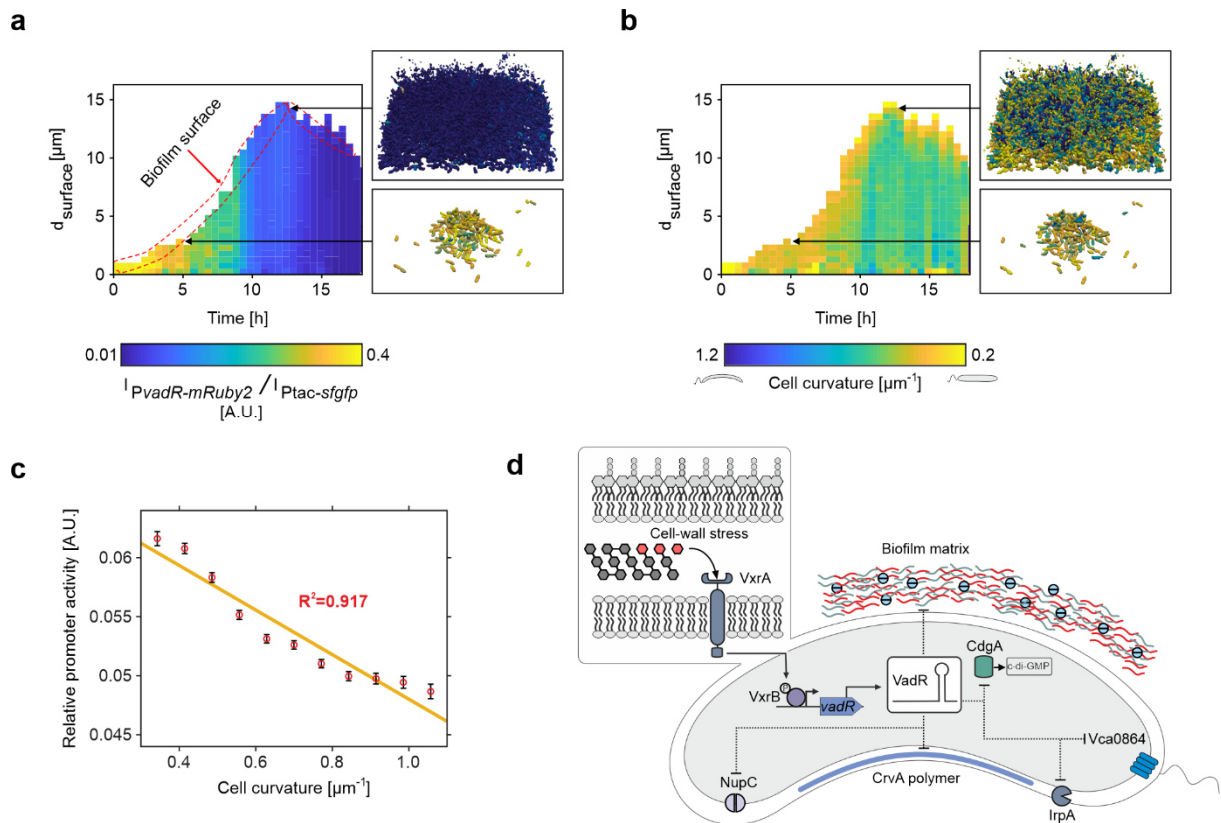
Figure 6

Figure 6: VadR controls cell curvature during biofilm development
(a) Relative activity of the *vadR* promoter during biofilm growth of *V. cholerae* wild-type. In each cell the fluorescence of mRuby2, expressed from the *vadR* promoter was normalized by the signal of the constitutive Ptac-promoter-driven sfGFP-fluorescence signal. Heatmap shows *vadR* promoter activity at both spatial (distance from surface of biofilm representing height of the biofilm) and temporal (time of biofilm growth) resolution. Subset of images show the cells from two time points and separate locations of the biofilm. These cells were rendered by ParaView[52] after final segmentation and analysis using BiofilmQ[51]. The color of each cell represents the activity of the *vadR* promoter. **(b)** Spatio-temporal heatmap showing cell curvature of each cell for *V. cholerae* biofilms. Cell curvature of individual cells was calculated using BiofilmQ[51]. To calculate the cell curvature of each cell inside the biofilms, similar positions of the biofilm as in (a) were selected for rendering. In these subset of images, the color represents the cell curvature of each cell. **(c)** A correlation graph was plotted for *vadR* promoter activity as function of cell curvature. Calculation of *vadR* promoter activity and cell curvature was done for *V. cholerae* wild-type biofilms grown in flow chambers. Each point represents >1000 cells for given time point in a biofilm. The error bars for each point correspond to the standard error. **(d)** Model showing the regulatory functions of the VadR sRNA in *V. cholerae*. Expression of *vadR* sRNA is controlled by the VxrAB two-component system. The sRNA regulates multiple biological processes, including cell shape and biofilm formation.

4 A conserved RNA seed-pairing domain directs small RNA-mediated stress resistance in enterobacteria

The full-text article is available online at:

https://www.embopress.org/doi/10.15252/embj.2019101650

The supplementary data is available online at:

https://www.embopress.org/action/downloadSupplement?doi=10.15252%2Fembj.2019101650&file=embj2019101650-sup-0001-Appendix.pdf

The corresponding source data files are available online at:

https://www.embopress.org/doi/10.15252/embj.2019101650

5 Concluding discussion

Parts of this chapter are adapted from:

Herzog R, Peschek N, Fröhlich KS, Schumacher K, Papenfort K. Three autoinducer molecules act in concert to control virulence gene expression in *Vibrio cholerae*. Nucleic Acids Res. 2019;47(6):3171-3183. doi:10.1093/nar/gky1320

Herzog R*, Peschek N*, Singh PK, Fröhlich KS, Schröger L, Meyer F, Bramkamp M, Drescher K, Papenfort K. RNA-mediated control of cell shape modulates antibiotic resistance in *Vibrio cholerae*. Manuscript

*these authors contributed equally to the work

Peschek N, Hoyos M, Herzog R, Förstner KU, Papenfort K. A conserved RNA seed-pairing domain directs small RNA-mediated stress resistance in enterobacteria. EMBO J. 2019;38(16). doi:10.15252/embj.2019101650

5.1 The role of the DPO pathway in *V. cholerae*

Cholera disease remains a major threat to human health in developing countries [82]. The pathogenicity of *V. cholerae* is primarily controlled by the bacterial communication process known as QS, which is based on the production, release, and subsequent recognition of AI molecules. Unlike many other enteric pathogens, *V. cholerae* produces virulence factors at low cell densities and shows reduced pathogenic behaviors in dense cultures with high AI concentrations. Thus, AI molecules are ideal candidates for alternative and highly-specific therapeutic strategies against *V. cholerae* infections. Indeed, a stable CAI-1 analog was already described as a potent repressor of virulence factor production [189]. However, understanding the underlying signal transduction pathway of an AI, its impact on pathogenic group behaviors, and its potential side-effects in other bacteria, are key requirements for its use as a therapeutic drug. This work revealed new insights into the DPO pathway and its biological functions in *V. cholerae* (chapter 2).

5.1.1 Post-transcriptional control of the *aphA* messenger

DPO is the most recently discovered AI molecule in *V. cholerae*. It is sensed by the cytoplasmic transcription factor VqmA, and the only validated target site of activated VqmA is a quasi-palindromic sequence in the promoter region of *vqmR* [1], [102], [190]. VqmR is an Hfq-dependent sRNA, and at the beginning of this work, VqmR has been characterized as a direct repressor of eight mRNAs [1]. One of these encodes for the biofilm master regulator VpsT, and induced VqmR expression inhibits biofilm formation in *V. cholerae* [1], [74]. In this work, the regulon of VqmR was extended by five mRNAs (chapter 2, Table 1). One of these transcripts encodes for the QS master regulator at LCD, AphA, which governs virulence factor production in *V. cholerae*. In contrast to all other VqmR targets, *aphA* regulation occurs independently of the two highly conserved base-pairing regions R1 and R2 of VqmR. Instead, VqmR uses a third conserved binding site (R3) located in the single-stranded region of its Rho-independent terminator stem-loop to block *aphA* translation by base-pairing with the RBS (chapter 2, Figure 2).

In accordance with this new regulatory link, the deletion of *vqmR* resulted in elevated AphA levels at late exponential and stationary growth phases (chapter 2, Figure 3A). At LCD, the lack of *vqmR* did not affect *aphA* mRNA and protein abundances, and only the overexpression or DPO-mediated induction of VqmR in this growth phase markedly reduced AphA levels (chapter 2, Figures 3A, C). These observations are in line with our understanding of the QS mode at LCD, in which the Qrrs are highly expressed, whereas VqmR levels are relatively low. Indeed, the Qrr4 sRNA, which is the most abundant Qrr sRNA in *V. cholerae*, accumulated to > 900 copies/cell in an LCD-locked *V.*

harveyi strain [73], [124]. In contrast, the calculated abundance of VqmR at LCD was approximately 100 copies/cell in *V. cholerae* [1]. VqmR and the Qrr2-4 sRNAs reciprocally regulate *aphA* at the post-transcriptional level and in an Hfq-dependent manner (chapter 2, Figure S1B and [110]). Thus, at LCD, the Qrrs and the *aphA* mRNA are assumed to be frequently bound to Hfq in order to facilitate sRNA-mRNA duplex formations.

Another explanation for the ineffective regulation of *aphA* through VqmR at LCD could be that the Qrrs render the *aphA* transcript less susceptible to VqmR base-pairing. The mechanism of Qrr-mediated activation of *aphA* in *V. cholerae* is not fully understood. Data from post-transcriptional reporter assays indicated that the Qrr2-4 sRNAs use a conserved base-pairing region, which is absent in Qrr1, to target a conserved sequence element in the far upstream region of the *aphA* 5' UTR (chapter 2, Figure S5 and [110]). It was hypothesized that the 5' UTR of *aphA* folds into a stable hairpin structure, which potentially sequesters the RBS and thus blocks *aphA* translation. However, this hypothesis could not be validated experimentally [110]. Alternatively, the Qrr2-4 sRNAs could increase the stability of the *aphA* transcript, for example, through additional recruitment of Hfq or other chaperones or by blocking nuclease cleavage sites. The recruitment of additional factors to the TIR of *aphA* could potentially prevent the duplex formation between *aphA* and VqmR.

With increasing cell density, AIs accumulate. Once a threshold is reached, the Qrrs are no longer transcribed, and HapR is made. HapR represses AphA on the transcriptional level, however, additional post-transcriptional inhibition of *aphA* via VqmR is required to successfully switch to a full QS output at HCD (chapter 2, Figure 5). Multiple feedback loops exist in the QS system of *V. cholerae* to keep all regulators in a balanced state, to ensure rapid transitions from LCD to HCD, or from HCD to LCD QS mode (chapter 1, Figure 4). Interestingly, no autoregulatory feedback loops were identified for either VqmA or VqmR. Given that VqmR is a highly abundant sRNA at HCD with a half-life of > 32 min [1], it seems inevitable that the cell needs to adjust either VqmR levels or VqmR's ability to regulate *aphA*, in order to quickly switch from an HCD to an LCD state. Besides the hypothesized roles of the Qrrs and the *aphA* 5' UTR in this regard, it is also possible that VqmR autoregulates its levels upon binding to *aphA*. More precisely, VqmR base-pairing via the R3 region could partially or even fully open the Rho-independent terminator stem-loop of VqmR (chapter 2, Figure 2A), which is an important factor for sRNA stability [191], [192].

The Rho-independent terminator stem-loop of VqmR consists of one A-U and six G-C base-pairs, which is sufficient to protect the sRNA from 3' → 5' exonucleolytic decay through PNPase and

RNase II [1], [193]. VqmR is also protected from the 3' → 5' exonuclease RNase R since binding of this RNase requires an extended single-stranded region at the 3' end of an RNA, which is not present in VqmR [194]. However, *in vitro* experiments demonstrated that stem-loop structures of only five or less G-C base-pairs do not protect from PNPase [193]. Thus, if one or more of the nucleotides 138-144 of VqmR base-pair with *aphA* as predicted (chapter 2, Figure 2D), VqmR could be rendered accessible for degradation through PNPase. Indeed, it was previously demonstrated that PNPase removes a Rho-independent terminator *in vivo*, and further, that PNPase is the major nuclease of Hfq-unbound sRNAs [49], [195]. An extensive pairing between the terminator loop of VqmR and *aphA*, as it was bioinformatically predicted (chapter 2, Figure 2D), could break open the whole terminator stem-loop and thus additionally allow decay through RNase II and RNase R.

A well-studied example of an sRNA that opens its 3' hairpin structure to regulate a target RNA is RNA I encoded on the plasmid ColE1. RNA I is expressed on the opposite strand of its target RNA, RNA II, which in its processed form, functions as a primer for plasmid replication [196], [197]. Hybridization of RNA I to RNA II prevents primer maturation and thus inhibits the replication of the plasmid [196], [197]. Binding of RNA I to RNA II is a multi-step process. Initially, the complementary single-stranded regions in the hairpin structures of both RNAs form transient duplexes. Next, the unstructured 5' sequence of RNA I anneals to its complementary sequence in RNA II. In a third step, the pairing propagates progressively, causing the unfolding of all hairpin structures and resulting in a perfectly aligned RNA-RNA duplex [198]. In contrast to VqmR, RNA I in its hybridized state with RNA II lacks a single-stranded 3' sequence, which could serve as a template for 3' → 5' exonucleases. To remove RNA I, its 3' end is polyadenylated by the enzyme PAP1, thereby facilitating exonucleolytic decay through PNPase and RNase II [199]–[201]. Notably, the decay of RNA I is initiated by endonucleolytic cleavage close to the 5' end through RNase E [202].

To summarize, VqmR could become subject to rapid sRNA turnover as soon as it binds to the *aphA* messenger since this interaction could facilitate 3' → 5' exonucleolytic decay. This type of regulation could contribute to a fast transition of a population from HCD to LCD QS mode. Interestingly, a similar mechanism, in which only the sRNA regulator is degraded upon binding to *aphA*, was previously suggested for the Qrr3 sRNA in *V. harveyi* [124]. Further research is required to elucidate the fate of the Rho-independent terminator stem-loop of VqmR upon base-pairing to *aphA* and to identify the enzymes involved in the turnover of both RNAs.

5.1.2 DPO-dependent gene regulation in *V. cholerae*

Bacteria constantly perceive and integrate information from their environment. To track their own cell numbers and the overall abundance of foreign cells, bacteria sense intra- and interspecies AI molecules, respectively. In *V. cholerae*, CAI-1 fulfills the function as an intragenus communication signal since homologs of its synthase and receptor are only present in *Vibrios* and a limited number of other genera [91], [92]. AI-2 is produced and detected by many genera, and thus, acts as an interspecies AI signal [93]. The scope of DPO in bacterial signaling is not yet fully understood. It shows characteristics of both, an intraspecies as well as an interspecies communication signal since the cognate DPO receptor protein, VqmA, seems to be a *Vibrio*-specific factor, whereas the synthase Tdh is a ubiquitous enzyme [74].

It was previously shown that binding of CAI-1 to its receptor, CqsS, has a greater impact on QS activation than AI-2 binding to LuxPQ [91], [203]. However, it was not known how these two AIs and the DPO system contribute to the overall QS output of *V. cholerae*. In this work, the impact of every single AI molecule and all possible AI combinations on the transcriptome of *V. cholerae* was investigated (chapter 2, Figure 6). Several conclusions can be drawn from this analysis. First, CAI-1 is the most potent AI, followed by DPO and AI-2. Second, combinations of AIs increase the number of regulated genes. Third, the spectrum of regulated genes of the two QS pathways, i.e., the shared CAI-1/AI-2 and the DPO pathway, largely overlap. The latter observation can be explained by the fact that all AIs lead to the repression of *aphA*, and consequently, to the activation of HapR (chapter 2, Figure 1). It seems likely that HapR is responsible for the differential expression of most of the genes in the AI RNA-seq experiment. This hypothesis is in line with the results of a previous study, in which the transcriptomes of *V. cholerae* wild-type and *hapR* mutant cells were analyzed at stationary growth phase [119]. Almost half of the differentially expressed genes (46 %) were also differentially regulated in our AI RNA-seq experiment. The homolog of HapR in *V. harveyi* is LuxR, and its regulon was shown to include 625 genes [225]. According to the KEGG database (https://www.kegg.jp/kegg/kegg2.html), 395 different homologs of these genes exist in the genome of *V. cholerae.* Interestingly, only ≈ 16 % of these genes were differentially expressed in our RNA-seq analysis of AI functions in *V. cholerae*. The low number of overlapping genes can be explained by the distinct life-cycles of *V. cholerae* and *V. harveyi*, which require species-specific QS-mediated responses in different ecological niches. Further, it was demonstrated that CAI-1 modestly increases VqmR levels (chapter 2, Figure 5), which explains why VqmR, and all of its known targets that were captured in the RNA-seq analysis, were also regulated in the presence of this AI.

Indeed, only four out of the 420 differentially expressed genes were significantly regulated (> 2-fold, FDR corrected p-value ≤ 0.01) by DPO, but not by either CAI-1, AI-2, or both. These four genes were *vibA* (encoding a vibriobactin-specific 2,3-dihydro-2,3-dihydroxybenzoate dehydrogenase), *malS* (encoding an alpha-amylase), *vca0888* (encoding a LuxR-type transcription factor), and *putP* (encoding a sodium/proline symporter)(Figure 8A). The *vibA* and *malS* transcripts were significantly increased upon treatment with DPO. However, this regulation was lost in combination with other AIs. In the case of *malS*, upregulation was also observed in the presence of CAI-1 (+1.95-fold) and AI-2 (+1.69-fold). The *putP* mRNA was consistently down-regulated in all DPO-treated cultures, but it was also affected by the combination of CAI-1 and AI-2 (-1.88-fold). In *V. cholerae*, *putP* is cotranscribed with the *putA* gene in the bicistronic *putAP* operon [204]. Since *putA* mRNA levels did not significantly change under any tested AI condition, DPO-mediated transcriptional regulation of *putP* via VqmA seems unlikely. Although *putP* was not differentially regulated in the transcriptome analysis of VqmR-overexpressing cells (chapter 2, Table 1), post-transcriptional control through VqmR can not be fully excluded, since the experimental setup was different in the AI experiment. More precisely, cells were tested at different densities (OD$_{600}$ of 0.5 vs. 0.2) and in different media (LB vs. M9 minimal medium), which could both affect *putAP* expression and VqmR-mediated regulation.
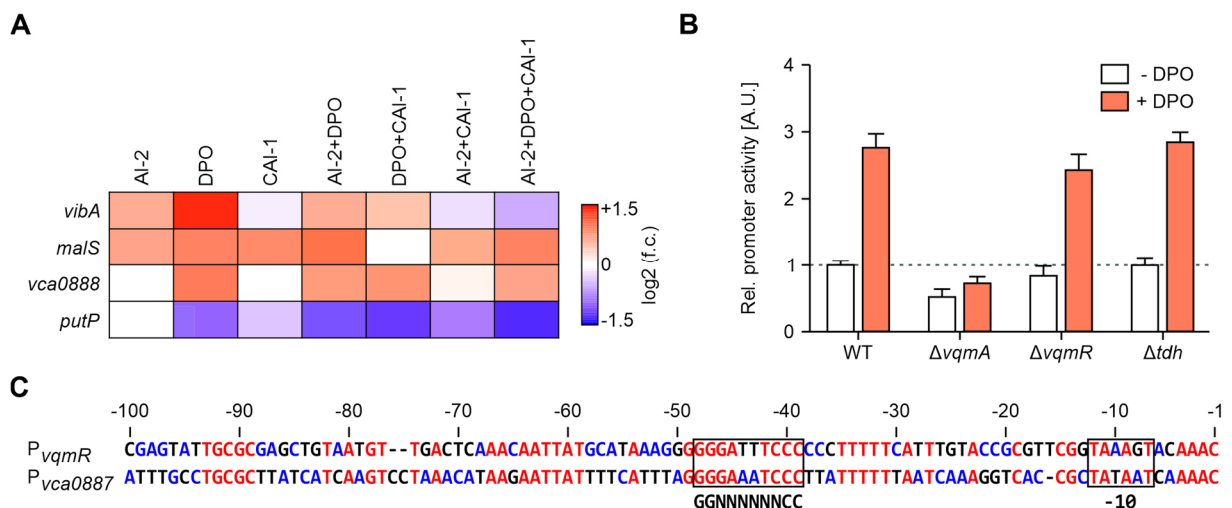
Figure 8 DPO-specific gene regulation in *V. cholerae*. A) The heatmap displays genes that were significantly regulated by DPO but not by CAI-1 or AI-2 in the global transcriptomic analysis of *chapter 2, Figure 6*. B) A transcriptional reporter of the *vca0887-0888* operon was tested in the indicated *V. cholerae* strains. Measurements were conducted after 16h of bacterial growth in L-threonine-free medium, in the presence or absence of DPO (100 µM final conc.). Error bars show SD of three biological replicates. Figure was adapted from [205] C) Alignment of the promoter regions of *vqmR* and *vca0887-0888.* Numbers illustrate the relative distance to the transcriptional start site of *vca0887-0888*. The putative VqmA binding sites and the -10 boxes are boxed.

In contrast to the other three mRNAs, *vca0888* was exclusively as well as consistently up-regulated by DPO. Similar to *putP*, *vca0888* is the second gene of a bicistronic operon. The first gene, *vca0887*, is annotated as a pseudogene and was therefore not included in the RNA-seq analysis. VqmR overexpression did not affect *vca0888* mRNA levels. Interestingly, *vca0888* was shown to be > 20-fold upregulated in *V. cholerae* cells that constitutively overexpressed VqmA [206]. To test if VqmA controls the *vca0887-0888* operon, a plasmid-based transcriptional reporter of this operon was analyzed in *V. cholerae* wild-type and single deletion mutants of the DPO-system (Figure 8B) [205]. In the absence of DPO, the promoter activity in the *vqmA* mutant was ≈ 2-fold decreased when compared to the other strains. The addition of DPO significantly increased the promoter activity by a factor of approximately 2.5 in the wild-type, Δ*vqmR*, and Δ*tdh* strains, however, it did not change in the *vqmA* mutant, indicating that VqmA is indeed a transcription factor of the *vca0887-0888* operon. So far, the promoter of *vqmR* is the only validated binding site of VqmA. A recently solved crystal structure for the DPO-VqmA-DNA complex revealed that VqmA recognizes a $GG(N)_6CC$ motif in the promoter region of *vqmR*, which also exists in the promoter of the *vca0887-0888* operon (Figure 8C) [102].

Together, these data strongly support the hypothesis that VqmA binds to and activates the promoter of the *vca0887-0888* operon. Initial experiments indicated that the *vca0887* pseudogene encodes two protein products: a truncated protein as it was expected from the *vca0887* DNA sequence and a less abundant full-length protein [205]. The latter shares 61 % amino-acid identity to the HchA protein of *E. coli*, an enzyme that converts toxic methylglyoxal to D-lactate [207]. Methylglyoxal (MGO) is formed by the oxidation of aminoacetone (AA), which is a by-product of catabolic L-threonine degradation and a precursor molecule of DPO [74], [208]. Thus it is tempting to speculate that high DPO levels could correlate with high levels of MGO and that VqmA-mediated activation of the *vca0887* gene could reduce the levels of toxic MGO. However, this function of the Vca0887 full-length protein could not yet be demonstrated experimentally [205]. It will be of considerable interest to investigate whether one or both of the Vca0887 protein variants are functional and eventually involved in L-threonine metabolism. Moreover, it should be studied how the uncharacterized LuxR-type transcription factor Vca0888, which lacks homologs outside the *Vibrio* genus, intertwines with the QS system of *V. cholerae*.

The conversion of AA to MGO could be prevented by a condensation reaction between AA and an activated L-alanine molecule, yielding linear *N*-alanyl-aminoacetone (Ala-AA) [74]. Ala-AA is a proposed intermediate in the DPO pathway and suspected to convert spontaneously into DPO

upon intramolecular cyclization and subsequent dehydration, tautomerization, and oxidation [74]. In line with this proposed mechanism, supplementation of a *tdh* deletion mutant with Ala-AA resulted in the concentration-dependent activation of VqmA and the *vqmR* promoter [74]. However, unpublished data of isotope-labelling experiments did not confirm the role of Ala-AA as the precursor molecule of DPO. Instead, the data indicated that Ala-AA binds and thereby activates VqmA directly in its linear form [209]. Furthermore, Ala-AA most likely occupies the same binding-pocket on VqmA as DPO, but with a weaker affinity than DPO [209]. Both ligands of VqmA lead to the activation of the *vqmR* promoter with comparable strength. Thus, it seems unlikely that the binding of either DPO or Ala-AA causes differential structural rearrangements of VqmA that would direct VqmA to different promoter sites. It will be interesting to test whether DPO and Ala-AA accumulate at different stages of growth or in different environments, thereby activating VqmA in distinct contexts.

VqmA is a LuxR-type transcription factor. Recent results suggest that, in contrast to other LuxR-type QS receptor-transcription factors, VqmA does not require the presence of a ligand to fold properly and to bind DNA [209]. Indeed, basal *vqmR* promoter activity was observed in a *tdh* but not in a *vqmA* deletion background [209]. In the same vein, VqmR accumulates to low levels in a *V. cholerae tdh* mutant strain and is not detectable in a *vqmA*-lacking strain (chapter 2, Figure 2B). Nevertheless, given the low abundance of VqmR in the absence of DPO, it seems unlikely that the basal activity of VqmA results in significant changes in global gene expression. Instead, it can be hypothesized that the properly folded structure of VqmA in the absence of ligands accelerates the switch from LCD to HCD QS mode. Recently, the structure of VqmA was also demonstrated to change in response to ligand-independent cues, i.e., oxygen and bile salts [210]. In this unpublished study, VqmA formed intermolecular disulfide bonds under anaerobic conditions and in the presence of DPO. Intermolecular disulfide bonds increased DPO-VqmA-mediated activation of the VqmR promoter, but they were disrupted in the presence of bile-salts. Under aerobic conditions, VqmA formed intramolecular disulfide bonds, which decreased VqmA activity [210]. Interestingly, it was also shown that CAI-1 is not produced in the absence of oxygen [210]. This implies that, in contrast to our *in vitro* transcriptomic analyses under aerobic conditions, CAI-1 could play only a minor role in the anaerobic environment of the human small intestine. Besides an anaerobic environment, *V. cholerae* also encounters bile salts in the human small intestine. Anaerobic conditions and bile salts show antagonistic effects on the activity of VqmA. The concentration of bile salts is higher in the intestinal lumen than in the vicinity of the intestinal villi, which are colonized by *V. cholerae* in the course of host infection [118]. Thus, it can be speculated

that the inhibitory effect of bile on the activity of VqmA is strongest in early phases of infection, whereas in later stages, VqmA activity is boosted by a low concentration of bile and high levels of DPO.

5.1.3 On the role of DPO and pyrazines as interspecies communication signals

The results of the transcriptome analysis of AI functions in *V. cholerae* demonstrated that intragenus communication via CAI-1 outranks interspecies communication via AI-2 in terms of global gene regulation. DPO, which is also produced by *E. coli* and potentially many other bacteria, was ranked between CAI-1 and AI-2 [190]. It was previously hypothesized that the commensal bacterium *Blautia obeum* (formerly known as *Ruminococcus obeum*) also produces DPO [190]. This hypothesis was based on the observation that co-cultivation of *B. obeum* and *V. cholerae* in mice restricted *V. cholerae* colonization, and this effect was mediated by VqmA [211]. The authors of this study also compared the transcriptomes of *V. cholerae ΔluxS* cells that were obtained from fecal samples of mice, which were either mono-colonized with *V. cholerae ΔluxS* or co-colonized with *V. cholerae ΔluxS* and *B. obeum* [211]. In this RNA-seq analysis, VqmA was > 25-fold upregulated in the co-cultivated cells. However, at that time, VqmR was not yet discovered and consequently missing in the analysis. Moreover, the translational start site of *vqmA* was still misannotated in the reference genome [1]. Indeed, a re-analysis of the RNA-seq dataset revealed that *vqmA* was not differentially expressed during the co-cultivation experiment, but *vqmR*, which was the strongest regulated gene (Table 1).

High levels of VqmR could mediate the observed colonization defect of *V. cholerae* by repressing *aphA* and *vpsT*. Notably, the numbers of *Vibrio*-specific reads obtained from the fecal samples of co-colonized mice were low. In fact, *aphA* was the only direct target of VqmR that could be included in the analysis since the *aphA* locus was covered by at least ten unique gene reads in every sample, which was set as a cutoff to obtain reliable results. Interestingly, *aphA* was not differentially expressed, despite the high levels of VqmR. An explanation for this result could be that *V. cholerae ΔluxS* accumulates to higher cell numbers in the mono-colonized mice than in mice that were pre-colonized with *B. obeum*. Thus, the concentration of the intragenus and most potent AI, CAI-1, could be higher in the small intestines of mono-colonized mice, leading to the increased production of HapR. HapR-mediated repression of *aphA* in mono-cultivated *V. cholerae* cells could mask the regulatory effect of VqmR on *aphA* in co-cultivated *V. cholerae* cells when the transcriptomes of both groups are compared. Indeed, *hapR* levels in co-cultivated *V. cholerae* cells were mildly reduced (-1.91-fold, FDR p-value = 0.01) when compared to mono-cultivated *V.*

cholerae. Besides VqmR, several other transcripts were also highly upregulated in the presence of *B. obeum* (Table 1). However, none of these were differentially expressed in the presence of DPO, CAI-1, or AI-2 (chapter 2, Table S1), indicating that their expression could be induced by QS-unrelated factors produced by *B. obeum* or in response to the competition with *B. obeum* for limited nutrients and co-factors.

Table 1 Differentially expressed genes in co-cultivated *V. cholerae* cells compared to mono-cultivated cells.

Gene	Description[a]	Fold change[b]
vqmR	Small regulatory RNA[c]	+72.55
vca0700	Endo-chitodextinase	+10.66
vc1096	Glyceraldehyde-3-phosphate dehydrogenase	+10.24
wbeG	RfbG protein	+10.06
nfo	Deoxyribonuclease IV	+5.79
vca0547	Hypothetical protein	+5.30
bfr	Bacterioferritin	+5.28
vca0963	Hypothetical protein	+4.80

[a]Description based on the annotation at KEGG (https://www.kegg.jp/kegg/kegg2.html)

[b]Fold change obtained by EDGE analysis as described in the Methods section of chapter 3. Raw data were obtained from the European Nucleotide Archive with the accession number PRJEB6358. Sample Vc1Ro2.m2 was excluded from the analysis due to the low number of total reads. A read minimum per gene was set to ≥ 10. Genes that were at least 4-fold differentially regulated and statistically significant (FDR-adjusted p-value ≤ 1E-07) are listed.

[c]Not annotated at KEGG. Identified by differential RNA-seq [1]

A recent study further fuelled the hypothesis that the synthesis of DPO is widespread among bacteria [212]. Spent media from various Gram-negative and Gram-positive bacteria, including important human pathogens like *Klebsiella pneumoniae*, *Pseudomonas aeruginosa*, *Salmonella Typhimurium*, and *Staphylococcus aureus*, were analyzed by mass spectrometry. In all investigated media, a peak corresponding to the mass of DPO was detected [212]. Importantly, the DPO peak is indistinguishable from the peak of a novel pyrazin-based AI molecule identified in the same study in enterohemorrhagic *E. coli*. This molecule is 3,6-dimethylpyrazin-2-ol and referred to as AI-3 [212]. Like DPO, AI-3 derives from the catabolic degradation of L-threonine to AA through Tdh. However, AI-3 is formed by the head-to-tail condensation of two AA molecules, in contrast to DPO, which assembles from one AA and one L-alanine molecule [190], [212]. It was assumed that AI-3 binds to the QseC receptor in *E. coli*, which activates the response regulator QseB. Indeed, the addition of AI-3 induced QseB/C-dependent changes in gene expression [212].

Although structurally highly related, these changes were not observed when DPO was added [212]. Noteworthy, the tested DPO concentration was 5 nM, which was already demonstrated to be insufficient to activate the *vqmR* promoter in a VqmA-dependent manner in *V. cholerae* [190]. The signal-sensing domain of QseC shows a high degree of conservation among different bacteria. Hence, it will be exciting to test whether DPO is recognized by QseC at higher concentrations, which would establish the role of pyrazines as interspecies communication signals. To this end, it should also be investigated whether AI-3 is another ligand of VqmA.

5.2 The role of sRNAs in the cell envelope stress response of *V. cholerae*

Maintenance of cell envelope homeostasis is a crucial and constant task for bacteria. Multiple stress response systems have evolved to adequately adapt to and counteract a variety of cell envelope-damaging cues. Commonly, these systems employ either an alternative sigma factor or a TCS to activate beneficial genes on a global scale. In addition to transcriptional regulators, the functionality of well-studied systems, for example, the Sigma E, Sigma S, Cpx, and Rcs stress response systems of *E. coli*, also critically depend on the action of one or more sRNAs [213]. However, why are sRNAs so frequently involved in stress response systems, and what are their advantages over transcriptional regulators? One apparent reason is that sRNAs build an additional, post-transcriptional, layer of regulation. Transcriptional regulators can only affect the rate of *de novo* transcription, but they have no control over the fate of existing mRNAs. However, under cell envelope stress, it is of utmost importance to prevent the ongoing synthesis of unfavorable proteins, which would further impair cell envelope integrity. sRNAs specifically block the translation of these unwanted transcripts and promote their nucleolytic decay. Thus, to achieve full repression of a target gene, combinations of transcriptional repressors and sRNAs are required [214]. Regarding the derepression of targets upon stress relief, sRNAs provide superior dynamics compared to transcription factors [215]. Given that sRNAs often undergo coupled degradation with their respective target mRNAs, they are rapidly removed after the stress-inducing signal disappeared [21]. This work revealed that, like in *E. coli*, stress response systems in *V. cholerae* depend on sRNAs. More precisely, the VadR sRNA was characterized as a critical VxrAB-controlled regulator to endure β-lactam stress (chapter 3), and the MicV sRNA was demonstrated to function cooperatively with VrrA in the σ^E response (chapter 4).

5.2.1   The VadR sRNA is a regulator of cell shape and biofilm formation and increases antibiotic tolerance

The current work identified the VadR sRNA as an Hfq-dependent base-pairing sRNA in *V. cholerae*, which is strictly controlled by the VxrB response regulator of the VxrAB TCS (chapter 3, Figures 1D and S1). The sensor histidine kinase of this system, VxrA, is activated under cell wall-damaging conditions by an unknown factor. Phosphorylated VxrB positively autoregulates the *vxrABCDE* operon and additionally affects the expression of > 300 genes [170]. Given the high number of regulated genes, it is not surprising that multiple phenotypes and biological processes were linked to the VxrAB system. Specifically, VxrB was described as a positive regulator of biofilm formation, type VI secretion, and peptidoglycan synthesis [170], [172], [186], [187]. Importantly, the functionality of the VxrAB system is not restricted to cell wall-damaging conditions. For example, a *V. cholerae vxrB* deletion mutant shows significantly decreased activation of the VPS-II gene cluster during exponential growth in standard LB media [187]. Under the same conditions, *vxrB* mutant cells display a marked increase in cell diameter, which indicates that Vxr-mediated peptidoglycan synthesis is also a house-keeping function. Likewise, VxrB-mediated expression of VadR occurs throughout bacterial growth in LB medium (chapter 3, Figure 1C). Consequently, the VadR sRNA was studied in two contexts: Under standard culturing conditions and in the presence of penicillin G (PenG), a β-lactam antibiotic that inhibits cell wall synthesis and which is a known activator of the VxrAB stress response [170]. This work revealed that VadR fulfills key roles in both contexts, as a regulator of biofilm formation and cell shape.

The periplasmic polymer CrvA is the structural determinant of the comma-shaped morphology of *Vibrios* [153]. It was hypothesized that QS controls *crvA* expression since cell curvature increases in a cell density-dependent manner. However, the results obtained from AI supplementation experiments and strains lacking AI synthases were not entirely conclusive [153]. Indeed, the presence of CAI-1, AI-2, or DPO, or any combination of these molecules, showed no significant effect on *crvA* mRNA levels (chapter 2, Figure 6). The present work identified the QS-independent VadR sRNA as the first direct regulator of *crvA* expression. VadR uses its conserved 5' seed sequence to base-pair with the RBS of *crvA*, and thus, reduces CrvA synthesis (chapter 3, Figures 3B, F, and 4A). Chromosomal deletion of *vadR* caused increased cell bending, whereas overexpression of VadR led to the opposite effect (chapter 3, Figures 4B, C).

The cell shape of a bacterium is also an important determinant for the formation of biofilms [148]–[150]. In growing *V. cholerae* biofilms, it was observed that the cells had lost their characteristic

curved-rod morphology, and instead, assembled as relatively straight rods [151]. This phenotype can now be explained by means of the VadR sRNA, which reduces cell curvature by blocking the synthesis of CrvA (chapter 3, Figure 4). Moreover, the VadR promoter was most active in the initial phase of biofilm formation and inactive in mature biofilms (chapter 3, Figure 6A). Simultaneous tracking of the cell curvature state of every single cell in the developing biofilm revealed a pronounced negative correlation of the VadR promoter activity and cell curvature (chapter 3, Figures 6B, C). VadR not only affects the morphology of cells within a biofilm, but it also regulates the process of biofilm formation itself. Indeed, most genes that were differentially regulated upon overexpression of VadR corresponded to a single biofilm cluster, including both VPS gene clusters as well as the genes encoding the major biofilm matrix proteins RbmA and RbmC (chapter 3, Figures 2A, B).

The biological relevance of VadR-mediated regulation of curvature and biofilm formation in the absence of cell wall stress is unclear. On the one hand, it can be speculated that a straight cell morphology at LCD leads to more efficient cell-cell adhesion processes, which could be beneficial for the initiation and proliferation of biofilms [151]. The high abundance of VadR at LCD, when biofilm genes are predominantly expressed, the high activity of the *vadR* promoter in growing biofilms, and the fact that *vxrB* mutant cells showed reduced biofilm formation [187], support this idea. On the other hand, VadR actively represses essential biofilm genes. Further, for the α-proteobacterium *C. crescentus*, a straight rod morphology was previously shown to be unfavorable for colonization and biofilm formation when compared to curved rod cells [150]. Future work is required to understand the role of VadR as a mediator of cell shape and biofilm formation in the absence of stress-inducing agents. To this end, strains that carry chromosomal point mutations in *crvA* or in the targeted biofilm genes, which disrupt VadR base-pairing but maintain the gene's function, could be tested in microfluidic devices.

V. cholerae shows a high tolerance to β-lactam antibiotics [216]. In the presence of such cell wall-targeting molecules, *V. cholerae* forms viable nondividing spheres, which lack a peptidoglycan layer. Once the antibiotic is removed, the spheres revert to normal rod shapes and start to divide again [216]. The VxrAB TCS is essential for the recovery process as it orchestrates the expression of the whole PG synthesis machinery [170]. Indeed, the capacity to form colonies after β-lactam treatment decreased by several logs in the *vxrAB* mutant when compared to wild-type [170]. The data presented in this work demonstrated that the β-lactam antibiotic PenG also induces *vadR* expression in a VxrAB-dependent manner (chapter 3, Figures 5A, B). Importantly, VadR is also a

critical component in the recovery process after antibiotic stress. Cells lacking the *vadR* gene displayed a > 50-fold reduction in cell survival after PenG treatment, whereas VadR overexpression increased viability (chapter 3, Figures 5C). Intriguingly, the beneficial effect of VadR appeared to be solely dependent on the regulation of the *crvA* mRNA. Chromosomal mutations in the *crvA* or *vadR* gene, which disrupted sRNA-mRNA base-pairing, led to similar cell survival rates as observed for the *vadR* deletion mutant (chapter 3, Figures 5C). Elevated CrvA levels seem to inhibit the transition from spherical to rod-shaped cells. It can be speculated that the transport of CrvA monomers through the inner membrane into the periplasm is an unfavorable event during cell envelope stress conditions, and VadR-mediated repression of *crvA* could reduce this additional stress.

The seed region of *vadR* and the *vxrA* gene are conserved among *Vibrios* (chapter 3, Figure 1B and [170]). However, the *crvA* gene is only present in curved *Vibrios*, which excludes the straight rod-shaped species *V. harveyi*, *V. alginolyticus*, and *V. parahaemolyticus* [153]. The VxrA homolog in *V. parahaemolyticus*, VbrK, seems to function as a direct β-lactam sensor, and the corresponding response regulator VbrR was demonstrated to induce the expression of *blaA*, a gene encoding a class A β-lactamase [171]. This enzyme actively degrades specific β-lactam antibiotics and thus confers antibiotic resistance in *V. parahaemolyticus* [171]. Interestingly, homologs of *blaA* can be found in all straight *Vibrio* species, indicating that in these organisms, VadR could fulfill a different role than in *V. cholerae*. This hypothesis is also supported by the fact that the *vadR* gene of straight *Vibrios* is perfectly conserved and additionally extended by 24 bp compared to the *vadR* gene of *V. cholerae* (chapter 3, Figure 1B). Notably, the genome of *V. cholerae* also harbors a β-lactamase, VarG, which could mediate PenG resistance [217]. When studied in *E. coli*, VarG conferred a modest resistance to PenG [217]. However, PenG treatment of *V. cholerae* cells results in growth arrest, which indicates that VarG plays, if at all, only a minor role in the cellular response to high concentrations of this antibiotic.

The VxrAB system is not the only system that contributes to the β-lactam tolerance of *V. cholerae*. Recently, it was demonstrated that PenG treatment also induces the expression of the alternative sigma factor σ^E [218]. The σ^E response was shown to be a vital factor for the successful recovery of spheres since cells that lacked the σ^E-encoding *rpoE* gene experienced a severe plating defect after PenG exposure [218]. It remains to be investigated which genes in the σ^E regulon mediate this phenotype.

5.2.2 The partially redundant MicV and VrrA sRNAs form the repressing arm of the σ^E response

The alternative sigma factor σ^E in association with RNA polymerase is a global activator of gene expression during outer membrane stress. In many Gram-negative bacteria, the σ^E regulon also includes one or more sRNAs to repress the synthesis of unfavorable proteins. In the present work, MicV was identified as the second σ^E-dependent sRNA in *V. cholerae* (chapter 4, Figures 1A-C). In contrast to the first discovered σ^E-dependent sRNA, VrrA, the stability of MicV critically depends on Hfq (chapter 4, Figure EV1D). Global transcriptome analysis revealed that the target mRNAs of MicV and VrrA predominantly encode proteins that integrate into or associate with the outer membrane (chapter 4, Table S2). All directly controlled mRNAs were down-regulated upon sRNA binding, demonstrating that both sRNAs act as the repressive arm of the σ^E response in *V. cholerae* (chapter 4, Figures 2C-E).

MicV and VrrA repress a shared and a smaller unique set of target transcripts, respectively (chapter 4, Figure 2B). They regulate the shared set of targets by utilizing an almost identical seed region (chapter 4, Figure 4A). The strength of regulation of the shared targets differs due to the involvement of additional nucleotides of one sRNA in the base-pairing interaction (chapter 4, Figure S3). VrrA regulates its unique targets via a second base-pairing region termed R2. In contrast, MicV uses the same seed sequence, which is also present in VrrA, to base-pair with all of its targets. Thus, the question remains of how MicV achieves unique target regulation. *In silico* base-pairing predictions indicated that the two nucleotides at the very 5' end of MicV, as well as the single nucleotide difference in the MicV-VrrA consensus sequence, could facilitate selective mRNA targeting by MicV (chapter 4, Figure S3C).

MicV and VrrA carry out redundant and non-redundant functions since both sRNAs are expressed under the same environmental conditions and regulate not only shared but also distinct target genes. Partial redundancy among sRNAs in stress response systems has been described before in other γ-proteobacteria. For example, during iron limitation in *S. enterica*, the ferric uptake regulator (Fur) liberates promoter regions on a global scale, including the promoters of the two sRNA genes *ryhB-1* and *ryhB-2*, a.k.a. *rfrA* and *rfrB*, respectively. Both sRNAs repress the synthesis of iron-dependent proteins to counteract iron depletion [219], [220]. Like MicV and VrrA, RyhB-1 and RyhB-2 each regulate a specific set of mRNAs and also a common set via a shared 33 nt consensus sequence [219]–[222]. Both sRNA pairs, MicV/VrrA and RyhB-1/RyhB-2, regulate some targets redundantly during outer membrane stress and iron starvation, respectively. However,

their underlying evolutionary development most likely differed. Given that the sequences and sRNA lengths of RyhB-1 and RyhB-2 are highly similar, it seems likely that one sRNA originated from a gene duplication event of the other sRNA. On the other hand, MicV and VrrA differ significantly in size and show only a low overall sequence identity (chapter 4, Figure 4A), which could indicate that these sRNAs evolved independently to execute similar regulatory functions.

The question of why two sRNAs evolve to fulfill partially redundant functions cannot be answered entirely. However, the striking difference between MicV and VrrA in their dependency on Hfq could provide one explanation. The half-life of MicV decreased dramatically in the absence of *hfq* from > 25 min to < 1 min, whereas the stability of VrrA was only mildly affected (chapter 4, Figure EV1D). It can be speculated that MicV preferentially regulates Hfq-associated mRNAs, while VrrA controls Hfq-unbound transcripts, which otherwise would be continuously translated. Indeed, it was previously demonstrated that VrrA regulates *ompA* in an Hfq-independent manner [182]. Again, parallels can be drawn between MicV and VrrA and the sRNAs involved in the iron stress response of another γ-proteobacterium. Like in *S. enterica*, iron homeostasis in *Yersinia pestis* is mediated by two Fur-regulated RyhB homologs, RyhB-1 and RyhB-2. As for MicV, the stability of RyhB-1 critically depends on Hfq, whereas similar to VrrA, the half-life of RyhB-2 is only mildly reduced in an *hfq* deletion mutant [223]. Future work could test the idea, if a different dependency on Hfq between two (partially) redundant sRNAs, provides distinct advantages in the presence of a specific stress. To this end, instead of using Hfq mutants, which could result in pleiotropic phenotypes, the sRNA sequences could be modified to enhance or reduce their affinities towards Hfq. For example, the insertion of an A/U-rich sequence upstream of the Rho-independent terminator loop of VrrA could increase the frequency of Hfq binding events [21]. It would be interesting to test whether this effect would also alter the VrrA-mediated regulation of *ompA*, and thus, cell survival in the presence of ethanol.

The *ompA* messenger is a shared target of MicV and VrrA, which is regulated through the highly similar seed sequence of both sRNAs (chapter 4, Figures 2C and S3A). The σ^E-dependent sRNA RybB utilizes the identical seed sequence as MicV to regulate *ompA* in *E. coli* (chapter 4, Figures 4A, C). Importantly, RybB was also able to repress a major OMP in *V. cholerae,* and in a reciprocal experiment, MicV and VrrA inhibited OMP production in *E. coli* (chapter 4, Figures 4B, C). These results led to the idea of an "OMP-regulating sRNA domain," which evolved independently in two different organisms to fulfill analogous biological functions. Indeed, in an unbiased laboratory selection experiment in the presence of ethanol, the shared OMP-regulating domain was highly

enriched since it allowed *ompA* repression and thus mediated an increased tolerance to ethanol (chapter 4, Figure 5). A synthetic and randomized sRNA library could also be useful for future studies of complex phenotypes. Instead of focusing on the evolving sRNA motifs, the global transcriptome could be analyzed by RNA-seq, for example, after treatment with an antimicrobial compound and multiple rounds of selection. This approach could reveal beneficial and detrimental genes whose corresponding transcripts are either up- or downregulated, respectively. A distinct advantage of this sRNA-based approach over transposon-based methods is that sRNAs can directly regulate the abundance of essential gene products. In contrast, a transposon insertion in a gene often results in a complete loss of function, which is why transposon insertions in essential genes lead to non-viable cells [224].

5.3 Conclusions and outlook

A key finding of this work is that the DPO-controlled VqmR sRNA regulates not only biofilm formation but also virulence gene expression in *V. cholerae*. Further, the global impact of all known autoinducers on the transcriptome of *V. cholerae* was determined, revealing combined effects on the regulation of multiple phenotypes. While the regulatory network of VqmR is now well studied, at least during standard laboratory growth conditions, little is known about the role of its activator, VqmA. The promoter region of *vqmR* is the only known target site of VqmA in *V. cholerae* [1], [102]. However, initial analyses indicated that VqmA could activate additional genes, and it will be interesting to study their role in the QS architecture of *V. cholerae*. There is increasing evidence that DPO production is far spread among commensal and pathogenic bacteria, for example, *E. coli*, *B. obeum*, *K. pneumoniae*, *P. aeruginosa*, and *S. aureus*, [74], [211], [212]. Future studies should verify DPO synthesis in these bacteria and, if verified, investigate whether DPO also affects their gene expression. A thorough understanding of DPO signaling and functionality in *V. cholerae*, as well as in other bacteria, could ultimately also facilitate the use of DPO, or functional DPO analogs, as a species-specific drug.

QS molecules were previously reported to induce cell bending in *V. cholerae* [153]. However, mRNA levels of the structural determinant of cell curvature in *V. cholerae*, CrvA, remained unaffected in the AI experiments conducted in chapter 2 of this work. Instead, the present work revealed the VadR sRNA as a post-transcriptional regulator of *crvA* and thus as the first sRNA that regulates the cell shape of a bacterium. VadR is controlled by the VxrAB TCS, which was previously linked to the processes of biofilm formation and cell wall damage repair [170], [187]. The results

presented here demonstrated that VadR also affects both of these processes. While a clear link between VadR-mediated regulation of *crvA* and increased tolerance to β-lactam antibiotics was revealed, it remains the subject of future studies to investigate the underlying mechanisms of this phenotype in greater detail. Likewise, the role of VadR in the process of biofilm formation requires further investigations. The expression of VadR is strongly induced in growing biofilms, and during biofilm promoting conditions at LCD, however, VadR represses several key biofilm elements at the post-transcriptional level. Testing a deletion mutant of *vadR* in growing biofilms could provide valuable information about the biological significance of these sRNA-target interactions.

For a high tolerance to β-lactam antibiotics, *V. cholerae* also requires the alternative sigma factor σ^E as an additional stress response system [218]. This work identified and functionally characterized the σ^E-dependent MicV sRNA. MicV and the VrrA sRNA carry out partially redundant functions in the σ^E stress response by using a highly similar base-pairing sequence. An almost identical sequence exists in the seed region of the σ^E-dependent RybB sRNA from *E. coli*. An important finding of this work is that these three sRNAs, MicV, VrrA, and RybB, can use this conserved sequence to regulate OMP production even in a heterologous host, demonstrating that sRNAs could potentially be annotated by functional domains. Future studies could investigate the evolutionary aspects of the OMP-regulatory domain of MicV, VrrA, and RybB. For example, it could be analyzed whether these three sRNAs share a common ancestor, which already harbored the conserved seed region (divergent evolution), or whether the seed sequence evolved independently in the three different sRNAs to fulfill similar biological functions (convergent evolution).

In summary, this study deepens our understanding of sRNAs involved in the regulation of complex phenotypes like virulence factor production, biofilm formation, cell shape, and tolerance to different cell envelope stresses in the major human pathogen *V. cholerae*. Given that the four characterized sRNAs, VqmR, VadR, MicV, and VrrA, are widely conserved among *Vibrios*, it will be exciting to investigate whether they fulfill similar roles in different *Vibrio* species.

References for Chapters 1 and 5

[1]   K. Papenfort, K. U. Förstner, J.-P. Cong, C. M. Sharma, and B. L. Bassler, "Differential RNA-seq of *Vibrio cholerae* identifies the VqmR small RNA as a regulator of biofilm formation.," *Proc. Natl. Acad. Sci. U. S. A.*, pp. 1–10, 2015.

[2]   H. C. Flemming and S. Wuertz, "Bacteria and archaea on Earth and their abundance in biofilms," *Nat. Rev. Microbiol.*, vol. 17, no. 4, pp. 247–260, Apr. 2019.

[3]   A. J. Westermann, S. A. Gorski, and J. Vogel, "Dual RNA-seq of pathogen and host," *Nature Reviews Microbiology*, vol. 10, no. 9., pp. 618–630, 14-Sep-2012.

[4]   J. Kortmann and F. Narberhaus, "Bacterial RNA thermometers: Molecular zippers and switches," *Nature Reviews Microbiology*, vol. 10, no. 4. pp. 255–265, 16-Apr-2012.

[5]   N. Pavlova, D. Kaloudas, and R. Penchovsky, "Riboswitch distribution, structure, and function in bacteria," *Gene*, vol. 708., pp. 38–48, 05-Aug-2019.

[6]   E. G. H. Wagner and P. Romby, "Small RNAs in Bacteria and Archaea: Who They Are, What They Do, and How They Do It," in *Advances in Genetics*, vol. 90, 2015, pp. 133–208.

[7]   J. Hör, S. A. Gorski, and J. Vogel, "Bacterial RNA Biology on a Genome Scale," *Molecular Cell*, vol. 70, no. 5, pp. 785–799, 07-Jun-2018.

[8]   M. Nitzan, R. Rehani, and H. Margalit, "Integration of Bacterial Small RNAs in Regulatory Networks," *Annu. Rev. Biophys.*, vol. 46, no. 1, pp. 131–148, May 2017.

[9]   L. S. Waters and G. Storz, "Regulatory RNAs in Bacteria," *Cell*, vol. 136, no. 4. pp. 615–628, 20-Feb-2009.

[10]   C. M. Sharma *et al.*, "The primary transcriptome of the major human pathogen *Helicobacter pylori*," *Nature*, vol. 464, no. 7286, pp. 250–255, Mar. 2010.

[11]   Y. Chao, K. Papenfort, R. Reinhardt, C. M. Sharma, and J. Vogel, "An atlas of Hfq-bound transcripts reveals 3′ UTRs as a genomic reservoir of regulatory small RNAs," *EMBO J.*, vol. 31, no. 20, pp. 4005–4019, Oct. 2012.

[12]   A. Jousselin, L. Metzinger, and B. Felden, "On the facultative requirement of the bacterial RNA chaperone, Hfq," *Trends Microbiol.*, vol. 17, no. 9, pp. 399–405, Sep. 2009.

[13]   H. T. Tsui, H. E. Leung, and M. E. Winkler, "Characterization of broadly pleiotropic phenotypes caused by an hfq insertion mutation in *Escherichia coli* K-12," *Mol. Microbiol.*, vol. 13, no. 1, pp. 35–49, Jul. 1994.

[14]   A. Sittka, V. Pfeiffer, K. Tedin, and J. Vogel, "The RNA chaperone Hfq is essential for the virulence of *Salmonella typhimurium*," *Mol. Microbiol.*, vol. 63, no. 1, pp. 193–217, Jan. 2007.

[15]   Y. Ding, B. M. Davis, and M. K. Waldor, "Hfq is essential for *Vibrio cholerae* virulence and downregulates σE expression," *Mol. Microbiol.*, vol. 53, no. 1, pp. 345–354, Jul. 2004.

[16] C. Romilly, I. Caldelari, D. Parmentier, E. Liolliou, P. Romby, and P. Fechter, "Current knowledge on regulatory RNAs and their machineries in *Staphylococcus aureus*.," *RNA Biol.*, vol. 9, no. 4, pp. 402–13, Apr. 2012.

[17] T. Rochat *et al.*, "Tracking the Elusive Function of *Bacillus subtilis* Hfq," *PLoS One*, vol. 10, no. 4, p. e0124977, Apr. 2015.

[18] M. T. Franze De Fernandez, L. Eoyang, and J. T. August, "Factor fraction required for the synthesis of bacteriophage Qβ-RNA," *Nature*, vol. 219, no. 5154, pp. 588–590, Aug. 1968.

[19] H. A. Vincent *et al.*, "Characterization of *Vibrio cholerae* Hfq provides novel insights into the role of the Hfq C-terminal region," *J. Mol. Biol.*, vol. 420, no. 1–2, pp. 56–69, Jun. 2012.

[20] T. M. Link, P. Valentin-Hansen, and R. G. Brennan, "Structure of *Escherichia coli* Hfq bound to polyriboadenylate RNA," *Proc. Natl. Acad. Sci. U. S. A.*, vol. 106, no. 46, pp. 19292–19297, Nov. 2009.

[21] D. J. Schu, A. Zhang, S. Gottesman, and G. Storz, "Alternative Hfq-sRNA interaction modes dictate alternative mRNA recognition," *EMBO J.*, vol. 34, no. 20, pp. 2557–2573, Oct. 2015.

[22] E. Sauer, S. Schmidt, and O. Weichenrieder, "Small RNA binding to the lateral surface of Hfq hexamers and structural rearrangements upon mRNA target recognition," *Proc. Natl. Acad. Sci. U. S. A.*, vol. 109, no. 24, pp. 9396–9401, Jun. 2012.

[23] A. Zhang, K. M. Wassarman, J. Ortega, A. C. Steven, and G. Storz, "The Sm-like Hfq protein increases OxyS RNA interaction with target mRNAs," *Mol. Cell*, vol. 9, no. 1, pp. 11–22, Jan. 2002.

[24] M. A. Schumacher, R. F. Pearson, T. Møller, P. Valentin-Hansen, and R. G. Brennan, "Structures of the pleiotropic translational regulator Hfq and an Hfq-RNA complex: a bacterial Sm-like protein.," *EMBO J.*, vol. 21, no. 13, pp. 3546–56, Jul. 2002.

[25] E. Holmqvist *et al.*, " Global RNA recognition patterns of post-transcriptional regulators Hfq and CsrA revealed by UV crosslinking in vivo ," *EMBO J.*, vol. 35, no. 9, pp. 991–1011, May 2016.

[26] C. Sauter, J. Basquin, and D. Suck, "Sm-like proteins in Eubacteria: The crystal structure of the Hfq protein from *Escherichia coli*," *Nucleic Acids Res.*, vol. 31, no. 14, pp. 4091–4098, Jul. 2003.

[27] S. Panja, D. J. Schu, and S. A. Woodson, "Conserved arginines on the rim of Hfq catalyze base pair formation and exchange.," *Nucleic Acids Res.*, vol. 41, no. 15, pp. 7536–46, Aug. 2013.

[28] A. Zheng, S. Panja, and S. A. Woodson, "Arginine Patch Predicts the RNA Annealing Activity of Hfq from Gram-Negative and Gram-Positive Bacteria.," *J. Mol. Biol.*, vol. 428, no. 11, pp. 2259–2264, Jun. 2016.

[29] Y. Peng, J. E. Curtis, X. Fang, and S. A. Woodson, "Structural model of an mRNA in complex with the bacterial chaperone Hfq," *Proc. Natl. Acad. Sci. U. S. A.*, vol. 111, no. 48, pp. 17134–17139, Dec. 2014.

[30] V. Arluison *et al.*, "The C-terminal domain of *Escherichia coli* Hfq increases the stability of the hexamer," *Eur. J. Biochem.*, vol. 271, no. 7, pp. 1258–1265, Apr. 2004.

[31] E. Sonnleitner, I. Moll, and U. Bläsi, "Functional replacement of the *Escherichia coli hfq* gene by the homologue of *Pseudomonas aeruginosa*," *Microbiology*, vol. 148, no. 3, pp. 883–891, Mar. 2002.

[32] A. Santiago-Frangos *et al.*, "*Caulobacter crescentus* Hfq structure reveals a conserved mechanism of RNA annealing regulation," *Proc. Natl. Acad. Sci. U. S. A.*, vol. 166, no. 22, pp. 10978–10987, May 2019.

[33] A. Fender, J. Elf, K. Hampel, B. Zimmermann, and E. G. H. Wagner, "RNAs actively cycle on the Sm-like protein Hfq.," *Genes Dev.*, vol. 24, no. 23, pp. 2621–6, Dec. 2010.

[34] T. Künne, D. C. Swarts, and S. J. J. Brouns, "Planting the seed: Target recognition of short guide RNAs," *Trends in Microbiology*, vol. 22, no. 2. pp. 74–83, Feb-2014.

[35] K. Papenfort, M. Bouvier, F. Mika, C. M. Sharma, and J. Vogel, "Evidence for an autonomous 5' target recognition domain in an Hfq-associated small RNA.," *Proc. Natl. Acad. Sci. U. S. A.*, vol. 107, no. 47, pp. 20435–40, Nov. 2010.

[36] T. J. Soper, K. Doxzen, and S. A. Woodson, "Major role for mRNA binding and restructuring in sRNA recruitment by Hfq.," *RNA*, vol. 17, no. 8, pp. 1544–50, Aug. 2011.

[37] A. Santiago-Frangos and S. A. Woodson, "Hfq chaperone brings speed dating to bacterial sRNA," *Wiley Interdiscip. Rev. RNA*, vol. 9, no. 4, p. e1475, Jul. 2018.

[38] S. Panja, R. Paul, M. M. Greenberg, and S. A. Woodson, "Light-Triggered RNA Annealing by an RNA Chaperone.," *Angew. Chem. Int. Ed. Engl.*, vol. 54, no. 25, pp. 7281–4, Jun. 2015.

[39] K. Papenfort, V. Pfeiffer, F. Mika, S. Lucchini, J. C. D. Hinton, and J. Vogel, "σE-dependent small RNAs of *Salmonella* respond to membrane stress by accelerating global *omp* mRNA decay," *Mol. Microbiol.*, vol. 62, no. 6, pp. 1674–1688, Dec. 2006.

[40] E. G. H. Wagner, "Cycling of RNAs on Hfq," *RNA Biology*, vol. 10, no. 4. Taylor and Francis Inc., pp. 619–626, Apr. 2013.

[41] R. Hussein and H. N. Lim, "Disruption of small RNA signaling caused by competition for Hfq.," *Proc. Natl. Acad. Sci. U. S. A.*, vol. 108, no. 3, pp. 1110–5, Jan. 2011.

[42] G. G. Carmichael, K. Weber, A. Niveleau, and A. J. Wahba, "The host factor required for RNA phage Qbeta RNA replication in vitro. Intracellular location, quantitation, and purification by polyadenylate-cellulose chromatography.," *J. Biol. Chem.*, vol. 250, no. 10, pp. 3607–612, May 1975.

[43] M. Kajitani, A. Kato, A. Wada, Y. Inokuchi, and A. Ishihama, "Regulation of the *Escherichia coli hfq* gene encoding the host factor for phage Q(β)," *Journal of Bacteriology*, vol. 176, no. 2, pp. 531–534, 1994.

[44] T. A. Azam, A. Iwata, A. Nishimura, S. Ueda, and A. Ishihama, "Growth phase-dependent variation in protein composition of the *Escherichia coli* nucleoid," *J. Bacteriol.*, vol. 181, no. 20, pp. 6361–6370, Oct. 1999.

[45] A. Santiago-Frangos, K. Kavita, D. J. Schu, S. Gottesman, and S. A. Woodson, "C-terminal domain of the RNA chaperone Hfq drives sRNA competition and release of target RNA," *Proc. Natl. Acad. Sci. U. S. A.*, vol. 113, no. 41, pp. E6089–E6096, Oct. 2016.

[46] A. Santiago-Frangos, J. R. Jeliazkov, J. J. Gray, and S. A. Woodson, "Acidic C-terminal domains autoregulate the RNA chaperone Hfq," *Elife*, vol. 6, Aug. 2017.

[47] A. S. Olsen, J. Møller-Jensen, R. G. Brennan, and P. Valentin-Hansen, "C-Terminally Truncated Derivatives of *Escherichia coli* Hfq Are Proficient in Riboregulation," *J. Mol. Biol.*, vol. 404, no. 2, pp. 173–182, Nov. 2010.

[48] K. Moon and S. Gottesman, "Competition among Hfq-binding small RNAs in *Escherichia coli*," *Mol. Microbiol.*, vol. 82, no. 6, pp. 1545–1562, Dec. 2011.

[49] J. M. Andrade, V. Pobre, A. M. Matos, and C. M. Arraiano, "The crucial role of PNPase in the degradation of small RNAs that are not associated with Hfq," *RNA*, vol. 18, no. 4, pp. 844–855, Apr. 2012.

[50] I. Moll, T. Afonyushkin, O. Vytvytska, V. R. Kaberdin, and U. Bläsi, "Coincident Hfq binding and RNase E cleavage sites on mRNA and small regulatory RNAs," *RNA*, vol. 9, no. 11, pp. 1308–1314, Nov. 2003.

[51] T. Morita, K. Maki, and H. Aiba, "RNase E-based ribonucleoprotein complexes: Mechanical basis of mRNA destabilization mediated by bacterial noncoding RNAs," *Genes Dev.*, vol. 19, no. 18, pp. 2176–2186, Sep. 2005.

[52] B. K. Mohanty, V. F. Maples, and S. R. Kushner, "The Sm-like protein Hfq regulates polyadenylation dependent mRNA decay in *Escherichia coli*," *Mol. Microbiol.*, vol. 54, no. 4, pp. 905–920, Nov. 2004.

[53] T. Mizuno, M. Y. Chou, and M. Inouye, "A unique mechanism regulating gene expression: translational inhibition by a complementary RNA transcript (micRNA).," *Proc. Natl. Acad. Sci. U. S. A.*, vol. 81, no. 7, pp. 1966–70, Apr. 1984.

[54] C. M. Sharma, F. Darfeuille, T. H. Plantinga, and J. Vogel, "A small RNA regulates multiple ABC transporter mRNAs by targeting C/A-rich elements inside and upstream of ribosome-binding sites.," *Genes Dev.*, vol. 21, no. 21, pp. 2804–17, Nov. 2007.

[55] Q. Yang, N. Figueroa-Bossi, and L. Bossi, "Translation Enhancing ACA Motifs and Their Silencing by a Bacterial Small Regulatory RNA," *PLoS Genet.*, vol. 10, no. 1, p. e1004026, Jan. 2014.

[56] M. S. Azam and C. K. Vanderpool, "Translation inhibition from a distance: the small RNA SgrS silences a ribosomal protein S1-dependent enhancer," *Mol. Microbiol.*, vol. 114, no. 3, pp. 391-408, Apr. 2020.

[57] F. Darfeuille, C. Unoson, J. Vogel, and E. G. H. Wagner, "An Antisense RNA Inhibits Translation by Competing with Standby Ribosomes," *Mol. Cell*, vol. 26, no. 3, pp. 381–392, May 2007.

[58] B. Veĉerek, I. Moll, and U. Bläsi, "Control of Fur synthesis by the non-coding RNA RyhB and iron-responsive decoding," *EMBO J.*, vol. 26, no. 4, pp. 965–975, Feb. 2007.

[59] G. Desnoyers and E. Massé, "Noncanonical repression of translation initiation through small RNA recruitment of the RNA chaperone Hfq.," *Genes Dev.*, vol. 26, no. 7, pp. 726–39, Apr. 2012.

[60] E. Massé, F. E. Escorcia, and S. Gottesman, "Coupled degradation of a small regulatory RNA and its mRNA targets in *Escherichia coli*," *Genes Dev.*, vol. 17, no. 19, pp. 2374–2383, Oct. 2003.

[61] T. Morita, Y. Mochizuki, and H. Aiba, "Translational repression is sufficient for gene silencing by bacterial small noncoding RNAs in the absence of mRNA destruction," *Proc. Natl. Acad. Sci. U. S. A.*, vol. 103, no. 13, pp. 4858–4863, Mar. 2006.

[62] V. Pfeiffer, K. Papenfort, S. Lucchini, J. C. D. Hinton, and J. Vogel, "Coding sequence targeting by MicC RNA reveals bacterial mRNA silencing downstream of translational initiation.," *Nat. Struct. Mol. Biol.*, vol. 16, no. 8, pp. 840–6, Aug. 2009.

[63] M.-C. Carrier, D. Lalaouna, and E. Massé, "Broadening the Definition of Bacterial Small RNAs: Characteristics and Mechanisms of Action," *Annu. Rev. Microbiol.*, vol. 72, no. 1, pp. 141–161, Sep. 2018.

[64] K. Papenfort and C. K. Vanderpool, "Target activation by regulatory RNAs in bacteria.," *FEMS Microbiol. Rev.*, vol. 39, no. 3, pp. 362–78, May 2015.

[65] K. S. Fröhlich and J. Vogel, "Activation of gene expression by small RNA," *Curr. Opin. Microbiol.*, vol. 12, no. 6, pp. 674–682, Dec. 2009.

[66] E. Morfeldt, D. Taylor, A. von Gabain, and S. Arvidson, "Activation of alpha-toxin translation in *Staphylococcus aureus* by the trans-encoded antisense RNA, RNAIII.," *EMBO J.*, vol. 14, no. 18, pp. 4569–4577, Sep. 1995.

[67] K. Papenfort and C. K. Vanderpool, "Target activation by regulatory RNAs in bacteria," *FEMS Microbiology Reviews*, vol. 39, no. 3. pp. 362–378, May 2015.

[68] A. Resch, T. Afonyushkin, T. B. Lombo, K. J. Mcdowall, U. Bläsi, and V. R. Kaberdin, "Translational activation by the noncoding RNA DsrA involves alternative RNase III processing in the *rpoS* 5′-leader," *RNA*, vol. 14, no. 3, pp. 454–459, Mar. 2008.

[69] H. Salvail, M.-P. Caron, J. Bélanger, and E. Massé, "Antagonistic functions between the RNA chaperone Hfq and an sRNA regulate sensitivity to the antibiotic colicin," *EMBO J.*, vol. 32, no. 20, pp. 2764–2778, Sep. 2013.

[70] K. Papenfort, Y. Sun, M. Miyakoshi, C. K. Vanderpool, and J. Vogel, "Small RNA-mediated activation of sugar phosphatase mRNA regulates glucose homeostasis," *Cell*, vol. 153, no. 2, pp. 426–437, Apr. 2013.

[71] J. Richards and J. G. Belasco, "Obstacles to Scanning by RNase E Govern Bacterial mRNA Lifetimes by Hindering Access to Distal Cleavage Sites," *Mol. Cell*, vol. 74, no. 2, pp. 284-295.e5, Apr. 2019.

[72] E. Holmqvist and G. H. Wagner, "Impact of bacterial sRNAs in stress responses," *Biochemical Society Transactions*, vol. 45, no. 6. Portland Press Ltd, pp. 1203–1212, 15-Dec-2017.

[73] D. H. Lenz *et al.*, "The small RNA chaperone Hfq and multiple small RNAs control quorum sensing in *Vibrio harveyi* and *Vibrio cholerae*.," *Cell*, vol. 118, no. 1, pp. 69–82, Jul. 2004.

[74] K. Papenfort, J. E. Silpe, K. R. Schramma, J.-P. Cong, M. R. Seyedsayamdost, and B. L. Bassler, "A *Vibrio cholerae* autoinducer–receptor pair that controls biofilm formation," *Nat. Chem. Biol.*, vol. 13, no. 5, pp. 551–557, Mar. 2017.

[75] C. Matz, D. McDougald, A. M. Moreno, P. Y. Yung, F. H. Yildiz, and S. Kjelleberg, "Biofilm formation and phenotypic variation enhance predation-driven persistence of *Vibrio cholerae*," *Proc. Natl. Acad. Sci. U. S. A.*, vol. 102, no. 46, pp. 16819–16824, Nov. 2005.

[76] S. Beyhan and F. H. Yildiz, "Smooth to rugose phase variation in *Vibrio cholerae* can be mediated by a single nucleotide change that targets c-di-GMP signalling pathway," *Mol. Microbiol.*, vol. 63, no. 4, pp. 995–1007, Feb. 2007.

[77] J. Zhu and J. J. Mekalanos, "Quorum sensing-dependent biofilms enhance colonization in *Vibrio cholerae*," *Dev. Cell*, vol. 5, no. 4, pp. 647–656, Oct. 2003.

[78] R. Tamayo, B. Patimalla, and A. Camilli, "Growth in a biofilm induces a hyperinfectious phenotype in *Vibrio cholerae*," *Infect. Immun.*, vol. 78, no. 8, pp. 3560–3569, Aug. 2010.

[79] A. L. Gallego-Hernandez *et al.*, "Upregulation of virulence genes promotes *Vibrio cholerae* biofilm hyperinfectivity," *Proc. Natl. Acad. Sci.*, vol. 117, no. 20, pp. 11010-11017, Apr. 2020.

[80] D. A. Herrington, R. H. Hall, G. Losonsky, J. J. Mekalanos, R. K. Taylor, and M. M. Levine, "Toxin, toxin-coregulated pili, and the toxR regulon are essential for *Vibrio cholerae* pathogenesis in humans," *J. Exp. Med.*, vol. 168, no. 4, pp. 1487–1492, Oct. 1988.

[81] M. K. Waldor and J. J. Mekalanos, "Lysogenic Conversion by a Filamentous Phage Encoding Cholera Toxin," *Science*, vol. 272, no. 5270, pp. 1910–1914, Jun. 1996.

[82] J. Deen, M. A. Mengel, and J. D. Clemens, "Epidemiology of cholera," *Vaccine*, vol. 38., pp. A31–A40, 29-Feb-2020.

[83] S. M. Faruque, K. Biswas, S. M. Nashir Udden, Q. S. Ahmad, D. A. Sack, and G. Balakrish Nair, "Transmissibility of cholera: In vivo-formed biofilms and their relationship to infectivity and persistence in the environment," *Proc. Natl. Acad. Sci. U. S. A.*, vol. 103, no. 16, pp. 6350–6355, Apr. 2006.

[84] K. Papenfort and B. L. Bassler, "Quorum sensing signal-response systems in Gram-negative bacteria," *Nature Reviews Microbiology*, vol. 14, no. 9., pp. 576–588, Sep. 2016.

[85] S. T. Rutherford and B. L. Bassler, "Bacterial quorum sensing: Its role in virulence and possibilities for its control," *Cold Spring Harbor Perspectives in Medicine*, vol. 2, no. 11., Nov. 2012.

[86]   D. A. Higgins, M. E. Pomianek, C. M. Kraml, R. K. Taylor, M. F. Semmelhack, and B. L. Bassler, "The major *Vibrio cholerae* autoinducer and its role in virulence factor production.," *Nature*, vol. 450, no. 7171, pp. 883–6, Dec. 2007.

[87]   Y. Wei, L. J. Perez, W. L. Ng, M. F. Semmelhack, and B. L. Bassler, "Mechanism of *Vibrio cholerae* autoinducer-1 biosynthesis," *ACS Chem. Biol.*, vol. 6, no. 4, pp. 356–365, Apr. 2011.

[88]   R. C. Kelly *et al.*, "The *Vibrio cholerae* quorum-sensing autoinducer CAI-1: Analysis of the biosynthetic enzyme CqsA," *Nat. Chem. Biol.*, vol. 5, no. 12, pp. 891–895, Dec. 2009.

[89]   W. Liang, S. Z. Sultan, A. J. Silva, and J. A. Benitez, "Cyclic AMP post-transcriptionally regulates the biosynthesis of a major bacterial autoinducer to modulate the cell density required to activate quorum sensing," *FEBS Lett.*, vol. 582, no. 27, pp. 3744–3750, Nov. 2008.

[90]   W. Liang, A. Pascual-Montano, A. J. Silva, and J. A. Benitez, "The cyclic AMP receptor protein modulates quorum sensing, motility and multiple genes that affect intestinal colonization in *Vibrio cholerae*.," *Microbiology*, vol. 153, no. 9, pp. 2964–2975, Sep. 2007.

[91]   M. B. Miller, K. Skorupski, D. H. Lenz, R. K. Taylor, and B. L. Bassler, "Parallel quorum sensing systems converge to regulate virulence in *Vibrio cholerae*.," *Cell*, vol. 110, no. 3, pp. 303–14, Aug. 2002.

[92]   J. M. Henke and B. L. Bassler, "Three parallel quorum-sensing systems regulate gene expression in *Vibrio harveyi*," *J. Bacteriol.*, vol. 186, no. 20, pp. 6902–6914, Oct. 2004.

[93]   C. S. Pereira, J. A. Thompson, and K. B. Xavier, "AI-2-mediated signalling in bacteria," *FEMS Microbiol. Rev.*, vol. 37, no. 2, pp. 156–181, Mar. 2013.

[94]   S. T. Miller *et al.*, "*Salmonella typhimurium* recognizes a chemically distinct form of the bacterial quorum-sensing signal AI-2," *Mol. Cell*, vol. 15, no. 5, pp. 677–687, Sep. 2004.

[95]   M. M. Meijler *et al.*, "Synthesis and biological validation of a ubiquitous quorum-sensing molecule," *Angew. Chemie - Int. Ed.*, vol. 43, no. 16, pp. 2106–2108, Apr. 2004.

[96]   X. Chen *et al.*, "Structural identification of a bacterial quorum-sensing signal containing boron," *Nature*, vol. 415, no. 6871, pp. 545–549, Jan. 2002.

[97]   M. G. Surette, M. B. Miller, and B. L. Bassler, "Quorum sensing in *Escherichia coli*, *Salmonella typhimurium*, and *Vibrio harveyi*: A new family of genes responsible for autoinducer production," *Proc. Natl. Acad. Sci. U. S. A.*, vol. 96, no. 4, pp. 1639–1644, Feb. 1999.

[98]   S. Schauder, K. Shokat, M. G. Surette, and B. L. Bassler, "The LuxS family of bacterial autoinducers: Biosynthesis of a novel quorum-sensing signal molecule," *Mol. Microbiol.*, vol. 41, no. 2, pp. 463–476, Jul. 2001.

[99]   J. E. Silpe and B. L. Bassler, "A Host-Produced Quorum-Sensing Autoinducer Controls a Phage Lysis-Lysogeny Decision," *Cell*, vol. 176, no. 1–2, pp. 268-280.e13, Jan. 2019.

[100] B. L. Bassler, M. Wright, and M. R. Silverman, "Multiple signalling systems controlling expression of luminescence in *Vibrio harveyi*: sequence and function of genes encoding a second sensory pathway," *Mol. Microbiol.*, vol. 13, no. 2, pp. 273–286, Jul. 1994.

[101] M. B. Neiditch, M. J. Federle, S. T. Miller, B. L. Bassler, and F. M. Hughson, "Regulation of LuxPQ receptor activity by the quorum-sensing signal autoinducer-2," *Mol. Cell*, vol. 18, no. 5, pp. 507–518, May 2005.

[102] H. Wu *et al.*, "Crystal structure of the *Vibrio cholerae* VqmA–ligand–DNA complex provides insight into ligand-binding mechanisms relevant for drug design," *J. Biol. Chem.*, vol. 294, no. 8, pp. 2580–2592, 2019.

[103] W. L. Ng *et al.*, "Probing bacterial transmembrane histidine kinase receptor-ligand interactions with natural and synthetic molecules," *Proc. Natl. Acad. Sci. U. S. A.*, vol. 107, no. 12, pp. 5575–5580, Mar. 2010.

[104] M. B. Neiditch *et al.*, "Ligand-Induced Asymmetry in Histidine Sensor Kinase Complex Regulates Quorum Sensing," *Cell*, vol. 126, no. 6, pp. 1095–1108, Sep. 2006.

[105] J. A. Freeman and B. L. Bassler, "Sequence and function of LuxU: a two-component phosphorelay protein that regulates quorum sensing in *Vibrio harveyi*.," *J. Bacteriol.*, vol. 181, no. 3, pp. 899–906, Feb. 1999.

[106] J. A. Freeman and B. L. Bassler, "A genetic analysis of the function of LuxO, a two-component response regulator involved in quorum sensing in *Vibrio harveyi*," *Mol. Microbiol.*, vol. 31, no. 2, pp. 665–677, Jan. 1999.

[107] B. L. Bassler, M. Wright, and M. R. Silverman, "Sequence and function of LuxO, a negative regulator of luminescence in *Vibrio harveyi*.," *Mol. Microbiol.*, vol. 12, no. 3, pp. 403–12, May 1994.

[108] B. N. Lilley and B. L. Bassler, "Regulation of quorum sensing in *Vibrio harveyi* by LuxO and Sigma-54," *Mol. Microbiol.*, vol. 36, no. 4, pp. 940–954, May 2000.

[109] S. T. Rutherford, J. C. Van Kessel, Y. Shao, and B. L. Bassler, "AphA and LuxR/HapR reciprocally control quorum sensing in vibrios," *Genes Dev.*, vol. 25, no. 4, pp. 397–408, Feb. 2011.

[110] Y. Shao and B. L. Bassler, "Quorum-sensing non-coding small RNAs use unique pairing regions to differentially control mRNA targets," *Mol. Microbiol.*, vol. 83, no. 3, pp. 599–611, Feb. 2012.

[111] M. Yang, E. M. Frey, Z. Liu, R. Bishar, and J. Zhu, "The virulence transcriptional activator AphA enhances biofilm formation by *Vibrio cholerae* by activating expression of the biofilm regulator VpsT.," *Infect. Immun.*, vol. 78, no. 2, pp. 697–703, Feb. 2010.

[112] K. Skorupski and R. K. Taylor, "A new level in the Vibrio cholerae ToxR virulence cascade: AphA is required for transcriptional activation of the *tcpPH* operon," *Mol. Microbiol.*, vol. 31, no. 3, pp. 763–771, Feb. 1999.

[113] G. Kovacikova and K. Skorupski, "A *Vibrio cholerae* LysR homolog, AphB, cooperates with AphA at the *tcpPH* promoter to activate expression of the ToxR virulence cascade," *J. Bacteriol.*, vol. 181, no. 14, pp. 4250–4256, Jul. 1999.

[114] L. R. Swem, D. L. Swem, N. S. Wingreen, and B. L. Bassler, "Deducing Receptor Signaling Parameters from In Vivo Analysis: LuxN/AI-1 Quorum Sensing in *Vibrio harveyi*," *Cell*, vol. 134, no. 3, pp. 461–473, Aug. 2008.

[115] Y. Wei, W. L. Ng, J. Cong, and B. L. Bassler, "Ligand and antagonist driven regulation of the *Vibrio cholerae* quorum-sensing receptor CqsS," *Mol. Microbiol.*, vol. 83, no. 6, pp. 1095–1108, Mar. 2012.

[116] G. Kovacikova and K. Skorupski, "Regulation of virulence gene expression in *Vibrio cholerae* by quorum sensing: HapR functions at the *aphA* promoter," *Mol. Microbiol.*, vol. 46, no. 4, pp. 1135–1147, Nov. 2002.

[117] C. M. Waters, W. Lu, J. D. Rabinowitz, and B. L. Bassler, "Quorum sensing controls biofilm formation in *Vibrio cholerae* through modulation of cyclic Di-GMP levels and repression of *vpsT*," *J. Bacteriol.*, vol. 190, no. 7, pp. 2527–2536, Apr. 2008.

[118] A. J. Silva and J. A. Benitez, "*Vibrio cholerae* Biofilms and Cholera Pathogenesis," *PLoS Neglected Tropical Diseases*, vol. 10, no. 2., Feb. 2016.

[119] A. T. Nielsen, N. A. Dolganov, G. Otto, M. C. Miller, Y. W. Cheng, and G. K. Schoolnik, "RpoS controls the *Vibrio cholerae* mucosal escape response," *PLoS Pathog.*, vol. 2, no. 10, pp. 0933–0948, Oct. 2006.

[120] S. L. Svenningsen, K. C. Tu, and B. L. Bassler, "Gene dosage compensation calibrates four regulatory RNAs to control *Vibrio cholerae* quorum sensing," *EMBO J.*, vol. 28, no. 4, pp. 429–439, Feb. 2009.

[121] W. Lin, G. Kovacikova, and K. Skorupski, "Requirements for *Vibrio cholerae* HapR binding and transcriptional repression at the *hapR* promoter are distinct from those at the *aphA* promoter," *J. Bacteriol.*, vol. 187, no. 9, pp. 3013–3019, May 2005.

[122] W. Lin, G. Kovacikova, and K. Skorupski, "The quorum sensing regulator HapR downregulates the expression of the virulence gene transcription factor AphA in *Vibrio cholerae* by antagonizing Lrp- and VpsR-mediated activation," *Mol. Microbiol.*, vol. 64, no. 4, pp. 953–967, May 2007.

[123] A. Becskei and L. Serrano, "Engineering stability in gene networks by autoregulation," *Nature*, vol. 405, no. 6786, pp. 590–593, Jun. 2000.

[124] L. Feng *et al.*, "A Qrr noncoding RNA deploys four different regulatory mechanisms to optimize quorum-sensing dynamics," *Cell*, vol. 160, no. 1–2, pp. 228–240, Jan. 2015.

[125] S. L. Svenningsen, C. M. Waters, and B. L. Bassler, "A negative feedback loop involving small RNAs accelerates *Vibrio cholerae*'s transition out of quorum-sensing mode.," *Genes Dev.*, vol. 22, no. 2, pp. 226–38, Jan. 2008.

[126] Y. Wang, K. C. Tu, N. P. Ong, B. L. Bassler, and N. S. Wingreen, "Protein-level fluctuation correlation at the microcolony level and its application to the *Vibrio harveyi* quorum-sensing circuit," *Biophys. J.*, vol. 100, no. 12, pp. 3045–3053, Jun. 2011.

[127] G. Kovacikova and K. Skorupski, "Overlapping binding sites for the virulence gene regulators AphA, AphB and cAMP-CRP at the *Vibrio cholerae* TcpPH promoter," *Mol. Microbiol.*, vol. 41, no. 2, pp. 393–407, Jul. 2001.

[128] N. A. Beck, E. S. Krukonis, and V. J. DiRita, "TcpH influences virulence gene expression in *Vibrio cholerae* by inhibiting degradation of the transcription activator TcpP.," *J. Bacteriol.*, vol. 186, no. 24, pp. 8309–16, Dec. 2004.

[129] C. C. Häse and J. J. Mekalanos, "TcpP protein is a positive regulator of virulence gene expression in *Vibrio cholerae*," *Proc. Natl. Acad. Sci. U. S. A.*, vol. 95, no. 2, pp. 730–734, Jan. 1998.

[130] V. J. DiRita and J. J. Mekalanos, "Periplasmic interaction between two membrane regulatory proteins, ToxR and ToxS, results in signal transduction and transcriptional activation.," *Cell*, vol. 64, no. 1, pp. 29–37, Jan. 1991.

[131] V. L. Miller, R. K. Taylor, and J. J. Mekalanos, "Cholera toxin transcriptional activator ToxR is a transmembrane DNA binding protein.," *Cell*, vol. 48, no. 2, pp. 271–9, Jan. 1987.

[132] E. S. Krukonis, R. R. Yu, and V. J. Dirita, "The *Vibrio cholerae* ToxR/TcpP/ToxT virulence cascade: distinct roles for two membrane-localized transcriptional activators on a single promoter.," *Mol. Microbiol.*, vol. 38, no. 1, pp. 67–84, Oct. 2000.

[133] R. K. Taylor, V. L. Miller, D. B. Furlong, and J. J. Mekalanos, "Use of *phoA* gene fusions to identify a pilus colonization factor coordinately regulated with cholera toxin," *Proc. Natl. Acad. Sci. U. S. A.*, vol. 84, no. 9, pp. 2833–2837, May 1987.

[134] E. J. Nelson, J. B. Harris, J. G. Morris, S. B. Calderwood, and A. Camilli, "Cholera transmission: The host, pathogen and bacteriophage dynamic," *Nature Reviews Microbiology*, vol. 7, no. 10. pp. 693–702, 2009.

[135] P. Cuatrecasas, "Gangliosides and Membrane Receptors for Cholera Toxin," *Biochemistry*, vol. 12, no. 18, pp. 3558–3566, Aug. 1973.

[136] M. J. Betley, V. L. Miller, and J. J. Mekalanos, "Genetics of Bacterial Enterotoxins," *Annu. Rev. Microbiol.*, vol. 40, no. 1, pp. 577–605, Oct. 1986.

[137] D. M. Gill and R. Meren, "ADP-ribosylation of membrane proteins catalyzed by cholera toxin: basis of the activation of adenylate cyclase," *Proc. Natl. Acad. Sci. U. S. A.*, vol. 75, no. 7, pp. 3050–3054, Jul. 1978.

[138] J. B. Harris, R. C. LaRocque, F. Qadri, E. T. Ryan, and S. B. Calderwood, "Cholera," *The Lancet*, vol. 379, no. 9835, pp. 2466–2476, Jun. 2012.

[139] P. V. Krasteva *et al.*, "*Vibrio cholerae* VpsT regulates matrix production and motility by directly sensing cyclic di-GMP," *Science*, vol. 327, no. 5967, pp. 866–868, Feb. 2010.

[140] S. Beyhan, K. Bilecen, S. R. Salama, C. Casper-Lindley, and F. H. Yildiz, "Regulation of rugosity and biofilm formation in *Vibrio cholerae*: comparison of VpsT and VpsR regulons and epistasis analysis of *vpsT*, *vpsR*, and *hapR*.," *J. Bacteriol.*, vol. 189, no. 2, pp. 388–402, Jan. 2007.

[141] D. Srivastava, R. C. Harris, and C. M. Waters, "Integration of cyclic di-GMP and quorum sensing in the control of *vpsT* and *aphA* in *Vibrio cholerae*," *J. Bacteriol.*, vol. 193, no. 22, pp. 6331–6341, Nov. 2011.

[142] J. K. Teschler *et al.*, "Living in the matrix: Assembly and control of Vibrio cholerae biofilms," *Nat. Rev. Microbiol.*, vol. 13, no. 5., pp. 255–268, May 2015.

[143] A. S. Utada *et al.*, "*Vibrio cholerae* use pili and flagella synergistically to effect motility switching and conditional surface attachment," *Nat. Commun.*, vol. 5, p. 4913, Sep. 2014.

[144] K. A. Floyd *et al.*, "c-di-GMP modulates type IV MSHA pilus retraction and surface attachment in *Vibrio cholerae*," *Nat. Commun.*, vol. 11, no. 1, p. 1549, Dec. 2020.

[145] J. C. N. Fong, K. A. Syed, K. E. Klose, and F. H. Yildiz, "Role of Vibrio polysaccharide (vps) genes in VPS production, biofilm formation and *Vibrio cholerae* pathogenesis," *Microbiology*, vol. 156, no. 9, pp. 2757–2769, Sep. 2010.

[146] V. Berk *et al.*, "Molecular architecture and assembly principles of *Vibrio cholerae* biofilms," *Science*, vol. 337, no. 6091, pp. 236–239, Jul. 2012.

[147] A. Seper *et al.*, "Extracellular nucleases and extracellular DNA play important roles in *Vibrio cholerae* biofilm formation," *Mol. Microbiol.*, vol. 82, no. 4, pp. 1015–1037, Nov. 2011.

[148] B. R. Wucher, T. M. Bartlett, M. Hoyos, K. Papenfort, A. Persat, and C. D. Nadell, "*Vibrio cholerae* filamentation promotes chitin surface attachment at the expense of competition in biofilms," *Proc. Natl. Acad. Sci. U. S. A.*, vol. 116, no. 28, pp. 14216–14221, Jul. 2019.

[149] W. P. J. Smith, Y. Davit, J. M. Osborne, W. D. Kim, K. R. Foster, and J. M. Pitt-Francis, "Cell morphology drives spatial patterning in microbial communities," *Proc. Natl. Acad. Sci. U. S. A.*, vol. 114, no. 3, pp. E280–E286, Jan. 2017.

[150] A. Persat, H. A. Stone, and Z. Gitai, "The curved shape of *Caulobacter crescentus* enhances surface colonization in flow," *Nat. Commun.*, vol. 5, no. 1, pp. 1–9, May 2014.

[151] K. Drescher *et al.*, "Architectural transitions in *Vibrio cholerae* biofilms at single-cell resolution.," *Proc. Natl. Acad. Sci. U. S. A.*, vol. 113, no. 14, pp. E2066-72, Apr. 2016.

[152] J.-V. Höltje, "Growth of the Stress-Bearing and Shape-Maintaining Murein Sacculus of *Escherichia coli*," *Microbiol. Mol. Biol. Rev.*, vol. 62, no. 1, pp. 181–203, Mar. 1998.

[153] T. M. Bartlett *et al.*, "A Periplasmic Polymer Curves Vibrio cholerae and Promotes Pathogenesis In Brief Article A Periplasmic Polymer Curves *Vibrio cholerae* and Promotes Pathogenesis," *Cell*, vol. 168, pp. 172–185, Jan. 2017.

[154] A. Typas, M. Banzhaf, C. A. Gross, and W. Vollmer, "From the regulation of peptidoglycan synthesis to bacterial growth and morphology," *Nat. Rev. Microbiol.*, vol. 10, no. 2. pp. 123–136, Feb. 2012.

[155] D. C. Yang, K. M. Blair, and N. R. Salama, "Staying in Shape: the Impact of Cell Shape on Bacterial Survival in Diverse Environments.," *Microbiol. Mol. Biol. Rev.*, vol. 80, no. 1, pp. 187–203, Mar. 2016.

[156] E. C. Garner, R. Bernard, W. Wang, X. Zhuang, D. Z. Rudner, and T. Mitchison, "Coupled, circumferential motions of the cell wall synthesis machinery and MreB filaments in *B. subtilis*," *Science*, vol. 333, no. 6039, pp. 222–225, Jul. 2011.

[157] J. Domínguez-Escobar, A. Chastanet, A. H. Crevenna, V. Fromion, R. Wedlich-Söldner, and R. Carballido-López, "Processive movement of MreB-associated cell wall biosynthetic complexes in bacteria," *Science*, vol. 333, no. 6039, pp. 225–228, Jul. 2011.

[158] P. Srivastava, G. Demarre, T. S. Karpova, J. McNally, and D. K. Chattoraj, "Changes in nucleoid morphology and origin localization upon inhibition or alteration of the actin homolog, MreB, of *Vibrio cholerae*," *J. Bacteriol.*, vol. 189, no. 20, pp. 7450–7463, Oct. 2007.

[159] P. Szwedziak and J. Löwe, "Do the divisome and elongasome share a common evolutionary past?," *Curr. Opin. Microbiol.*, vol. 16, no. 6. pp. 745–751, Dec-2013.

[160] H. Shi, B. P. Bratton, Z. Gitai, and K. C. Huang, "How to Build a Bacterial Cell: MreB as the Foreman of *E. coli* Construction," *Cell*, vol. 172, no. 6., pp. 1294–1305, Mar 2018.

[161] J. Wagstaff and J. Löwe, "Prokaryotic cytoskeletons: Protein filaments organizing small cells," *Nat. Rev. Microbiol.*, vol. 16, no. 4, pp. 187–201, Apr. 2018.

[162] K. Richardson, "Roles of motility and flagellar structure in pathogenicity of *Vibrio cholerae*: Analysis of motility mutants in three animal models," *Infect. Immun.*, vol. 59, no. 8, pp. 2727–2736, Aug. 1991.

[163] C. M. DeAngelis, J. Saul-McBeth, and J. S. Matson, "Vibrio responses to extracytoplasmic stress," *Environmental Microbiology Reports*, vol. 10, no. 5., pp. 511–521, Oct 2018.

[164] A. M. Mitchell and T. J. Silhavy, "Envelope stress responses: balancing damage repair and toxicity," *Nat. Rev. Microbiol.*, vol. 17, no. 7., pp. 417–428, Jul. 2019.

[165] N. Acosta, S. Pukatzki, and T. L. Raivio, "The Cpx system regulates virulence gene expression in *Vibrio cholerae*," *Infect. Immun.*, vol. 83, no. 6, pp. 2396–2408, Mar. 2015.

[166] G. Kovacikova and K. Skorupski, "The alternative sigma factor σE plays an important role in intestinal survival and virulence in *Vibrio cholerae*," *Infect. Immun.*, vol. 70, no. 10, pp. 5355–5362, Oct. 2002.

[167] C. M. DeAngelis, D. Nag, J. H. Withey, and J. S. Matson, "Characterization of the *Vibrio cholerae* Phage Shock Protein Response," in *J. Bacteriol.*, vol. 201, no. 14., pp. e00761-18, Jun. 2019

[168] E. Wall, N. Majdalani, and S. Gottesman, "The Complex Rcs Regulatory Cascade," *Annu. Rev. Microbiol.*, vol. 72, no. 1, pp. 111–139, Sep. 2018.

[169] R. G. Raffa and T. L. Raivio, "A third envelope stress signal transduction pathway in *Escherichia coli*," *Mol. Microbiol.*, vol. 45, no. 6, pp. 1599–1611, Sep. 2002.

[170] T. Dörr, L. Alvarez, F. Delgado, B. M. Davis, F. Cava, and M. K. Waldor, "A cell wall damage response mediated by a sensor kinase/response regulator pair enables beta-lactam tolerance," *Proc. Natl. Acad. Sci. U. S. A.*, vol. 113, no. 2, pp. 404–409, Jan. 2016.

[171] L. Li, Q. Wang, H. Zhang, M. Yang, M. I. Khan, and X. Zhou, "Sensor histidine kinase is a β-lactam receptor and induces resistance to β-lactam antibiotics," *Proc. Natl. Acad. Sci. U. S. A.*, vol. 113, no. 6, pp. 1648–1653, Feb. 2016.

[172] S. J. Hersch *et al.*, "Envelope stress responses defend against type six secretion system attacks independently of immunity proteins," *Nat. Microbiol.*, May 2020.

[173] S. E. Ades, L. E. Connolly, B. M. Alba, and C. A. Gross, "The *Escherichia coli* sigma(E)-dependent extracytoplasmic stress response is controlled by the regulated proteolysis of an anti-sigma factor.," *Genes Dev.*, vol. 13, no. 18, pp. 2449–61, Sep. 1999.

[174] R. Chaba *et al.*, "Signal integration by DegS and RseB governs the σE- mediated envelope stress response in *Escherichia coli*," *Proc. Natl. Acad. Sci. U. S. A.*, vol. 108, no. 5, pp. 2106–2111, Feb. 2011.

[175] S. Lima, M. S. Guo, R. Chaba, C. A. Gross, and R. T. Sauer, "Dual molecular signals mediate the bacterial response to outer-membrane stress," *Science*, vol. 340, no. 6134, pp. 837–841, May 2013.

[176] N. P. Walsh, B. M. Alba, B. Bose, C. A. Gross, and R. T. Sauer, "OMP peptide signals initiate the envelope-stress response by activating DegS protease via relief of inhibition mediated by its PDZ domain.," *Cell*, vol. 113, no. 1, pp. 61–71, Apr. 2003.

[177] K. Kanehara, K. Ito, and Y. Akiyama, "YaeL (EcfE) activates the σE pathway of stress response through a site-2 cleavage of anti-σE, RseA," *Genes Dev.*, vol. 16, no. 16, pp. 2147–2155, Aug. 2002.

[178] V. A. Rhodius, W. C. Suh, G. Nonaka, J. West, and C. A. Gross, "Conserved and variable functions of the sigmaE stress response in related genomes.," *PLoS Biol.*, vol. 4, no. 1, p. e2, Jan. 2006.

[179] E. B. Gogol, V. A. Rhodius, K. Papenfort, J. Vogel, and C. A. Gross, "Small RNAs endow a transcriptional activator with essential repressor functions for single-tier control of a global stress regulon.," *Proc. Natl. Acad. Sci. U. S. A.*, vol. 108, no. 31, pp. 12875–80, 2011.

[180] V. K. Mutalik, G. Nonaka, S. E. Ades, V. A. Rhodius, and C. A. Gross, "Promoter strength properties of the complete sigma E regulon of *Escherichia coli* and *Salmonella enterica*," *J. Bacteriol.*, vol. 191, no. 23, pp. 7279–7287, Dec. 2009.

[181] M. S. Guo, T. B. Updegrove, E. B. Gogol, S. A. Shabalina, C. A. Gross, and G. Storz, "MicL, a new σE-dependent sRNA, combats envelope stress by repressing synthesis of Lpp, the major outer membrane lipoprotein," *Genes Dev.*, vol. 28, no. 14, pp. 1620–1634, Jul. 2014.

[182] T. Song *et al.*, "A new *Vibrio cholerae* sRNA modulates colonization and affects release of outer membrane vesicles.," *Mol. Microbiol.*, vol. 70, no. 1, pp. 100–11, Oct. 2008.

[183] T. Song, D. Sabharwal, and S. N. Wai, "VrrA mediates Hfq-dependent regulation of OmpT synthesis in *Vibrio cholerae*.," *J. Mol. Biol.*, vol. 400, no. 4, pp. 682–8, Jul. 2010.

[184] T. Song *et al.*, "*Vibrio cholerae* utilizes direct sRNA regulation in expression of a biofilm matrix protein.," *PLoS One*, vol. 9, no. 7, p. e101280, Jul. 2014.

[185] D. Sabharwal, T. Song, K. Papenfort, and S. N. Wai, "The VrrA sRNA controls a stationary phase survival factor Vrp of *Vibrio cholerae*.," *RNA Biol.*, vol. 12, no. 2, pp. 186–96, Dec. 2015.

[186] A. T. Cheng, K. M. Ottemann, and F. H. Yildiz, "*Vibrio cholerae* Response Regulator VxrB Controls Colonization and Regulates the Type VI Secretion System," *PLOS Pathog.*, vol. 11, no. 5, p. e1004933, May 2015.

[187] J. K. Teschler, A. T. Cheng, and F. H. Yildiz, "The two-component signal transduction system VxrAB positively regulates *Vibrio cholerae* biofilm formation," *J. Bacteriol.*, vol. 199, no. 18, Sep. 2017.

[188] J. Yan and B. L. Bassler, "Surviving as a Community: Antibiotic Tolerance and Persistence in Bacterial Biofilms," *Cell Host Microbe*, vol. 26, no. 1., pp. 15–21, Jul. 2019.

[189] L. J. Perez, T. K. Karagounis, A. Hurley, B. L. Bassler, and M. F. Semmelhack, "Highly Potent, Chemically Stable Quorum Sensing Agonists for *Vibrio cholerae*.," *Chem. Sci.*, vol. 5, no. 1, pp. 151–155, Jan. 2014.

[190] K. Papenfort, J. E. Silpe, K. R. Schramma, J. P. Cong, M. R. Seyedsayamdost, and B. L. Bassler, "A *Vibrio cholerae* autoinducer-receptor pair that controls biofilm formation," *Nat. Chem. Biol.*, vol. 13, no. 5, pp. 551–557, May 2017.

[191] H. Abe and H. Aiba, "Differential contributions of two elements of rho-independent terminator to transcription termination and mRNA stabilization," *Biochimie*, 1996, vol. 78, no. 11–12, pp. 1035–1042.

[192] B. K. Mohanty and S. R. Kushner, "Enzymes Involved in Posttranscriptional RNA Metabolism in Gram-Negative Bacteria," *Microbiol. Spectr.*, vol. 6, no. 2, Apr. 2018.

[193] C. Spickler and G. A. Mackie, "Action of RNase II and polynucleotide phosphorylase against RNAs containing stem-loops of defined structure," *J. Bacteriol.*, vol. 182, no. 9, pp. 2422–2427, May 2000.

[194] Z. F. Cheng and M. P. Deutscher, "An important role for RNase R in mRNA decay," *Mol. Cell*, vol. 17, no. 2, pp. 313–318, Jan. 2005.

[195] B. K. Mohanty and S. R. Kushner, "Processing of the *Escherichia coli leuX* tRNA transcript, encoding tRNA Leu5 , requires either the 3' -> 5' exoribonuclease polynucleotide phosphorylase or RNase P to remove the Rho-independent transcription terminator," *Nucleic Acids Res.*, vol. 38, no. 2, pp. 597–607, Jan. 2010.

[196] J. Tomizawa, T. Itoh, G. Selzer, and T. Som, "Inhibition of ColE1 RNA primer formation by a plasmid-specified small RNA.," *Proc. Natl. Acad. Sci. U. S. A.*, vol. 78, no. 3, pp. 1421–1425, Mar. 1981.

[197] R. M. Lacatena and G. Cesareni, "Base pairing of RNA I with its complementary sequence in the primer precursor inhibits ColE1 replication," *Nature*, vol. 294, no. 5842, pp. 623–626, 1981.

[198] J. ichi Tomizawa, "Control of ColE1 plasmid replication: Initial interaction of RNA I and the primer transcript is reversible," *Cell*, vol. 40, no. 3, pp. 527–535, Mar. 1985.

[199] L. He, F. Söderbom, E. G. H. Wagner, U. Binnie, N. Binns, and M. Masters, "PcnB is required for the rapid degradation of RNAI, the antisense RNA that controls the copy number of ColE1-related plasmids," *Mol. Microbiol.*, vol. 9, no. 6, pp. 1131–1142, Sep. 1993.

[200] S. Brantl, "Plasmid Replication Control by Antisense RNAs," *Microbiol. Spectr.*, vol. 2, no. 4, Aug. 2014.

[201] F. Xu, L. C. Sue, and S. N. Cohen, "The *Escherichia coli pcnB* gene promotes adenylylation of antisense RNAI of ColE1-type plasmids in vivo and degradation of RNAI decay intermediates," *Proc. Natl. Acad. Sci. U. S. A.*, vol. 90, no. 14, pp. 6756–6760, Jul. 1993.

[202] S. Lin-Chao and S. N. Cohen, "The rate of processing and degradation of antisense RNAI regulates the replication of ColE1-type plasmids in vivo," *Cell*, vol. 65, no. 7, pp. 1233–1242, Jun. 1991.

[203] A. Hurley and B. L. Bassler, "Asymmetric regulation of quorum-sensing receptors drives autoinducer-specific gene expression programs in *Vibrio cholerae*," *PLoS Genet.*, vol. 13, no. 5, May 2017.

[204] J. H. Lee, N. Y. Park, M. H. Lee, and S. H. Choi, "Characterization of the *Vibrio vulnificus putAP* operon, encoding proline dehydrogenase and proline permease, and its differential expression in response to osmotic stress," *J. Bacteriol.*, vol. 185, no. 13, pp. 3842–3852, Jul. 2003.

[205] K. Schumacher, "DPO-mediated gene expression control in *Vibrio cholerae*," Master's Thesis, Ludwig-Maximilians-University Munich, 2019.

[206] Z. Liu, A. Hsiao, A. Joelsson, and J. Zhu, "The transcriptional regulator VqmA increases expression of the quorum-sensing activator HapR in *Vibrio cholerae*," *J. Bacteriol.*, vol. 188, no. 7, pp. 2446–2453, Apr. 2006.

[207] K. P. Subedi, D. Choi, I. Kim, B. Min, and C. Park, "Hsp31 of *Escherichia coli* K-12 is glyoxalase III," *Mol. Microbiol.*, vol. 81, no. 4, pp. 926–936, Aug. 2011.

[208] W. H. Elliott, "Methylglyoxal formation from aminoacetone by Ox plasma," *Nature*, vol. 185, no. 4711, pp. 467–468, Feb. 1960.

[209] X. Huang *et al.*, "Mechanism underlying autoinducer recognition in the *Vibrio cholerae* DPO-VqmA quorum-sensing pathway.," *J. Biol. Chem.*, vol. 295, no. 10, pp. 2916-2931, Mar. 2020.

[210] A. A. Mashruwala and B. L. Bassler, "The *Vibrio cholerae* quorum-sensing protein VqmA integrates cell density, environmental, and host-derived cues into the control of virulence," *bioRxiv*, p. 2020.05.04.076810, May 2020.

[211] A. Hsiao *et al.*, "Members of the human gut microbiota involved in recovery from *Vibrio cholerae* infection," *Nature*, vol. 515, no. 7527, pp. 423–426, Nov. 2014.

[212] C. S. Kim *et al.*, "Characterization of Autoinducer-3 Structure and Biosynthesis in *E. coli*," *ACS Cent. Sci.*, vol. 6, no. 2, pp. 197–206, Feb. 2020.

[213] K. S. Fröhlich and S. Gottesman, "Small Regulatory RNAs in the Enterobacterial Response to Envelope Damage and Oxidative Stress.," *Microbiol. Spectr.*, vol. 6, no. 4, Jul. 2018.

[214] E. Levine and T. Hwa, "Small RNAs establish gene expression thresholds," *Curr. Opin. Microbiol.*, vol. 11, no. 6. pp. 574–579, Dec. 2008.

[215] Y. Shimoni *et al.*, "Regulation of gene expression by small non-coding RNAs: A quantitative view," *Mol. Syst. Biol.*, vol. 3, no. 138, Sep. 2007.

[216] T. Dörr, B. M. Davis, and M. K. Waldor, "Endopeptidase-Mediated Beta Lactam Tolerance," *PLoS Pathog.*, vol. 11, no. 4, p. e1004850, Apr. 2015.

[217] H. T. V. Lin *et al.*, "The *Vibrio cholerae var* regulon encodes a metallo-β-lactamase and an antibiotic efflux pump, which are regulated by VarR, a LysR-type transcription factor," *PLoS One*, vol. 12, no. 9, Sep. 2017.

[218] A. I. Weaver *et al.*, "Genetic determinants of penicillin tolerance in *Vibrio cholerae*," *Antimicrob. Agents Chemother.*, vol. 62, no. 10, Oct. 2018.

[219] J. R. Ellermeier and J. M. Slauch, "Fur regulates expression of the *Salmonella* pathogenicity island 1 type III secretion system through HilD," *J. Bacteriol.*, vol. 190, no. 2, pp. 476–486, Jan. 2008.

[220] G. Padalon-Brauch *et al.*, "Small RNAs encoded within genetic islands of *Salmonella typhimurium* show host-induced expression and role in virulence," *Nucleic Acids Res.*, vol. 36, no. 6, pp. 1913–1927, Apr. 2008.

[221] J. N. Kim and Y. M. Kwon, "Identification of target transcripts regulated by small RNA RyhB homologs in *Salmonella*: RyhB-2 regulates motility phenotype," *Microbiol. Res.*, vol. 168, no. 10, pp. 621–629, Dec. 2013.

[222] J. N. Kim and Y. M. Kwon, "Genetic and phenotypic characterization of the RyhB regulon in *Salmonella Typhimurium*," *Microbiol. Res.*, vol. 168, no. 1, pp. 41–49, Jan. 2013.

[223] Z. Deng *et al.*, "Two sRNA RyhB homologs from *Yersinia pestis* biovar microtus expressed in vivo have differential Hfq-dependent stability," *Res. Microbiol.*, vol. 163, no. 6–7, pp. 413–418, Jul. 2012.

[224] Y. M. Kwon, S. C. Ricke, and R. K. Mandal, "Transposon sequencing: methods and expanding applications," *Appl. Microbiol. and Biotechnol.*, vol. 100, no. 1., pp. 31–43, Jan. 2016.

[225] J. C. Van Kessel, S. T. Rutherford, Y. Shao, A. F. Utria, and B. L. Bassler, "Individual and combined roles of the master regulators *apha* and *luxr* in control of the *Vibrio harveyi* quorum-sensing regulon," *J. Bacteriol.*, vol. 195, no. 3, pp. 436–443, Feb. 2013.

Supplemental Information – Chapter 3

RNA-mediated control of cell shape modulates antibiotic resistance in *Vibrio cholerae*

Roman Herzog[1,2*], Nikolai Peschek[1,2*], Praveen K. Singh[3], Kathrin S. Fröhlich[1,2], Luise Schröger[1,2], Fabian Meyer[1,4], Marc Bramkamp[1,4], Knut Drescher[3,5], and Kai Papenfort[1,2,6#]

[1] Friedrich Schiller University, Institute of Microbiology, 07745 Jena, Germany

[2] Faculty of Biology I, Ludwig-Maximilians-University of Munich, 82152 Martinsried, Germany

[3] Max Planck Institute for Terrestrial Microbiology, 35043 Marburg, Germany

[4] Institute for General Microbiology, Christian-Albrechts-University, Kiel, Germany,

[5] Department of Physics, Philipps-Universität Marburg, 35032 Marburg, Germany

[6] Microverse Cluster, Friedrich Schiller University Jena, 07743 Jena, Germany.

* These authors contributed equally

\# Corresponding author:

Kai Papenfort

E-mail: kai.papenfort@uni-jena.de

Phone: +49-3641-939-5753

This supplement contains:

Supplementary Figures

Supplementary Materials and Methods

Supplemental References

Tables S1-4

TABLE OF CONTENTS

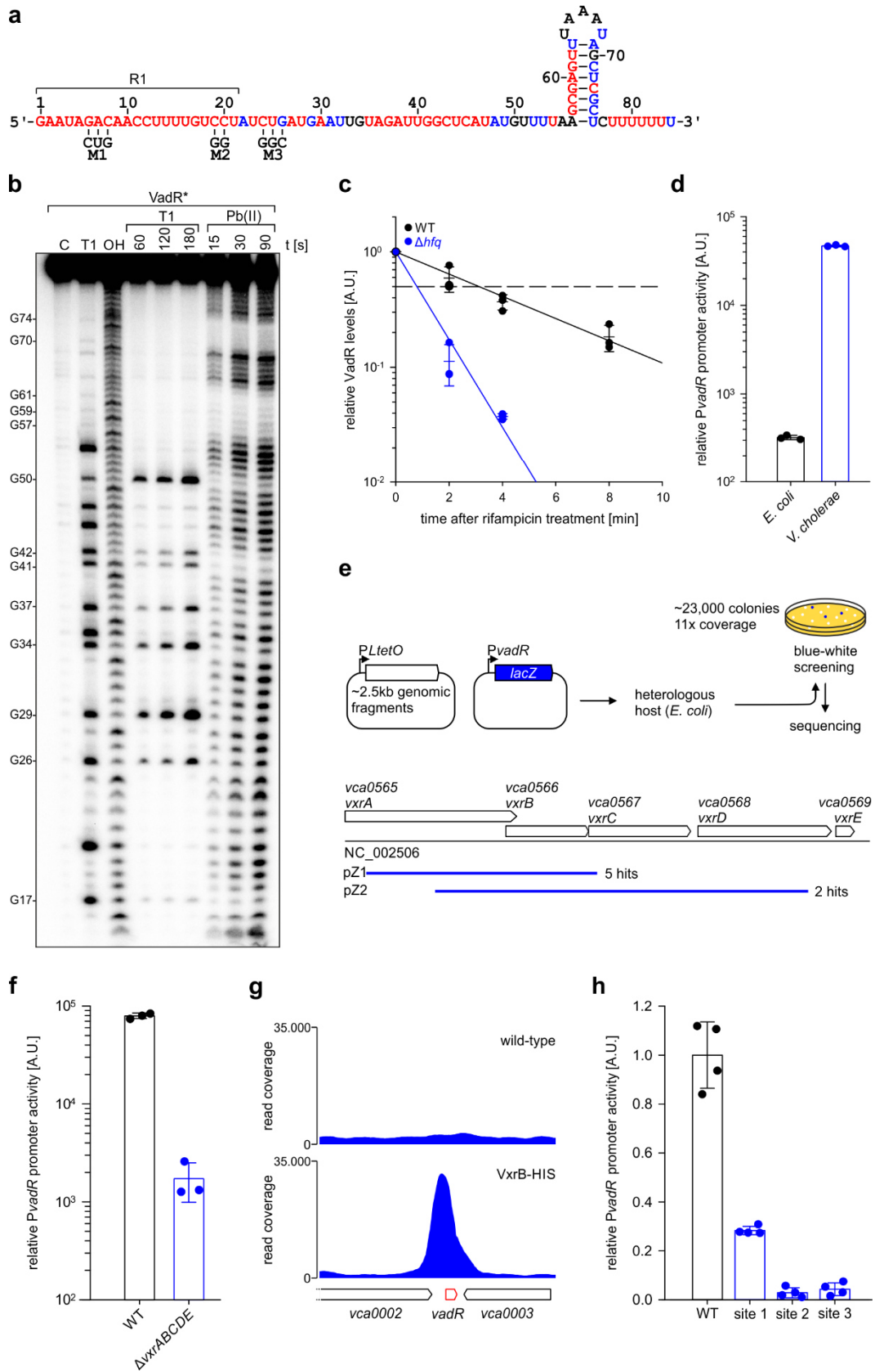**Supplementary Materials and Methods**

Figure S1

Figure S1: Structure and transcriptional control of the VadR sRNA

(a) The secondary structure of the VadR sRNA predicted by structure probing experiments (b).

(b) Secondary structure probing of the VadR sRNA. VadR was synthesized *in vitro* and labelled with ^{32}P. Enzymatic treatment was performed using RNase T1, or lead-acetate (Pb(II)). The untreated control is labelled with C, denatured ladders for RNase T1 and alkaline ladder are provided and labelled with T1 and OH, respectively. Guanin residues are labelled on the left side.

(c) Rifampicin treatment to determine half-life of the VadR sRNA, in wild-type or *hfq* mutant strains. The dashes represent the mean pf biological replicates ± SD, *n* = 3.

(d) VadR promoter activities in *E. coli* and *V. cholerae* cultures grown for 16h in LB were determined using a fluorescent transcriptional reporter. Data are the mean of biological replicates ± SD, *n* = 3.

(e) Upper part: Experimental outline to identify transcription factors affecting *vadR* transcription. Lower part: Identified fragments that yielded blue colonies.

(f) *V. cholerae* wild-type and *vxrABCDE* mutant strains were grown to OD_{600} = 0.5 and VadR promoter activities were measured. Bars show the mean of biological replicates ± SD, *n* = 3.

(g) ChIP-seq data from *V. cholerae* wild-type and *vxrB-HIS* strains, which were treated with Penicillin G for 3h[1]. Data was re-analyzed and read coverages for the *vadR* genomic locus were plotted.

(h) Three putative VxrB binding sites in the promoter region of *vadR* were deleted. The resulting strains and *V. cholerae* wild-type were cultivated to OD_{600} = 1.0 and assayed for *vadR* promoter activities using a fluorescent transcriptional reporter. Bars represent the mean of biological replicates ± SD, *n* = 4. The mean of wild-type cells was set to 1.

Figure S2
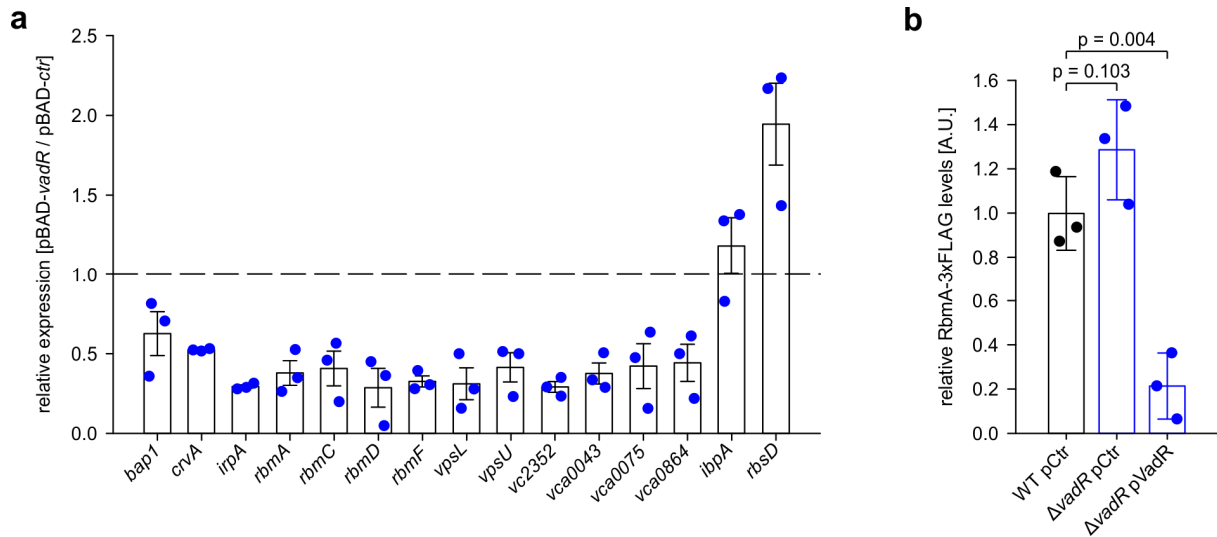
Figure S2: RNA-seq target validation and VadR-mediated regulation of RbmA

(a) qRT-PCR analysis after short period VadR expression. Expression was calculated relative to an empty vector control (pBAD-ctr). Bars represent mean of biological replicates ± SE, n = 3.

(b) Western analysis of RbmA-3xFLAG levels in *V. cholerae* wild-type and *vadR* mutant strains carrying either an empty control plasmid (pCtr) or a constitutive *vadR* overexpression plasmid. Cells were grown at 30 °C without agitation. Whole cell protein fractions were harvested at OD_{600} = 0.4. Bars indicate mean of biological replicates ± SD, n = 3. Statistical significance was determined using one-way ANOVA and post-hoc Holm-Sidak test.

Figure S3
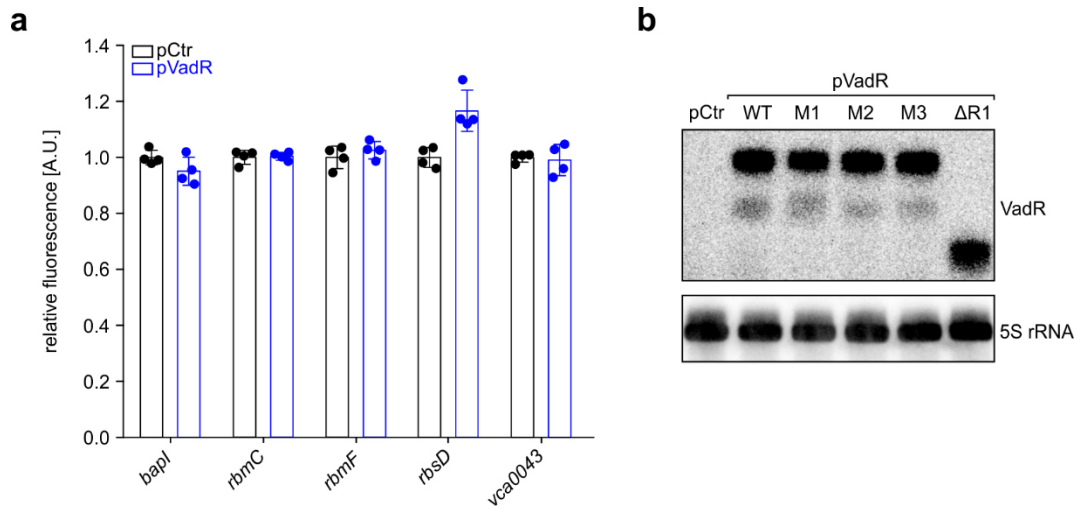
Figure S3: Indirectly regulated genes by VadR and expression of VadR variants

(a) Genes which are not post-transcriptionally regulated by VadR. Fluorescence intensities of *E. coli* strains carrying the gene-specific reporter and the control plasmid (pCtr) were set to 1. Bars show mean of biological replicates ± SD, *n* = 4.

(b) Northern analysis confirms similar expression levels of all plasmid-borne VadR variants used in this study. RNA was obtained from *E. coli* cells at OD_{600} = 1.0, which were overexpressing the indicated *vadR* variants.

Figure S4

a
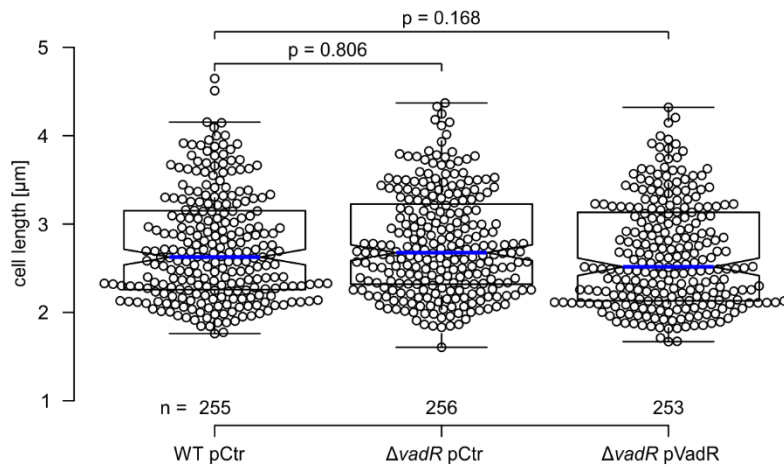
b
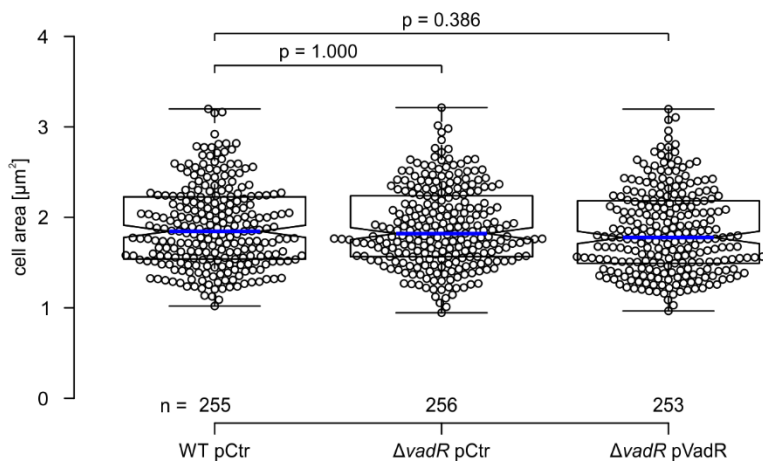
Figure S4: VadR does not affect the length and area of *V. cholerae* cells
(a-b) Analysis of cell length (a) and cell area (b) in –Cef samples of Fig. 4b. A blue line indicates the median, boxes represent 25th and 75th percentiles, whiskers represent 5th and 95th percentiles and notches indicate 95% confidence intervals for each median. *n* of each set is listed above the x-axis. Statistical significance was determined using Kruskal-Wallis test and post-hoc Dunn's test.
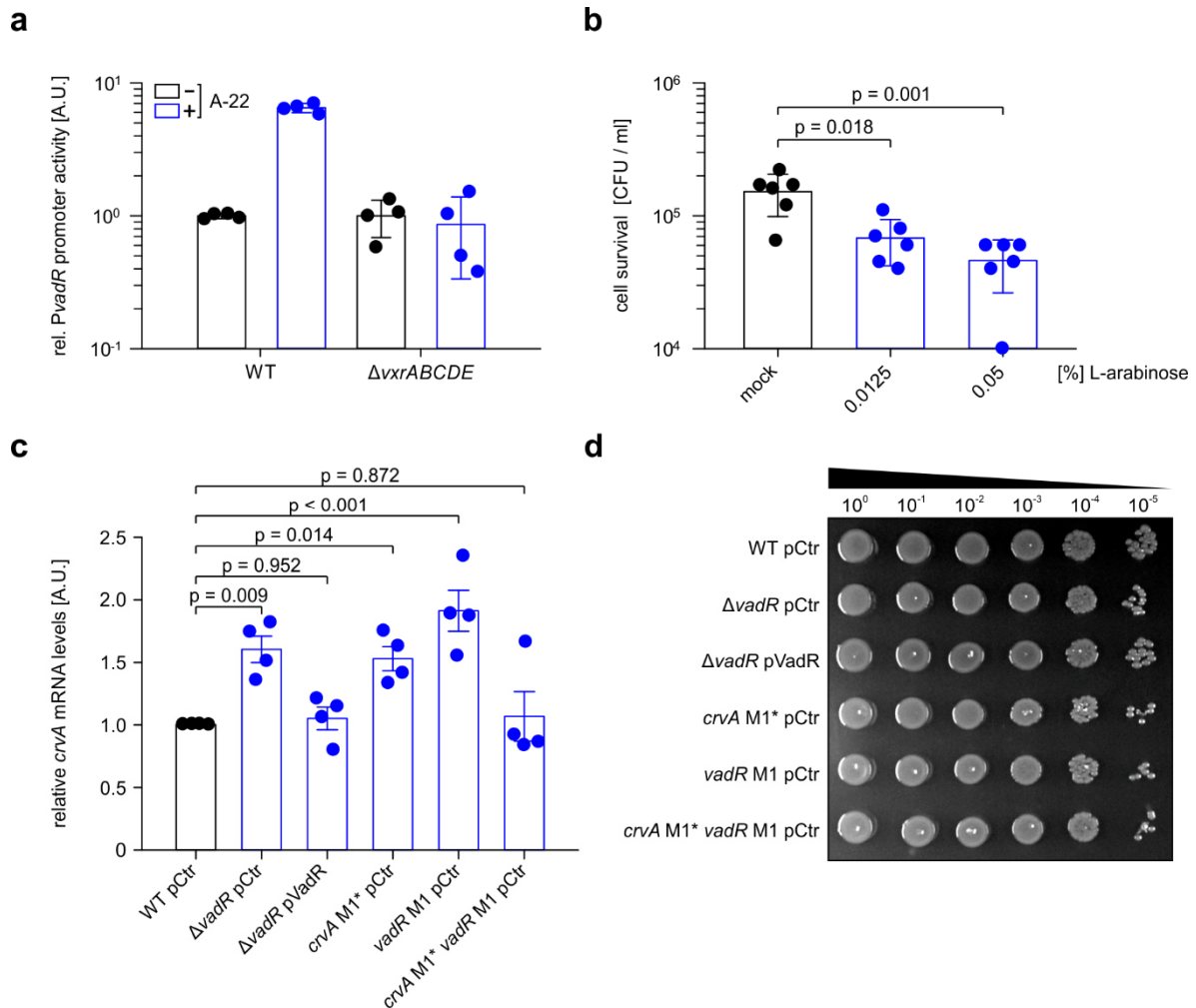
Figure S5: The VadR promoter responds to A22 treatment and V. cholerae depends on tight crvA regulation to overcome Penicillin G stress

(a) *V. cholerae* wild-type and *vxrABCDE* mutant strains were grown to OD_{600} = 0.2. Cultures were split and one set was treated with A-22 (10 µg/ml final conc.), while the other set received the same volume of water as mock treatment. VadR promoter activities in both sets were measured after 3h using a fluorescent transcriptional reporter. Promoter activities of mock-treated strains were set to 1. Bars represent mean of biological replicates ± SD, *n* = 4.

(b) Expression of the *crvAB* operon was regulated by replacing its native promoter with a P_{BAD} promoter and by using different L-arabinose concentrations for induction. Cells harbored an empty control vector (pCtr) and were treated with penicillin G for 3h and colony forming units (CFUs) were counted. Bars show mean of biological replicates ± SD, *n* = 6. Statistical significance was determined using one-way ANOVA and post-hoc Holm-Sidak test.

(c) The indicated *V. cholerea* strains (x-axis) were grown to OD_{600} = 0.2 and treated with penicillin G for 30min. Total RNA was isolated and analyzed for *crvA* expression by qRT-PCR. Bars represent mean of biological replicates ± SE, *n* = 4, relative to *V. cholerae* wild-type. Statistical significance was determined using log10-transformed values for one-way ANOVA and post-hoc Holm-Sidak test.

(d) The indicated *V. cholerea* strains (y-axis) were grown to OD_{600} = 0.4 + 3h and assayed for CFUs by spotting serial dilutions on agar plates.

Supplementary Materials and Methods

Plasmid construction

All plasmids and DNA oligonucleotides used in this study are listed in Table S3 and Table S4, respectively. If not stated otherwise, all insert fragments were amplified from genomic DNA of *V. cholerae* C6706. The backbone for the overexpression plasmids pNP-001/003-006/008-010/013 was linearized with KPO-0092/1023 using pEVS143 as a PCR template. For the amplifications of the inserted sRNAs, the following combinations of oligonucleotides were used: KPO-1003/1004 (pNP-001), KPO-1024/1025 (pNP-003), KPO-1005/1006 (pNP-004), KPO-1015/1016 (pNP-005), KPO-1021/1022 (pNP-006), KPO-1009/1010 (pNP-008), KPO-1219/1220 (pNP-009), KPO-1001/1002 (pNP-010), and KPO-1017/1018 (pNP-013). Subsequently, linearized vector and sRNA inserts were treated with XbaI restriction enzyme and fused by ligation. The construction of overexpression plasmids pLS-014-020, pRH-005, and pSG-001/002 was achieved by Gibson assembly. pEVS143 backbone was linearized using KPO-0092/1397 (pLS-014-020) or KPO-0092/1023 (pRH-005, pSG-001/002). sRNA insert sequences were amplified using KPO-5835/5836 (pLS-014), KPO-5837/5838 (pLS-015), KPO-5841/5842 (pLS-016), KPO-5843/5844 (pLS-017), KPO-5845/5846 (pLS-018), KPO-5847/5848 (pLS-019), KPO-5849/5850 (pLS-020), KPO-1226/1227 (pRH-005), KPO-1858/1859 (pSG-001), and KPO-1860/1861 (pSG-002). Further, Gibson assembly was used to generate the inducible overexpression plasmids pMD-097, pNP-019, and pNP-123-127. For these plasmids, pMD-004 served as backbone and was linearized using KPO-0196/1397 (pMD-097 and pNP-019) or KPO-0196/1488 (pNP-123-127). Amplification of insert genes were achieved with oligonucleotide combinations KPO-2554/2555 (pMD-097), KPO-1400/1401 (pNP-019), KPO-4852/4918 (pNP-123), KPO-4852/4919 (pNP-125), KPO-4852/4920 (pNP-126), and KPO-4852/4921 (pNP-127). Plasmid pNP-124 was assembled from two insert fragments, which were amplified with oligonucleotides KPO-4852/4853 and KPO-4854/4855, respectively. Plasmids pEE-007 and pLS-026-028 were generated by oligonucleotide-directed mutagenesis of pNP-005 (pEE-007) and pAE-002 (pLS-026-028), using KPO-4098/4099 (pEE-007), KPO-5981/5982 (pLS-026), KPO-5983/5984 (pLS-027), and KPO-5985/5986 (pLS-028). The promoter region of *vadR* was amplified using KPO-1906/1907 and KPO-4410/4411 for plasmids pAE-002 and pNP-122, respectively. To generate pAE-002, the obtained fragment and the pCMW-1C vector were digested with SphI and SalI enzymes and fused by ligation. Likewise, pNP-122 was obtained by ligation after treating insert and pBBR1-MCS5-lacZ equally with restriction enzymes SpeI and SalI. 5' UTRs and initial coding sequences for the construction of the translational reporter plasmids pNP-064/070-073, pRG-011-013 and pRH-090/092 were amplified using KPO-1720/1721 (pNP-064), KPO-2067/2068 (pNP-070), KPO-2069/2070 (pNP-071), KPO-2071/2072 (pNP-072), KPO-

2065/2066 (pNP-073), KPO-3735/3736 (pNP-113), KPO-3739/3740 (pNP-114), KPO-3737/3738 (pNP-115), KPO-2383/2384 (pRG-011), KPO-2385/2386 (pRG-012), KPO-2389/2390 (pRG-013), KPO-5534/5535 (pRH-090), and KPO-5538/5539 (pRH-092). Restriction digests of the amplified fragments and the pXG10-SF vector were conducted using NsiI and NheI enzymes. Inserts and vectors were combined by ligation. Plasmid pMH-039 was generated by Gibson assembly, using KPO-1702/1703 to linearize the pXG10-SF vector and KPO-1801/2803 to amplify the insert fragment, respectively. To build the suicide plasmid pNP-133, flanking regions of the *vadR* locus were amplified using KPO-1294/1295 and KPO-1296/1297. The two fragments were combined by overlap PCR with KPO-1298/1299. Restriction digest of the obtained insert fragment and of the pKAS32 vector using KpnI and ArvII enzymes and subsequent ligation, yielded the functional plasmid. To build plasmid pRH-093, pNP-133 was linearized with KPO-5550/5551. The required insert was amplified from pNP-117 using KPO-5548/5549. Gibson assembly of both parts resulted in pRH-093. Plasmids pNP-128/132/134/135 and pRH-099 were obtained by Gibson assembly, using a pKAS32 vector, which was linearized with KPO-0267/0268. The single insert fragment of pNP-128 was amplified with KPO-5456/5457. The flanking regions of the *crvA* gene and the *vxrABCDE* operon were amplified using the two oligonucleotide combinations KPO-5450/5451, KPO-5452/5453 (pNP-134) and KPO-4621/4622, KPO-4625/4626 (pNP-135), respectively. To introduce a *crvA-3xFLAG* construct onto the chromosome of *V. cholerae*, plasmid pNP-132 was designed. The corresponding flanking regions were amplified using KPO-5442/5443 and KPO-5446/5447. Oligonucleotides KPO-5444/5445 were used to amplify the 3xFLAG epitope from template plasmid pRH-030. The *araC*-P_{BAD} insert of pRH-099 was amplified from pMD-004 using KPO-4529/0196. Flanking regions of the *crvAB* promoter were amplified using oligos KPO-6013/6014 and KPO-6015/6016, respectively. Plasmid pNUT1403 was generated by ligating the *vadR* promoter fused to *mruby2* gene, amplified with oligo pair KDO-0626 and KDO1721, at XbaI-SphI restriction site of pNUT542 plasmid. *mRuby2* gene was used from pNUT883 and *vadR* promoter region was amplified from plasmid pAE-002.

All mutations for compensatory base pair exchanges were introduced by oligonucleotide-directed mutagenesis using the oligonucleotides listed in Table S4, and the respective parental plasmids as a template.

Construction of *V. cholerae* mutant strains

All strains used in this study is are listed in Table S2. *V. cholerae* C6706 was used as the wild-type strain in this study. *V. cholerae* mutant strains were generated as described previously[2]. Conjugal transfer was used to introduce plasmids into *V. cholerae* from *E. coli* S17λpir donor strains. Transconjugants were selected using appropriate antibiotics, and 50 U/ml polymyxin B was used to select against *E. coli* donor strains.

Transcript stability experiments

Stability of VadR was determined as described previously[3]. Briefly, biological triplicates of V. cholerae wild-type (KPS-0014) and Δ*hfq* (KPS-0054) strains were grown to OD600 = 0.2 and transcription was terminated by addition of 250 µg/ml rifampicin. Transcript levels were probed and quantified using Northern blot analysis.

Quantitative real-time PCR

Total RNA was isolated using the SV Total RNA Isolation System (Promega), according to the manufacturer's instructions. qRT-PCR was performed using the Luna Universal One-Step RT-qPCR Kit (New England BioLabs) and the MyiQ™ Single-Color Real-Time PCR Detection System (Bio-Rad). *recA* was used as a reference gene.

Analysis of VxrB-HIS ChIP-seq data

The raw data of the VxrB-HIS ChIP experiment conducted by Shin et al.[1] was obtained from Gene Expression Omnibus (GEO) under the accession number GSE135009. The read files were imported into CLC Genomics Workbench v11 (Qiagen) and trimmed for quality using default parameters. Reads were mapped to the *V. cholerae* reference genome (NCBI accession numbers: NC_002505.1 and NC_002506.1) using the "RNA-Seq Analysis" tool with default parameters.

RNA *in vitro* analysis

A DNA template carrying the T7 promoter for *in vitro* synthesis of RNA was prepared by PCR using oligonucleotides KPO-5083 and KPO-5084. 200 ng of template DNA were *in vitro* transcribed using the AmpliScribe T7-Flash transcription kit (Epicentre) following the manufacturer's recommendations. RNA size and integrity were verified on denaturing polyacrylamide gels. For 5' end labelling, 20 pmol of RNA were dephosphorylated using 10 units of calf alkaline phosphatase (NEB), followed by P:C:I extraction and ethanol precipitation of RNA. Dephosphorylated RNA was incubated with [^{32}P]-γATP (20 µCi) and 1 unit of polynucleotide kinase (NEB) for 1h at 37°C. Unincorporated nucleotides were removed using Microspin G-50 Columns (GE Healtcare). Labelled RNA was loaded on a 6%/7M urea gel, cut from the gel, eluted overnight at 4°C in RNA elution buffer (0.1 M sodium acetate, 0.1% SDS, 10 mM EDTA), and recovered by P:C:I extraction.

RNA structure probing was carried out as described previously[4] with few modifications. In brief, for 0.4 pmol 5′-end-labelled VadR sRNA was denatured, quickly chilled on ice and supplemented with 1x structure buffer (0.01 M Tris [pH 7], 0.1 M KCl, 0.01 M MgCl$_2$) and 1 µg yeast RNA. Samples were incubated at 37°C, and treated with RNase T1 (0.1 U; Ambion no.

127

AM2283) for 60,120 and 180 sec, or with lead(II) acetate (final concentration, 5 mM; Sigma no. 316512) for 15, 30 and 90 sec.

Reactions were stopped by the addition of 2 vol. stop/precipitation buffer (1M guanidinium thiocyanate, 0.167% N-lauryl-sarcosine, 10 mM DTT, 83% 2-propanol). RNA was precipitated for 2 h at -20°C, and collected by centrifugation (30 min, 4°C, 13.000 rpm). Samples were dissolved in GLII loading buffer, and separated on 10% polyacrylamide sequencing gels.

Supplemental References

1.   Shin, J.-H. et al. A multifaceted cellular damage repair and prevention pathway promotes high level tolerance to β-lactam antibiotics. 777375 (2019).
2.   Papenfort, K. et al. A Vibrio cholerae autoinducer-receptor pair that controls biofilm formation. *Nat Chem Biol* **13**, 551-557 (2017).
3.   Papenfort, K., Forstner, K.U., Cong, J.P., Sharma, C.M. & Bassler, B.L. Differential RNA-seq of Vibrio cholerae identifies the VqmR small RNA as a regulator of biofilm formation. *Proc Natl Acad Sci U S A* **112**, E766-75 (2015).
4.   Frohlich, K.S., Papenfort, K., Fekete, A. & Vogel, J. A small RNA activates CFA synthase by isoform-specific mRNA stabilization. *EMBO J* **32**, 2963-79 (2013).
5.   Thelin, K.H. & Taylor, R.K. Toxin-coregulated pilus, but not mannose-sensitive hemagglutinin, is required for colonization by Vibrio cholerae O1 El Tor biotype and O139 strains. *Infect Immun* **64**, 2853-6 (1996).
6.   Svenningsen, S.L., Tu, K.C. & Bassler, B.L. Gene dosage compensation calibrates four regulatory RNAs to control Vibrio cholerae quorum sensing. *EMBO J* **28**, 429-39 (2009).
7.   Datsenko, K.A. & Wanner, B.L. One-step inactivation of chromosomal genes in Escherichia coli K-12 using PCR products. *Proc Natl Acad Sci U S A* **97**, 6640-5 (2000).
8.   de Lorenzo, V. & Timmis, K.N. Analysis and construction of stable phenotypes in gram-negative bacteria with Tn5- and Tn10-derived minitransposons. *Methods Enzymol* **235**, 386-405 (1994).
9.   Fried, L., Lassak, J. & Jung, K. A comprehensive toolbox for the rapid construction of lacZ fusion reporters. *J Microbiol Methods* **91**, 537-43 (2012).
10.   Herzog, R., Peschek, N., Frohlich, K.S., Schumacher, K. & Papenfort, K. Three autoinducer molecules act in concert to control virulence gene expression in Vibrio cholerae. *Nucleic Acids Res* **47**, 3171-3183 (2019).
11.   Waters, C.M. & Bassler, B.L. The Vibrio harveyi quorum-sensing system uses shared regulatory components to discriminate between multiple autoinducers. *Genes Dev* **20**, 2754-67 (2006).
12.   Nadell, C.D., Drescher, K., Wingreen, N.S. & Bassler, B.L. Extracellular matrix structure governs invasion resistance in bacterial biofilms. *ISME J* **9**, 1700-9 (2015).
13.   Yan, J., Sharo, A.G., Stone, H.A., Wingreen, N.S. & Bassler, B.L. Vibrio cholerae biofilm growth program and architecture revealed by single-cell live imaging. *Proc Natl Acad Sci U S A* **113**, E5337-43 (2016).
14.   Skorupski, K. & Taylor, R.K. Positive selection vectors for allelic exchange. *Gene* **169**, 47-52 (1996).
15.   Corcoran, C.P. et al. Superfolder GFP reporters validate diverse new mRNA targets of the classic porin regulator, MicF RNA. *Mol Microbiol* **84**, 428-45 (2012).
16.   Donnell, Z. Regulation of cqsA and cqsS in Vibrio cholerae. (Princeton, NJ : Princeton University, 2015).

Table S1 Genes differentially regulated by *vadR* pulse expression

ID	Gene	Description#	Fold change*
vc0932	*rbmE*	uncharacterized protein	-4.70
vc0934	*vpsL*	capsular polysaccharide biosynthesis glycosyltransferase	-4.61
vc0933	*rbmF*	uncharacterized protein	-4.57
vc0928	*rbmA*	rugosity and biofilm structure modulator A	-3.58
vc0935	*vpsM*	polysaccharide biosynthesis protein	-3.48
vc0936	*vpsN*	polysaccharide biosynthesis/export protein	-3.23
vc0917	*vpsA*	UDP-N-acetylglucosamine 2-epimerase	-3.19
vc0919	*vpsC*	serine O-acetyltransferase	-3.03
vc0918	*vpsB*	UDP-N-acetyl-D-mannosaminuronic acid dehydrogenase	-2.92
vc0916	*vpsU*	tyrosine-protein phosphatase	-2.83
vc0931	*rbmD*	hypothetical protein	-2.71
vca0043		hypothetical protein	-2.55
vca0864		methyl-accepting chemotaxis protein	-2.53
vc0920	*vpsD*	polysaccharide biosynthesis protein	-2.47
vc1888	*bap1*	extracellular matrix protein	-2.38
vc0937	*vpsO*	polysaccharide biosynthesis transport protein	-2.38
vc1264	*irpA*	iron-regulated protein A	-2.34
vc0938	*vpsP*	polysaccharide biosynthesis protein	-2.14
vc2352		concentrative nucleoside transporter, CNT familiy	-1.97
vca0075		hypothetical protein	-1.89
vca1075	*crvA*	hypothetical protein	-1.81
vc0930	*rbmC*	rugosity and biofilm structure modulator C	-1.79
vca0044		pseudogene	-1.77
vca0074		diguanylate cyclase	-1.77
vc0018	*ibpA*	molecular chaperone IbpA	-1.76
vca0129	*rbsC*	ribose transport system permease protein	1.81
vca0128	*rbsA*	ribose transport system ATP-binding protein	1.96
vca0127	*rbsD*	D-ribose pyranase	2.22

#Description is based on the annotation at KEGG (https://www.genome.jp/kegg)

*Fold change is based on transcriptomic analysis of pBAD-derived *vadR* expression using RNA-seq. Genes with a fold-change of at least 1.75-fold in either condition and a FDR adjusted p-value ≤ 0.001 were considered to be differentially expressed.

Table S2 Bacterial strains used in this study

Strain	Relevant markers/ genotype	Reference/ source
V. cholerae		
KPS-0014	Wild-type C6706	[5]
KPS-0053	Δ*hapR* C6706	[3]
KPS-0054	Δ*hfq* C6706	[6]
KPVC-10126	Δ*vadR* C6706	This study
KPVC-12430	Δ*vxrABCDE* C6706	This study
KPVC-12817	Δ*crvA* C6706	This study
KPVC-12912	*crvA* M1* C6706	This study
KPVC-12913	*crvA::crvA-3xFLAG* C6706	This study
KPVC-12914	Δ*vadR crvA::crvA-3xFLAG* C6706	This study
KPVC-13214	*vadR* M1 C6706	This study
KPVC-13215	*vadR* M1 *crvA* M1* C6706	This study
KPVC-13223	*rbmA::rbmA-3xFLAG, rbmC::rbmC-3xFLAG, bapI::bapI-3xFLAG* C6706	This study
KPVC-13384	P$_{crvAB}$*::araC*-P$_{BAD}$ C6706	This study
KPVC-13439	Δ*hapR* Δ*rbmA* C6706	This study
E. coli		
BW25113	*lacI*⁺ *rrn*B$_{T14}$ Δ*lacZ*$_{WJ16}$ *hsdR514* Δ*araBAD*$_{AH33}$ Δ*rhaBAD*$_{LD78}$ *rph-1* Δ*(araB–D)567* Δ*(rhaD–B)568* Δ*lacZ4787(::rrnB-3) hsdR514 rph-1*	[7]
TOP10	*mcr*AΔ*(mrr-hsd*RMS-*mcr*BC) Φ80*lacZ*ΔM15Δ*lacX74deoRrec*A1 *ara*D139Δ*(ara-leu)*7697 *gal*U *gal*K *rps*L *end*A1 *nup*G	Invitrogen
S17λpir	Δ*lacU*169 (Φ*lacZ*ΔM15), *rec*A1, *end*A1, *hsd*R17, *thi-1*, *gyr*A96, *rel*A1, *λpir*	[8]

Table S3 Plasmids used in this study

Plasmid trivial name	Plasmid stock name-	Relevant fragment	Comment	Origin, marker	Reference
pBBR1MCS5-5-lacZ		*lacZ*	Promoterless plasmid for transcriptional reporters	pBBR1, Gent[R]	9
P*vadR-mKate2*	pAE-002	P*vadR-mKate2*	*vadR* transcriptional reporter plasmid	p15A, Cm[R]	This study
pCMW-1C	pCMW-1C	Cm[R] cassette	Promoterless plasmid for transcriptional reporters	p15A, Cm[R]	10
pCtr	pCMW-1K	Kan[R] cassette	Control plasmid	p15A, Kan[R]	11
pKAS32-Δ*rbmA*	pCN-007	up-/downstream flanks of *rbmA*	suicide plasmid for *rbmA* knockout	R6K, Amp[R]	12
pKAS32-*rbmA-3xFLAG*	pCN-018	3xFLAG	*rbmA-3xFLAG* allelic replacement	R6K, Amp[R]	12
pKAS32-*rbmC-3xFLAG*	pCN-019	3xFLAG	*rbmC-3xFLAG* allelic replacement	R6K, Amp[R]	12
pKAS32-*bapI-3xFLAG*	pCN-020	3xFLAG	*bap1-3xFLAG* allelic replacement	R6K, Amp[R]	13
pVadRΔR1	pEE-007	*vadR ΔR1*	*vadR ΔR1* expression plasmid	p15A, Kan[R]	This study
pEVS143	pEVS143	Ptac promoter	Constitutive over-expression plasmid	p15A, Kan[R]	3
pKAS32	pKAS32		suicide plasmid for allelic exchange	R6K, Amp[R]	14
pVcr025	pLS-014	*vcr025*	*vcr025* expression plasmid	p15A, Kan[R]	This study
pVcr062	pLS-015	*vcr062*	*vcr062* expression plasmid	p15A, Kan[R]	This study
pVcr058	pLS-016	*vcr058*	*vcr058* expression plasmid	p15A, Kan[R]	This study
pVcr071	pLS-017	*vcr071*	*vcr071* expression plasmid	p15A, Kan[R]	This study
pVcr067	pLS-018	*vcr067*	*vcr067* expression plasmid	p15A, Kan[R]	This study
pVcr094	pLS-019	*vcr094*	*vcr094* expression plasmid	p15A, Kan[R]	This study
pVcr099	pLS-020	*vcr099*	*vcr099* expression plasmid	p15A, Kan[R]	This study

pΔsite1-mKate2	pLS-026	PvadRΔsite1-mKate2	vadR transcriptional reporter plasmid	p15A, Cm^R	This study
pΔsite2-mKate2	pLS-027	PvadRΔsite2-mKate2	vadR transcriptional reporter plasmid	p15A, Cm^R	This study
pΔsite3-mKate2	pLS-028	PvadRΔsite3-mKate2	vadR transcriptional reporter plasmid	p15A, Cm^R	This study
pBAD	pMD-004		Control plasmid	p15A, Kan^R	[10]
pVcr084	pMD-097	vcr084	vcr084 expression plasmid	p15A, Kan^R	This study
pvca0864-gfp	pMH-039	vca0864-gfp	Translational reporter vca0864-gfp	pSC101*, Cm^R	This study
pVcr002	pNP-001	vcr002	vcr002 expression plasmid	p15A, Kan^R	This study
pVcr036	pNP-003	vcr036	vcr036 expression plasmid	p15A, Kan^R	This study
pVcr043	pNP-004	vcr043	vcr043 expression plasmid	p15A, Kan^R	This study
pVadR	pNP-005	vadR	vadR expression plasmid	p15A, Kan^R	This study
pVcr079	pNP-006	vcr079	vcr079 expression plasmid	p15A, Kan^R	This study
pVcr034	pNP-008	vcr034	vcr034 expression plasmid	p15A, Kan^R	This study
pVcr082	pNP-009	vcr082	vcr082 expression plasmid	p15A, Kan^R	This study
pVcr092	pNP-010	vcr092	vcr092 expression plasmid	p15A, Kan^R	This study
pVcr045	pNP-013	vcr045	vcr045 expression plasmid	p15A, Kan^R	This study
pBAD-vadR	pNP-019	P$_{BAD}$-vadR	Inducible vadR expression plasmid	p15A, Kan^R	This study
prbmC-gfp	pNP-064	rbmC-gfp	Translational reporter rbmC-gfp	pSC101*, Cm^R	This study
pvpsU-gfp	pNP-070	vpsU-gfp	Translational reporter vpsQ-gfp	pSC101*, Cm^R	This study
prbmA-gfp	pNP-071	rbmA-gfp	Translational reporter rbmA-gfp	pSC101*, Cm^R	This study
prbmD-gfp	pNP-072	rbmD-gfp	Translational reporter rbmD-gfp	pSC101*, Cm^R	This study
pvpsL-gfp	pNP-073	vpsL-gfp	Translational reporter vpsL-gfp	pSC101*, Cm^R	This study
pirpA-gfp	pNP-113	irpA-gfp	Translational reporter irpA-gfp	pSC101*, Cm^R	This study
pvc2352-gfp	pNP-114	vc2352-gfp	Translational reporter vc2352-gfp	pSC101*, Cm^R	This study

p*vca0043-gfp*	pNP-115	*vca0043-gfp*	Translational reporter *vca0043-gfp*	pSC101*, Cm^R	This study
p*crvA M1*-gfp*	pNP-116	*crvA M1*-gfp*	Translational reporter *crvA* M1-*gfp*	pSC101*, Cm^R	This study
pVadR M1	pNP-117	*vadR* M1	*vadR* M1 expression plasmid	p15A, Kan^R	This study
pVadR M3	pNP-118	*vadR* M3	*vadR* M3 expression plasmid	p15A, Kan^R	This study
p*vpsU M2*-gfp*	pNP-119	*vpsU M2*-gfp*	Translational reporter *vpsU* M2-*gfp*	pSC101*, Cm^R	This study
p*rbmA M1*-gfp*	pNP-120	*rbmA M1*-gfp*	Translational reporter *rbmA* M1-*gfp*	pSC101*, Cm^R	This study
p*vpsL M3*-gfp*	pNP-121	*vpsL M3*-gfp*	Translational reporter *vpsL* M3-*gfp*	pSC101*, Cm^R	This study
P*vadR-lacZ*	pNP-122	P*vadR-lacZ*	*vadR* transcriptional reporter plasmid	pBBR1, Gent^R	This study
pBAD-*vxrA*	pNP-123	*vxrA*	Inducible *vxrA* expression plasmid	p15A, Kan^R	This study
pBAD-*vxrAB*	pNP-124	*vxrAB*	Inducible *vxrAB* expression plasmid	p15A, Kan^R	This study
pBAD-*vxrABC*	pNP-125	*vxrABC*	Inducible *vxrABC* expression plasmid	p15A, Kan^R	This study
pBAD-*vxrABCD*	pNP-126	*vxrABCD*	Inducible *vxrABCD* expression plasmid	p15A, Kan^R	This study
pBAD-*vxrABCDE*	pNP-127	*vxrABCDE*	Inducible *vxrABCDE* expression plasmid	p15A, Kan^R	This study
pKAS32-Δ*crvA*	pNP-128	*crvA* region	*crvA* region	R6K, Amp^R	This study
pKAS32-*crvA* M1*	pNP-129	*crvA* M1*	*crvA* M1* allelic replacement	R6K, Amp^R	This study
pKAS32-*crvA-3xFLAG*	pNP-132	*crvA-3xFLAG*	*crvA-3xFLAG* allelic replacement	R6K, Amp^R	This study
pKAS32-Δ*vadR*	pNP-133	up-/downstream flanks *vadR*	suicide plasmid for *vadR* knockout	R6K, Amp^R	This study
pKAS32-Δ*crvA*	pNP-134	up-/downstream flanks *crvA*	suicide plasmid for *crvA* knockout	R6K, Amp^R	This study
pKAS32-Δ*vxrABCDE*	pNP-135	up-/downstream flanks *vxrABCDE*	suicide plasmid for *vxrABCDE* knockout	R6K, Amp^R	This study
pVadR M2	pNP-168	*vadR* M2	*vadR* M2 expression plasmid	p15A, Kan^R	This study
pNUT1403	pNUT1403	P*vadR-mRuby2*	*vadR* transcriptional reporter plasmid	pSC101, Gent^R	This study

p*bap1-gfp*	pRG-011	*bap1-gfp*	Translational reporter *bap1-gfp*	pSC101*, Cm^R	This study
p*crvA-gfp*	pRG-012	*crvA-gfp*	Translational reporter *crvA-gfp*	pSC101*, Cm^R	This study
p*rbmF-gfp*	pRG-013	*rbmF-gfp*	Translational reporter *rbmEF-gfp*	pSC101*, Cm^R	This study
pVcr098	pRH-005	*vcr098*	*vcr098* expression plasmid	p15A, Kan^R	This study
pKAS32-*aphA-3xFLAG*	pRH-030	3xFLAG	*aphA-3xFLAG* allelic replacement	R6K, Amp^R	[14]
p*vca0075-gfp*	pRH-090	*vca0075-gfp*	Translational reporter *vca0075-gfp*	pSC101*, Cm^R	This study
p*rbsD-gfp*	pRH-092	*rbsD-gfp*	Translational reporter *rbsD-gfp*	pSC101*, Cm^R	This study
pKAS32-*vadR* M1	pRH-093	*vadR* M1	*vadR* M1 allelic replacement	R6K, Amp^R	This study
pKAS32-*araC*-P$_{BAD}$	pRH-099	*araC*-P$_{BAD}$, flanking regions of P$_{crvAB}$	*araC*-P$_{BAD}$ allelic replacement	R6K, Amp^R	This study
pVcr017	pSG-001	*vcr017*	*vcr017* expression plasmid	p15A, Kan^R	This study
pVcr080	pSG-002	*vcr080*	*vcr080* expression plasmid	p15A, Kan^R	This study
pXG10-SF	pXG10SF	'*lacZ::gfp*	template plasmid for translational reporters	pSC101*, Cm^R	[15]
pCMW-1C-mKate2	pYH-010	mKate2	Promoterless plasmid for transcriptional reporters	P15A, Cm^R	[7]
pZ1	pZ1	*vcrAB* fragment 1	*vxrAB* fragment 1 expression plasmid	p15A, Cm^R	This study
pZ2	pZ2	*vcrAB* fragment 2	*vxrAB* fragment 2 expression plasmid	p15A, Cm^R	This study
pZach	pZND132	*V.ch.* genomic fragments	Genomic fragment expression plasmid	p15A, Cm^R	[16]

Table S4 DNA oligonucleotides used in this study

Sequences are given in 5' → 3' direction; 5' P denotes a 5' monophosphate

ID	Sequence	Description
KDO-0626	TAGCTCCTGAATTCCTAGGCCTG	pNUT1403
KDO-1721	GGGTCTAGAGCGGAGTGACTATAAAAAGGCGC	pNUT1403
KPO-0092	CCACACATTATACGAGCCGA	pNP-001/003-006/008-010/013, pSG001/002, pLS014-020, pRH-005
KPO-0196	GGAGAAACAGTAGAGAGTTGCG	pNP-019/123-127, pMD-097, pRH-099
KPO-0243	TTCGTTTCACTTCTGAGTTCGG	5S-rRNA probe
KPO-0267	TAATAGGCCTAGGATGCATATG	pNP-128/132/133/134/135, pRH-099
KPO-0268	CGTTAACAACCGGTACCTCTA	pNP-128/132/133/134/135, pRH-099
KPO-0331	GAGCCAATCTACAATTCATCAGA	VadR probe
KPO-1001	P-TCACAGAACCGCTGTGACCA	pNP-010
KPO-1002	GTTTTTTCTAGATTGACTACTTCATTCGCCAC	pNP-010
KPO-1003	P-GCAAACACATTGGTAAGATATTAG	pNP-001
KPO-1004	GTTTTTTCTAGATATAACCTGTTCAGAATGTGCT	pNP-001
KPO-1005	P-GTCATCTCGTTAGTCATTACGA	pNP-004
KPO-1006	GTTTTTTCTAGACACTGACAAACCGGTGTTGG	pNP-004
KPO-1009	P-ACTTACTTGGATAAATATGCATTG	pNP-008
KPO-1010	GTTTTTTCTAGAGTATTGTTTGTCTGTCATAAAGTT	pNP-008
KPO-1015	P-AATAGACAACCTTTTGTCCTATC	pNP-005
KPO-1016	GTTTTTTCTAGAATAGAAAGCACTGAGTCAGGA	pNP-005
KPO-1017	P-TTGCCCGCAAGCCACGGC	pNP-013
KPO-1018	GTTTTTTCTAGAAGGCGATTGGTCGTGTTGTT	pNP-013
KPO-1021	P-GTTTGAACCCCGGCGGCT	pNP-006
KPO-1022	GTTTTTTCTAGAAAACCGACTCCTTGCAAGAA	pNP-006
KPO-1023	GTTTTTTCTAGAGGATCCGGTGATTGATTGAG	pNP-001/003-006/008-010/013, pSG001/002, pRH-005
KPO-1024	P-ACCCAAAGGGTAGAGCAAAC	pNP-003
KPO-1025	GTTTTTTCTAGAGAAAACGAAGTAATCTTCACCTT	pNP-003
KPO-1219	P-AGCTTCGCTAGCGAAGAG	pNP-009
KPO-1220	GTTTTTTCTAGAGAATGTTGCGATCAAGTTCG	pNP-009
KPO-1226	TCGTATAATGTGTGGGTAAGGTTAGTGAGAACATTTCT	pRH-005
KPO-1227	ACCGGATCCTCTAGAAGTTTCAAATTTCGTGGACAGC	pRH-005
KPO-1294	GTACATTTTGGTGTGGGAGC	pNP-133
KPO-1295	GCACTGAGTCAGGATTTTGCGTATCGGCGGTTATTCGGTTC	pNP-133
KPO-1296	GCAAAATCCTGACTCAGTGC	pNP-133
KPO-1297	CAAACCCAGCTCTTTAGCTTC	pNP-133
KPO-1298	GTTTTTGGTACCGACGCGAGATTATTTCTTCC	pNP-133
KPO-1299	GTTTTTCCTAGGGATAGTCAGGCCGCTTTCG	pNP-133
KPO-1397	GATCCGGTGATTGATTGAGC	pNP-019, pMD-097, pLS014-020
KPO-1400	CGCAACTCTCTACTGTTTCTCCGAATAGACAACCTTTTGTCCTATC	pNP-019
KPO-1401	GCTCAATCAATCACCGGATCATAGAAAGCACTGAGTCAGGA	pNP-019

136

KPO-1488	TTTTTTCTAGATTAAATCAGAACGCAG	pNP-123-127
KPO-1702	ATGCATGTGCTCAGTATCTCTATC	pMH-039
KPO-1703	GCTAGCGGATCCGCTGG	pMH-039
KPO-1720	GAGATACTGAGCACATGCATAGGTTGTTATTAGCAATCCGCGATAC	pNP-064
KPO-1721	GAGCCAGCGGATCCGCTAGCCAACGACAAAAGACCGACAGCAAG	pNP-064
KPO-1801	CTGTCACCAATTACGCTGGTTTTTCCTTTTTATTAAC	pMH-039
KPO-1858	TCGGCTCGTATAATGTGTGGGCTAGCGAAAACTATAATCATAAAC	pSG-001
KPO-1859	CTCAATCAATCACCGGATCCGCTTTGATTGAGCAGACGTTG	pSG-001
KPO-1860	TCGGCTCGTATAATGTGTGGGCAAGTCAGTGGTGTTGG	pSG-002
KPO-1861	CTCAATCAATCACCGGATCCGTACTGTCAATATCGACCAC	pSG-002
KPO-1906	GTTTTTGCATGCGCTGCGTGTTGAAAACGATG	pAE-002
KPO-1907	GTTTTTGTCGACCTATTCGTGAAGCAGTGTATC	pAE-002
KPO-2065	GTTTTTATGCATAGATATTTCTATTGATAAAGATGTAGTCTT	pNP-073
KPO-2066	GTTTTTGCTAGCGCTATCAATTAATCGGTAGAAAAATTTAC	pNP-073
KPO-2067	GTTTTTATGCATACTCTGATAATGAGTAGATTGCG	pNP-070
KPO-2068	GTTTTTGCTAGCCTCTGCCATTGGCGAACGA	pNP-070
KPO-2069	GTTTTTATGCATTTAGCCAATGCAATTGTCTTAGATTTG	pNP-071
KPO-2070	GTTTTTGCTAGCATAAGAAGCCGTTGAAAATAACAATGC	pNP-071
KPO-2071	GTTTTTATGCATATGGCATGGCGGAGCAAGTTG	pNP-072
KPO-2072	GTTTTTGCTAGCACTGCCAAGAGGGATTGGTAAC	pNP-072
KPO-2378	GGTAACCCAGAAACTACCACTG	*recA* qRT-PCR
KPO-2379	CACCACTTCTTCGCCTTCTT	*recA* qRT-PCR
KPO-2383	GTTTTTATGCATGCTCTCAGCATATCGTTATTG	pRG-011
KPO-2384	GTTTTTGCTAGCGAATGCGGTGCTTTGAGTC	pRG-011
KPO-2385	GTTTTTATGCATGCTTAGATCTAAAGTTCAAAAAATCAG	pRG-012
KPO-2386	GTTTTTGCTAGCCGATGCAGATACCCATAAAGG	pRG-012
KPO-2389	GTTTTTATGCATAAAGAAATAATATGTATCGTTTATCG	pRG-013
KPO-2390	GTTTTTGCTAGCATTCATGCTAGGAAAAAATGCAATC	pRG-013
KPO-2554	CGCAACTCTCTACTGTTTCTCCTATTACAACAAGAGAGGCTC	pMD-097
KPO-2555	GCTCAATCAATCACCGGATCCAGACGCTACATCAAACTG	pMD-097
KPO-2803	GAGCCAGCGGATCCGCTAGCGACCACCCAACGCAGCAATC	pMH-039
KPO-3613	CTTGATTGGTTGGCGTGTATTG	*vpsL-O* qRT-PCR
KPO-3614	CTTGCCCTTGAGTAGTCATACC	*vpsL-O* qRT-PCR
KPO3615	CTTGTGGCGCACTTTCAATC	*rbmEF* qRT-PCR
KPO3616	GTGGATGACCAACGAGTACAA	*rbmEF* qRT-PCR
KPO-3617	GCTCTTACTGATGGTCGTATGT	*rbmA* qRT-PCR
KPO-3618	CTGCAACGACTTGAAGAGAAAC	*rbmA* qRT-PCR
KPO-3621	TAGTGCTGGCACGCTAAAG	*vpsQA-K* qRT-PCR
KPO-3622	TTGAGTCACTTGCTGGACTG	*vpsQA-K* qRT-PCR
KPO-3623	CTTGGTTGCCGCGTTATTG	*rbmD* qRT-PCR
KPO-3624	GCATAGAAGGCCTGACAGATAC	*rbmD* qRT-PCR
KPO-3625	GAGCTGCAAGGTAAGGGATAC	*vca0043-44* qRT-PCR
KPO-3626	AACTACAGACGGGCACAATC	*vca0043-44* qRT-PCR
KPO-3627	CAGTCCCTATCCGAGCATATTG	*vca0864* qRT-PCR
KPO-3628	GGTAAGCTCCTCTAACCGATAAC	*vca0864* qRT-PCR
KPO-3629	CCGTCTCTTACTGGTTCTTTGG	*bapI* qRT-PCR
KPO-3630	GTGTCACAGGAACGGCATAA	*bapI* qRT-PCR
KPO-3631	CGATCTTGAGTGGATGGAGAAG	*irpA* qRT-PCR
KPO-3632	ATAGCGAGCCCATACCAAAC	*irpA* qRT-PCR

KPO-3633	GCGTGAAAGTAGCGTGTTAGA	*crvA* qRT-PCR
KPO-3634	TTCTGCTTCGTCAGGTATTGG	*crvA* qRT-PCR
KPO-3635	CTGAGCTGTTTGCGGTAATG	*vc2352* qRT-PCR
KPO-3636	CCGCTACCAAGTATTCGATCT	*vc2352* qRT-PCR
KPO-3637	GGCATCGAACATCACGATACA	*vca0074-75* qRT-PCR
KPO-3638	CCATGGCAGTTCAGTGGTAAA	*vca0074-75* qRT-PCR
KPO-3641	TCGGCCATACCGATGAAATC	*rbsDACB* qRT-PCR
KPO-3642	AGTCAGCGCGAGATCAATAC	*rbsDACB* qRT-PCR
KPO-3643	GGTTCTGAGCTATGGAGCTATG	*rbmC* qRT-PCR
KPO-3644	ATCTCAACGATTCCGTCACC	*rbmC* qRT-PCR
KPO-3735	GTTTTTATGCATGAAATAACAAATGATAATAATTTGCAATTC	pNP-113
KPO-3736	GTTTTTGCTAGCCGCTGATGTAGTGAGCGTC	pNP-113
KPO-3737	GTTTTTATGCATAGCGAGTCACCAACTAATTTG	pNP-115
KPO-3738	GTTTTTGCTAGCTTCCAAAGCCACGCGATAAC	pNP-115
KPO-3739	GTTTTTATGCATGCTTAATCGCTCCATTTTGTAAC	pNP-114
KPO-3740	GTTTTTGCTAGCCAGTAGAACTGCGATTCCTAG	pNP-114
KPO-4098	TCGGCTCGTATAATGTGTGGATCTGATGAATTGTAGATTGGCT	pEE-007
KPO-4099	AATAGACAACCTTTTGTCCTATCTGATGAATTGATATGTTTTAAGC	pEE-007
KPO-4250	GAATACTGAACCTTTTGTCCTATCTG	pNP-117
KPO-4251	GTTCAGTATTCCCACACATTATACG	pNP-117
KPO-4252	GTTTCAGTTTCCCACTTTATGTGG	pNP-116
KPO-4253	GGAAACTGAAACTTTTGACAGCTTTG	pNP-116
KPO-4410	GTTTTTTACTAGTGCTGCGTGTTGAAAACGATG	pNP-122
KPO-4411	GTTTTTTGTCGACCTATTCGTGAAGCAGTGTATC	pNP-122
KPO-4529	TATAAGATCATAAAAGACCCTTCATTTATG	pRH-099
KPO-4621	AGAGGTACCGGTTGTTAACGCATCATCAAGTCCACACCACT	pNP-135
KPO-4622	TATCCGGTAAAGAGATATTCGAG	pNP-135
KPO-4625	GAATATCTCTTTACCGGATACACCAAACCTGCTAAAAACACG	pNP-135
KPO-4626	TATGCATCCTAGGCCTATTACGATACCGGTGAAGCTAATGA	pNP-135
KPO-4846	GATTGGCTTTGACCGTCTACT	*ibpA* qRT-PCR
KPO-4847	GCTCGATATTGTATGGAGGGTATC	*iboA* qRT-PCR
KPO-4852	CAACTCTCTACTGTTTCTCCGGATAATGCGTTATAGTTTTTGC	pNP-123-127
KPO-4853	TCAACGAGAAGCAGTGTCTG	pNP-124
KPO-4854	CAGACACTGCTTCTCGTTGAAGATGATAAAAACCTCGCTGAC	pNP-124
KPO-4855	CTGATTTAATCTAGAAAAAATGATCACGCTTTCATTTTGTAAC	pNP-124
KPO-4918	CTGATTTAATCTAGAAAAAATCAACGAGAAGCAGTGTCTG	pNP-123
KPO-4919	CTGATTTAATCTAGAAAAAACTATAGCGGCATATTGTCCAA	pNP-125
KPO-4920	CTGATTTAATCTAGAAAAAAGAGCCACACTATAAAGAGATG	pNP-126
KPO-4921	CTGATTTAATCTAGAAAAAAGAAAAATTGGCTACGATTATTACC	pNP-127
KPO-5083	GTTTTTTTTAATACGACTCACTATAGGAATAGACAACCTTTTGTCCT	In-vitro VadR
KPO-5084	AAAAAAAGAGCGAGCTATTTAAAC	In-vitro VadR
KPO-5442	AGAGGTACCGGTTGTTAACGGCTTAGATCTAAAGTTCAAAAAATCAG	pNP-132
KPO-5443	GCTGTCTTTGTTTGGTCTGAG	pNP-132
KPO-5444	TCAGACCAAACAAAGACAGCGACTACAAAGACCATGACGGTG	pNP-132
KPO-5445	ATCGTTGGATTTTTGTGCGGTTACTATTTATCGTCATCTTTGTAGTC	pNP-132
KPO-5446	CCGCACAAAAATCCAACGATTTC	pNP-132
KPO-5447	TATGCATCCTAGGCCTATTAGCAGCAATACTTCAACCGGAG	pNP-132
KPO-5450	AGAGGTACCGGTTGTTAACGGAGCTCAATAAGCGAGGAATTC	pNP-134
KPO-5451	GAAATATGCAAGCTGAGTTTTCC	pNP-134

KPO-5452	AAACTCAGCTTGCATATTTCGTCGGAATTCACAAACCTGTC	pNP-134
KPO-5453	TATGCATCCTAGGCCTATTAGAATGGTCTGATCGGAGGTG	pNP-134
KPO-5456	AGAGGTACCGGTTGTTAACGGAACGTACTTTGATTGGAAAAACC	pNP-128
KPO-5457	TATGCATCCTAGGCCTATTACTTCTTTCGATACGGTGACTTG	pNP-128
KPO-5458	GTTTCAGTTTCCCACTTTATGTGGCTAAAC	pNP-129
KPO-5459	GAAACTGAAACTTTTGACAGCTTTGTAGATAG	pNP-129
KPO-5534	GTTTTTATGCATCAAATAATGATGATTAGCCGTCAA G	pRH-090
KPO-5535	GTTTTTGCTAGCGTTCGATGCCAAAGCGAGAG	pRH-090
KPO-5538	GTTTTTATGCATGTAAACTATTATGTCATCGAAACG	pRH-092
KPO-5539	GTTTTTGCTAGCCACCAAGTAAGAGAGTTCAGAG	pRH-092
KPO-5548	CCGCCGATACACTGCTTCACGAATACTGAACCTTTTGTCCTATC	pRH-093
KPO-5549	GATTTTGCCAAATCGTAGGCAAAAAAAGAGCGAGCTATTTAAACTC	pRH-093
KPO-5550	TTCAGTATTCGTGAAGCAGTGTATCGGCGGTTATTCGGTTC	pRH-093
KPO-5551	CTTTTTTTGCCTACGATTTGGCAAAATCCTGACTCAGTGC	pRH-093
KPO-5552	GAGCGAGCTATTTAAACTCGC	VadR 3' probe
KPO-5692	GTTCAGTAACTTTAAAGGATCTATCATG	pNP-120
KPO-5693	GTTACTGAACCATTTGTTTTTACAACTG	pNP-120
KPO-5696	GTTACCGTATGAAGGTTAAAGGTTTATCAG	pNP-119
KPO-5697	CATACGGTAACTACGCACATGATTTAATATTG	pNP-119
KPO-5698	CAAGGTTTTGTCCTATCTGATGAATTG	pNP-168
KPO-5699	CAAAACCTTGTCTATTCCCACACATTA	pNP-168
KPO-5700	GTGGTATCTGATGAATTGTAGATTGG	pNP-118
KPO-5701	GATACCACAAAAGGTTGTCTATTCC	pNP-118
KPO-5743	GAACCAAAAAAGCAGAATACGCATTAC	pNP-121
KPO-5744	CTTTTTTTGGTTCATCACTAGACGCTC	pNP-121
KPO-5835	TCGGCTCGTATAATGTGTGGGCGGGTAAAACGCAACTAATC	pLS014
KPO-5836	GCTCAATCAATCACCGGATCCCACCATTTTATGCTCTAGAAATG	pLS014
KPO-5837	TCGGCTCGTATAATGTGTGGGAGAGGTACATAAGAGTTCAAG	pLS-015
KPO-5838	GCTCAATCAATCACCGGATCCGATGTTTTAGGGATATAAAAATAG	pLS-015
KPO-5841	TCGGCTCGTATAATGTGTGGATATATTTCCCAAAGTGGGAAATAG	pLS-016
KPO-5842	GCTCAATCAATCACCGGATCGGAATTGATATGATGAAGACAGAAA	pLS-016
KPO-5843	TCGGCTCGTATAATGTGTGGAGAATCGTTGCTAATCCTGCG	pLS-017
KPO-5844	GCTCAATCAATCACCGGATCCAATGCTCAGTCGTTTGGGTAT	pLS-017
KPO-5845	TCGGCTCGTATAATGTGTGGCCCGAACAGTCTATTTTGCTATTC	pLS-018
KPO-5846	GCTCAATCAATCACCGGATCCCAATCACATAGTCTGCCTATGC	pLS-018
KPO-5847	TCGGCTCGTATAATGTGTGGAATTTGATTATTCTGAATAACCATTAC	pLS-019
KPO-5848	GCTCAATCAATCACCGGATCGTGACTTGCAACTCCGAGT	pLS-019
KPO-5849	TCGGCTCGTATAATGTGTGGGAACTCAGTAGAATCGCTTAGG	pLS-020
KPO-5850	GCTCAATCAATCACCGGATCGCACCATTTTACCGTGGTTTAG	pLS-020
KPO-5981	GTTTTGTTAAACCTGACAACAGTCTGAC	pLS-026
KPO-5982	GTTTAACAAAACCAACGCCCAGCC	pLS-026
KPO-5983	AAACCAACAGTCTGACATTGAACCGAATAAC	pLS-027
KPO-5984	CTGTTGGTTTAAGTCACAAAACCAACGC	pLS-027
KPO-5985	CAGTCATTGAACCGAATAACCGCCG	pLS-028
KPO-5986	TCAATGACTGTTGTCAGGTTTAAGTCAC	pLS-028
KPO-6013	CAACTCTCTACTGTTTCTCC GCTTAGATCTAAAGTTCAAAAAATC	pRH-099
KPO-6014	TATGCATCCTAGGCCTATTA GTTCGCCCACTGTTTATCTTG	pRH-099
KPO-6015	GGGTCTTTTATGATCTTATA CGTTTTGAAGCAATTTGAGATACC	pRH-099
KPO-6016	AGAGGTACCGGTTGTTAACG GTAGTCACTAGGGTTTTGTCATC	pRH-099

Danksagung

Abschließend möchte ich einigen Personen danken, die mich während meiner Promotion begleitet haben.

Herrn Prof. Dr. Kai Papenfort danke ich für die Aufnahme in seine Arbeitsgruppe, für seinen mitreißenden wissenschaftlichen Enthusiasmus und für den engen Austausch, der zu jeder Tages- und Nachtzeit möglich war.

Ich danke allen Mitgliedern meiner Prüfungskommission, vor allem Herrn Prof. Dr. Heinrich Jung, der sich als Zweitgutachter meiner Doktorarbeit zur Verfügung gestellt hat. Mein besonderer Dank gilt auch meinem Promotionskomitee, bestehend aus Prof. Dr. Christof Osman, Prof. Dr. Ralf Heermann und Dr. Kathrin Fröhlich, das mir stets mit Rat und Tat zur Seite stand.

Der Graduiertenschule Life Science Munich (LSM) sowie der Joachim Herz Stiftung möchte ich für die idelle und finanzielle Förderung danken. Dankbar bin ich vor allem auch für die vielseitige Unterstützung seitens der (ehemaligen) Koordinatorinnen der LSM, Francisca Rosa Mende und Nadine Hamze.

Prof. Dr. David Grainger und Dr. James Haycocks danke ich für die vielen Eindrücke, die ich an der Universität Birmingham sammeln durfte und für die stets angenehme wissenschaftliche Zusammenarbeit. Für seinen unermüdlichen Einsatz für das „VadR"-Projekt, möchte ich mich ganz herzlich bei Dr. Praveen Singh vom Max-Planck-Institut für Terrestrische Mikrobiologie in Marburg bedanken.

Für die angenehme Arbeitsatmosphäre bedanke ich mich bei allen aktuellen und ehemaligen Mitgliedern der AG Papenfort, AG Heermann, AG K. Jung und AG H. Jung. Ein besonderer Dank geht an „meine" Studenten Kilian, Merlin, Andreas und vor allem an Luise, deren Hilfsbereitschaft keine (Landes-)Grenzen kannte. Danke Yannik für die zahlreichen späten, aber durch dich sehr unterhaltsamen Stunden im Labor. Danke Mona für deine stetige Hilfsbereitschaft. Vielen Dank Niko und Andreas dafür, dass ihr für die nötige Abwechslung im Arbeitsalltag gesorgt habt!

Für die hervorragenden Arbeitsbedingungen während der Zeit in München, möchte ich mich ganz herzlich bei Tatjana bedanken.

In ganz besonderem Maße danke ich meiner Familie. Danke für die durchgehende und bedingungslose Unterstützung während aller Höhen und Tiefen meiner Promotion.

Zu guter Letzt möchte ich mich bei der Person bedanken, die trotz all der Entbehrungen in den letzten Jahren wie ein Fels an meiner Seite stand. Danke Tatjana, für deine Liebe, dein Verständnis und deine Selbstlosigkeit.

Curriculum Vitae

Aus Datenschutzgründen entfernt.

Removed for protection of privacy.